Complex phase space representation of plasma waves: Theory and applications

Naren Ratan

New College

University of Oxford

A thesis submitted for the degree of

Doctor of Philosophy

Trinity 2017

Acknowledgements

I would like to take this chance to thank my supervisor, Peter Norreys, for his enormous generosity with both his time and knowledge and for the constant inspiration to explore new ideas. I would also like to thank Bob Bingham, Raoul Trines, and Nathan Sircombe for all of their considerable help over the years and for putting up with my bothering them. To the students in my group I would like to say thank you for teaching me so much about physics and other matters. It really has been a pleasure, and I hope we can continue our group meetings well into the future. And to all residents of the Simon room past and present I say thank you for bringing light to an intrinsically quite dark place. For all the years I have known them my parents have been incredibly supportive. No thank you could be enough for all of the kindness they have shown me. Finally, I would like to thank Chloe, my marvellous wife, without whom it is no exaggeration, and in fact the most unforgivable understatement, to say that I could not have done this.

I also gratefully acknowledge a grant from the EPSRC (Award Reference 1378659) as well as funding from the STFC, OxCHEDS, and EUROfusion.

Abstract

This thesis presents results on the description of plasma waves in terms of wavepackets. The wave field is decomposed into a distribution of wavepackets in a space of position, wavevector, time, and frequency. A complex structure joining each pair of Fourier conjugate variables into a single complex coordinate allows the efficient derivation of equations of motion for the phase space distribution by exploiting its analytic properties. The Wick symbol calculus, a mathematical tool generalizing many convenient properties of the Fourier transform to a local setting, is used to derive new exact phase space equations which maintain full information on the phase of the waves and include effects nonlocal in phase space such as harmonic generation. A general purpose asymptotic expansion of the Wick symbol product formula is used to treat dispersion, refraction, photon acceleration, and ponderomotive forces. Examples studied include the nonlinear Schrödinger equation, mode conversion, and the Vlasov equation. The structure of partially coherent wave fields is understood in terms of zeros in the phase space distribution caused by dislocations in its complex phase which are shown to be correlated with the field entropy. Simulations of plasma heating by crossing electron beams are understood by representing the resulting plasma waves in phase space. The local coherence properties of the beam driven Langmuir waves are studied numerically.

Contents

List of Figures

1 Introduction

This is a thesis about plasma physics, in particular the description of plasma waves in terms of wavepackets. In this introduction I give a brief historical overview of the development of plasma physics, giving the opportunity to introduce some key plasma concepts and valuable references. Following this I give an outline of the rest of the thesis.

1.1 Selected history of plasma physics

Here I present a necessarily much abridged discussion of some of the key developments in plasma physics. In this section I have drawn heavily on a recently written disciplinary history of plasma physics [1] which contains a great deal of historical information and many further references, as well as reference [2] which contains further information on fusion research in the UK, and the historical introduction of [3]. For the sake of definiteness I take a preliminary definition of a plasma as an ionized gas that exhibits collective behavior.

Given the prominent role played by gas discharges in the development of electromagnetism, plasmas were present in many early experiments which are described in reference [4]. In 1876 Crookes [5] asked if the gas in a discharge "should not be considered to have got beyond the gaseous state, and to have assumed a

fourth state of matter, in which its properties are as far removed from those of a gas as this is from a liquid", a description now very popular. In 1896 Birkeland gave an explanation of the aurora in terms of the effect of the magnetic field of the earth on cathode rays emitted by the sun [1]. In response to Marconi's transatlantic radio transmission in 1901, in 1902 Kennelly and Heaviside predicted that the radio waves had been reflected from a ionized layer in the atmosphere. In 1907 Lorentz' influential *Theory of Electrons* was published [6], the program of which, to explain all electromagnetic phenomena in terms of the vacuum electromagnetic field equations and the motions of electrons, plasma physics sits within very naturally.

In 1923 Debye and Hückel gave a theory of electrolytes [7] which described how the charge of a given ion was screened by other charges in the solution, a phenomenon which also occurs in plasmas, the screening occurring on the scale of what is now called the Debye length. An ideal plasma has a large number of particles in a Debye sphere, a sphere with the radius of the Debye length, this number being called the plasma parameter, in which case this charge screening is effective. In 1928 Langmuir introduce the term plasma for an ionized gas "containing balanced charges of ions and electrons" [8], and Langmuir and Tonks in 1929 gave the theory of and experiments on oscillations in ionized gases [9], describing the high frequency electron density waves caused by the electric field produced by modulations in electron density now known as Langmuir waves as well as the lower frequency ion-acoustic waves in which the electrons move with the ions. In 1931 Appleton and Hartree treated radio wave propagation in the ionosphere in terms of electron motion [3], [10], including the effect of propagation at any angle to the Earth's magnetic field on the dispersion of the waves. In 1934 Bennett gave a theory of the pinch effect by which a stream of electrons can be magnetically self focused [11].

Vlasov in 1938 gave his plasma kinetic equation, which contained a term representing the fields generated collectively by the charges in the plasma [12], an equation which we will study theoretically in Chapter 4 and numerically in Chapter 7. In 1942 Alfvén in a letter to Nature [13] announced his electromagnetic-hydrodynamic waves, now called Alfvén waves, magnetohydrodynamic waves along

magnetic field lines. In 1946 Landau developed his theory of the collisionless damping of Langmuir waves [14], now called Landau damping, which stimulated considerable theoretical development in plasma physics and which we will discuss in Chapter 4. 1950 saw the publication of Alfvén's *Cosmical Electrodynamics*, a very influential textbook containing discussions the guiding center orbits of charged particles in a magnetic field, the adiabatic invariance of the magnetic moment of a charged particle in a varying magnetic field, and of the freezing in of magnetic flux into a plasma.

In 1950 Sakharov and Tamm proposed the magnetic thermonuclear reactor [15], later renamed the tokamak, a toroidal device using magnetic fields to confine a fusion plasma. In 1951 Spitzer proposed the stellarator, a magnetic confinement fusion device with a twisted geometry [16], and in 1955 Spitzer's book *Physics of Fully Ionized Gases* was published, which included a treatment of the multiple small angle collisions between particles in the plasma leading to diffusion in velocity space [17]. In 1959 Buneman gave a theoretical and computational treatment of the two-stream instability [18], the instability of streams of particles drifting with respect to each other, which we will study in Chapter 6 and 7. This paper is also an early example of the use of computers to study plasmas numerically.

In 1960 Maiman constructed the first laser [19], and shortly after the laser was used in classified work involving the generation of plasmas [1] and the development of the inertial confinement fusion concept which uses lasers to compress and heat a pellet of fuel, work which was declassified in 1972 [20]. In 1964 Zel'dovich and Raizer's textbook *Physics of Shock Waves and High-Temperature Hydrodynamic Phenomena* [21] appeared, covering many aspects of high energy density physics, and including a useful discussion of the method of characteristics as we will use in Chapters 2 and 4. 1969 saw the publication of Sagdeev and Galeev's *Nonlinear Plasma Theory* [22], containing treatments of the nonlinear interactions between waves in a plasma as well as an early example of the phase space description of waves, that is the description of a wave field in terms of a distribution of wavepackets in a space of position and wavevector. This, the publication of an influential plasma physics text containing an early phase space representation of waves, is an

appropriate point to conclude this historical survey. Discussion of the extensive further development of the phase space description of waves, both inside and outside plasma physics, can be found in Chapter 4.

1.2 Outline of the thesis

This thesis presents some new methods for the description of plasma waves and their equations in terms of wavepackets, and falls into two parts. Chapters 2-5 deal with a new method for translating field equations, depending on position and time, into wavepacket equations which govern the evolution of the distribution of the wavepackets of varying locations, wavevectors and frequencies which make up the field. This phase space representation of wave equations has a long history, the key new aspect here is the use of the Wick symbol calculus for the derivation of equations for the coherent state distribution, a technique which leads to new phase space equations which have a number of physical and technical advantages. The material in Chapters 3-5 forms the basis of a paper due to be submitted shortly. Chapters 6 and 7 present analytical and numerical results on the heating of plasmas by the instability of crossing electron beams, including the understanding of this process using the description in terms of wavepackets and local coherence developed in the earlier chapters. Chapters 6 and 7 are based on work published in [23].

In preparation for the development of wavepacket methods, Chapter 2 covers methods of solving wave equations, contrasting the global approach of the Fourier and Laplace transform with the local methods of characteristics and random characteristics. All of this material is well known, although the treatment of the delta functions and principal value functions which occur when solving wave equations using the Fourier transform is new to my knowledge, as is the method of presentation of the Laplace transform as a field sourced by the function describing the distribution of modes in frequency and growth rate.

In Chapter 3 I describe the windowed Fourier transform, the coherent state distribution, and the Wick symbol calculus, which together provide an intuitive and powerful set of mathematical tools for calculating with phase space distributions.

This builds upon the Wick symbol calculus as developed by Berezin, and while most of the results are well known aspects of the presentation as well as the physical interpretation of some of the symbols calculated in terms of windowed Fourier transforms is also new. It is also my hope that this Chapter will provide a useful introduction to what is potentially an obscure subject.

In Chapter 4 I apply the Wick symbol calculus to systematically derive phase space representations of a number of equations of physical interest. I first treat an oscillator with varying frequency, studying the asymptotic expansion for slowly varying frequencies in detail. Secondly I treat an equation proposed by Schuster describing wave propagation in a medium, demonstrating how the method treats dispersion, refraction and photon acceleration, as well as effects such as harmonic generation which result from the medium varying on scales shorter than the wavelength of the waves. As a third example I take the nonlinear Schrödinger equation, which shows how the method naturally treats dispersion and ponderomotive forces. Next I solve a mode conversion problem by solving the corresponding complex phase space equation along rays. Lastly I treat the Vlasov equation and make contact with some modern developments concerning phase mixing in the study of Landau damping.

In Chapter 5 I present the complex phase space distribution of some incoherent wave fields and show that their coherence properties are determined by zeros in their phase space distributions resulting from dislocations in their complex phase, studying the relation between phase dislocations, coherence length and field entropy. These zeros are well known in other areas such as quantum chaos, but their use in an account of partial coherence in the phase space representation of plasma waves is new.

Chapters 6 and 7 are paired, Chapter 6 presenting the linear growth rate calculations for the instability of crossing beams in a plasma using a relativistic fluid model for the beams, Chapter 7 containing Vlasov-Maxwell simulations of this system using the VALIS code. This chapter uses numerically calculated phase space distributions to understand the coupling process and studies the local coherence properties of the waves.

Finally Chapter 8 contains a summary and discussion of future work.

2 Waves

In this chapter I describe some techniques essential for the study of waves, focusing on the Fourier and Laplace transform and the (random and ordinary) method of characteristics. The purpose of this chapter is twofold. Firstly it serves to introduce methods and notations which will be heavily leaned on subsequently. Secondly it contrasts the global approach to waves epitomized by the Fourier transform with the entirely local approach of the method of characteristics, so setting the scene for the wavepacket methods I will later develop which in some sense interpolate between the global and local methods.

2.1 Global methods

2.1.1 The Fourier transform

Euler did not believe (what would become) Fourier's theorem [24], [25], and who can blame him? It seems on the face of it surprising that we can write any function as a sum of sine waves. Two points allow the Fourier transform to pull off this feat: i) the phase of the Fourier transform varies in subtle and intricate ways to achieve the correct interference between the sine waves; and ii) the amplitude of the Fourier transform can become infinite in subtle and intricate ways. To handle the singular behaviour of the Fourier transform responsibly we can use infinite

and infinitesimal numbers (something Euler did believe in [26]). The complicated behaviour of the phase is intrinsic to the Fourier transform, but this difficulty is considerably alleviated by using wavepackets (Chapter 3).

The hyperfinite Fourier transform

The Fourier transform allows us to analyze a given function $u(x)$ into its components $F(k)$ of different wavevectors e^{ikx}, according to the formula

$$F(k) = \frac{1}{2\pi}\int_{-\infty}^{\infty} e^{-ikx}u(x)\,\mathrm{d}x. \tag{2.1}$$

The inverse Fourier transform allows us to synthesize a given function from its components according to the formula

$$u(x) = \int_{-\infty}^{\infty} F(k)e^{ikx}\,\mathrm{d}k. \tag{2.2}$$

The analysis formula (2.1) has the interpretation that $F(k)$ is the inner product of u with the complex exponential e_k, or $F = e_k^\dagger u$, and the synthesis formula (2.2) tells us that we can reconstruct u by superposing the basis functions e_k with the appropriate coefficients. When using the Fourier transform either to analyze or synthesize we routinely encounter integrals which do not exist in the ordinary sense because either $u(x)$ or $F(k)$ does not decay fast enough or even grows as $x \to \pm\infty$ or $k \to \pm\infty$. These equations can be made sense of using the theory of distributions [27]–[29], however we can simply treat them using the hyperreal numbers [30]–[32], a field of numbers which extends the real numbers with infinitesimal and infinite numbers but which otherwise satisfies all the properties of the real numbers. In particular we adopt the simple rule that rather than trying to take the limits implied by integrating between $\pm\infty$, we integrate between $\pm N$, where N is an infinite number. For example the constant function $u(x) = 1$ certainly does not decay at infinity but we can calculate its Fourier transform F_1 as

$$F_1(k) = \frac{1}{2\pi}\int_{-N}^{N} e^{-ikx}\,\mathrm{d}x \tag{2.3}$$

$$= \frac{N}{\pi}\,\mathrm{sinc}(Nk), \tag{2.4}$$

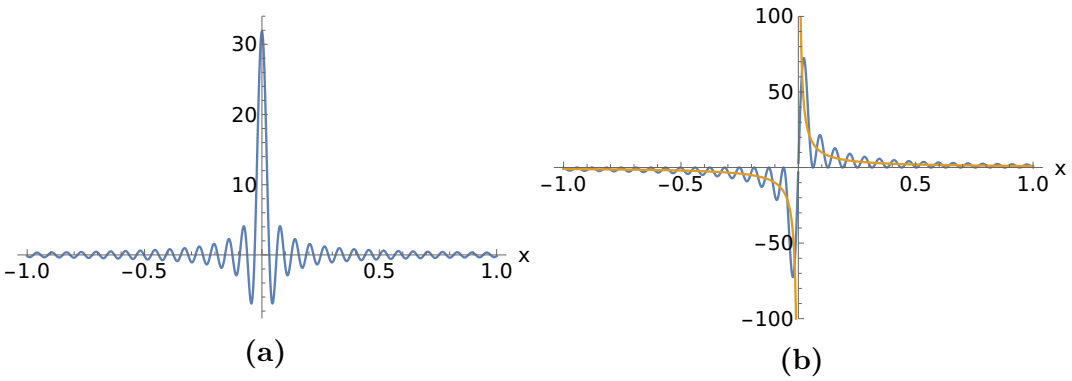

Figure 2.1: Plots showing (a) the function $\frac{N}{\pi}\operatorname{sinc}(Nx)$, a delta function, and (b) the function $\frac{1-\cos(Nx)}{x}$, a principal value function. The functions are plotted for finite N; for infinite N they are delta/principal value functions.

which we can verify is a delta function. For the Fourier transform F_H of the step function H we obtain

$$F_H(k) = \frac{1}{2\pi}\int_0^N e^{-ikx}\,\mathrm{d}x \tag{2.5}$$

$$= \frac{1}{2}\frac{N}{\pi}\operatorname{sinc}(Nk) + \frac{1}{2\pi i}\frac{1-\cos(Nk)}{k} \tag{2.6}$$

$$\equiv \frac{1}{2}\delta(k) + \frac{1}{2\pi i}\mathcal{P}\left(\frac{1}{k}\right), \tag{2.7}$$

where on the last line we have identified $\frac{N}{\pi}\operatorname{sinc}(Nk)$ as a delta function and $\frac{1}{k}(1-\cos(Nk))$ as a principal value function. Figure 2.1 shows plots of these two functions. The sinc function has a single central peak with high frequency oscillations in its tails, and it seems reasonable enough that it acts as a delta function. The function $\frac{1}{k}(1-\cos(Nk))$ is zero at the origin, with two spikes close to the origin which take it up to meet the curve $\frac{1}{x}$ (also shown), which it then oscillates about. This is how it acts as a principal value function; it is zero at the origin, and so inside an integral it excludes the value of its partner at zero, and when integrated the rapid oscillations average out to give behaviour like $\frac{1}{x}$ away from $x = 0$.

Solving differential equations

The Fourier transform is very useful for solving differential equations. In particular the hyperfinite Fourier transform gives a simple treatment of the delta functions and principal value functions which appear when solving wave equations with the Fourier

transform. As a simple first example we take the differential equation $\partial_x u = 0$, the simplest possible differential equation. Taking the Fourier transform of the equation we obtain 0 for the right hand side, while integrating the left hand side by parts gives

$$\frac{1}{2\pi}\int_{-N}^{N}(\partial_x u)\,e^{-ikx}\,\mathrm{d}x = \frac{1}{2\pi}[ue^{-ikx}]_{x=-N}^{x=N} + \frac{ik}{2\pi}\int_{-N}^{N} ue^{-ikx}\,\mathrm{d}x \tag{2.8}$$

$$= \frac{u(N)e^{-ikN} - u(-N)e^{ikN}}{2\pi} + ikF(k). \tag{2.9}$$

Now if u decays at $x = \pm\infty$, $u(N)$ and $u(-N)$ are infinitesimal and so the Fourier transform of $\partial_x u$ equals ikF up to infinitesimals. However we do not know $u(\pm N)$ since we have not solved the equation yet (and in fact here $u(N)$ and $u(-N)$ are not infinitesimal), so we introduce the unknown constants $\alpha = u(-N)$ and $\beta = u(N)$, in terms of which we find

$$F(k) = \frac{\alpha e^{ikN} - \beta e^{-ikN}}{2\pi ik}. \tag{2.10}$$

At first sight $F(k)$ appears to be undefined for $k = 0$, but in fact we know that $F(k)$ must exist for all k since the integral defining the hyperfinite Fourier transform exists for any k. This necessarily good behaviour imposes a constraint on α and β; to ensure that $F(k)$ is defined at $k = 0$ we require $\alpha = \beta$, and so

$$F(k) = \frac{\alpha N}{\pi}\,\mathrm{sinc}(Nk) \tag{2.11}$$

$$= \alpha\delta(k) \tag{2.12}$$

which upon inverting the Fourier transform gives $u(x) = \alpha$, the general solution of $\partial_x u = 0$.

As a second example we take the simplest equation for a Green function, $\partial_x u = \delta$, which illustrates the principal value functions encountered when finding Green functions. First of all applying the usual rule that the Fourier transform of the derivative is ik multiplied by the Fourier transform (and so informally an equation is Fourier transformed applying the rule $\partial_x \to ik$) and using the rule that the Fourier transform of a delta function is a constant (with our conventions $\frac{1}{2\pi}$),

we would obtain for the Fourier transform $\tilde{u}$ of u

$$ik\tilde{u} = \frac{1}{2\pi} \tag{2.13}$$

$$\tilde{u} = \frac{1}{2\pi k}. \tag{2.14}$$

Then when trying to invert the Fourier transform we would realize that the integral does not make sense, and argue that the correct thing to do is to in fact evaluate a contour integral, and choose the contour in order to match the boundary conditions we impose on u. This gets us the right answer, but by using the hyperfinite Fourier transform we can avoid dealing with undefined integrals which need to be 'fixed up'. The hyperfinite Fourier transform of $\partial_x u = \delta$ gives

$$\frac{u(N)e^{-ikN} - u(-N)e^{ikN}}{2\pi} + ikF(k) = \frac{1}{2\pi} \tag{2.15}$$

$$F(k) = \frac{1 + \alpha e^{ikN} - \beta e^{-ikN}}{2\pi ik} \tag{2.16}$$

where as before we have introduced the unknown constants $\alpha = u(-N)$ and $\beta = u(+N)$. Again we use the necessarily good behaviour of $F(k)$ at $k = 0$ to constrain α and β; in this case we require $\beta = \alpha + 1$, and so $F(k)$ is given by

$$F(k) = \left(\alpha + \frac{1}{2}\right)\frac{N}{\pi}\operatorname{sinc}(Nk) + \frac{1}{2\pi i}\frac{1 - \cos(Nk)}{k} \tag{2.17}$$

$$= \left(\alpha + \frac{1}{2}\right)\delta(k) + \frac{1}{2\pi i}\mathcal{P}\left(\frac{}{}\right), \tag{2.18}$$

the Fourier transform of the constant function α plus the step function H, which is indeed the general solution of $\partial_x u = \delta$. The condition that the solution u can only increase in value by one is really determined in the tiny region around $x = 0$, where the delta function acts, but when employing the Fourier transform manifests itself rather as a consistency condition constraining the values of u at $x = \pm N$, infinitely far apart, perceiving the localized jump only through its nonlocal effects.

As an example of solving a wave equation using the hyperfinite Fourier transform we take the advection equation (with which we will also illustrate the method of characteristics later),

$$\partial_t u + a\partial_x u = 0, \tag{2.19}$$

which describes a quantity u propagating to the right at speed a (we will verify its solution is $f(x-at)$ for some function f). In extending the hyperfinite Fourier transform to two dimensions x and t we have a choice in the shape of the (infinite) region in the x-t plane over which we integrate. The most immediate extension of the hyperfinite Fourier transform to two dimensions would be $\int_{-X}^{X}\int_{-T}^{T} f(x,t)e^{-i(kx+\omega t)}\,\mathrm{d}t\,\mathrm{d}x$, that is to integrate over a rectangle in the x-t plane. However another choice will be more convenient and is in fact closely tied to physics, which is to integrate over the diamond formed by two 'light-cones' formed from trajectories of particles travelling with velocity $\pm a$, the region D shown in Figure 2.2 (a). In these diagrams T and aT are infinite; we have 'zoomed out' by an infinite factor [33] to make the boundaries visible, and on any ordinary diagram the shaded regions would cover any amount of plane we could draw. While it here serves the fairly mundane purpose of allowing us to solve the advection equation, the introduction by Penrose of past and future null infinities in general relativity [34], [35] (using not infinite numbers but a conformal rescaling to bring infinity in to a finite distance) has led to many significant theoretical advances [36]. In any case whether motivated by physics or by convenience we introduce the two dimensional hyperfinite Fourier transform as

$$F(k,\omega) = \frac{1}{2\pi}\int_D u(x,t)e^{-i(kx-\omega t)}\,\mathrm{d}x\,\mathrm{d}t, \tag{2.20}$$

or

$$F(p,q) = \frac{1}{2\pi}\int_{-aT}^{aT}\int_{-aT}^{aT} u(r,s)e^{-i(pr+qs)}\,\mathrm{d}r\mathrm{d}s, \tag{2.21}$$

where we have introduced light-cone coordinates $r = x+at$ and $s = x-at$ and the corresponding Fourier transform variables $p = \frac{1}{2}\left(k-\frac{\omega}{a}\right)$ and $q = \frac{1}{2}\left(k+\frac{\omega}{a}\right)$, in terms of which the integral over D corresponds just to integrating with respect to r and s between $\pm aT$, thus avoiding integrals with variable limits. Now taking the hyperfinite Fourier transform of the advection equation, either directly or using the fact that $\partial_t u + a\partial_x u = 2a\partial_r u$, and integrating in parts in r, we obtain

for the Fourier transform $F(p,q)$

$$F(p,q) = \frac{1}{2\pi ip}\left(\left(\int_{-aT}^{aT} u(-aT,s)e^{-iqs}\,\mathrm{d}s\right)e^{ipaT} - \left(\int_{-aT}^{aT} u(-aT,s)e^{-iqs}\,\mathrm{d}s\right)e^{-ipaT}\right) \tag{2.22}$$

$$= \frac{\alpha(q)e^{ipaT} - \beta(q)e^{-ipaT}}{2\pi ip}, \tag{2.23}$$

where we have in this case introduced two unknown functions of q, $\alpha(q)$ and $\beta(q)$, which were introduced as the unknown Fourier transform of u along the boundaries N_+ and N_- shown in Figure 2.2 (b) in red and blue. Now the good behaviour of $F(p,q)$ imposes a constraint on the functions $\alpha(q)$ and $\beta(q)$, in this case that they must be equal for all q, and hence

$$F(p,q) = \alpha(q)\frac{aT}{\pi}\operatorname{sinc}(paT) \tag{2.24}$$

$$= \alpha(q)\delta(p), \tag{2.25}$$

and so

$$F(k,\omega) = \alpha(k+\frac{\omega}{a})\delta(k-\frac{\omega}{a}). \tag{2.26}$$

This expresses the Fourier transform $F(k,\omega)$ as the product of a delta function confining the Fourier transform to the surface $\omega = ka$, the dispersion surface, together with an arbitrary function along that surface which is in fact the Fourier transform of u at null infinity along N_+ and N_-.

2.1.2 The Laplace transform

The Laplace transform [37], [38] allows us to deal with waves which grow exponentially. Analogously to the Fourier synthesis of a function from oscillations $e^{i\omega t}$ of varying frequency ω, we can consider synthesizing a function from growing/damping oscillations $e^{\gamma t+i\omega t}$ of varying frequency ω and growth rate γ, according to the formula

$$u(t) = \iint g(\omega,\gamma)e^{(\gamma+i\omega)t}\,\mathrm{d}\omega\,\mathrm{d}\gamma, \tag{2.27}$$

in which we will call $g(\omega,\gamma)$ the mode distribution function. Physically we might think of $g(\omega,\gamma)$ as a distribution of damped radiating atoms, a spectrum of unstable

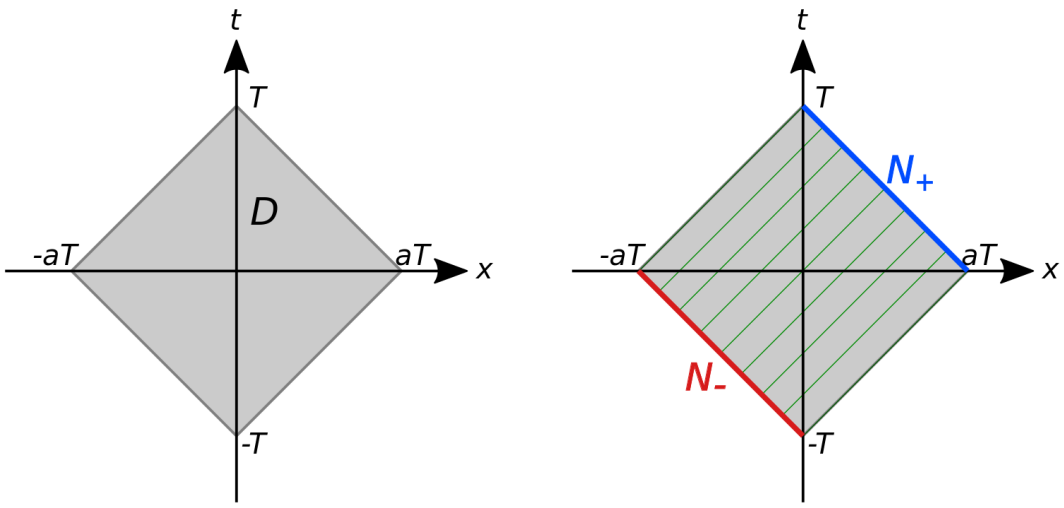

(a) **(b)**

Figure 2.2: The infinite region of integration D in the definition of the space-time hyperfinite Fourier transform. In (a) the region D is shown in gray, bounded by past and future 'light cones at infinity' formed from lines $x \pm at = \pm aT$, where T is infinite. In (b) the lines $N_\pm$ along which the boundary values are required in order to Fourier transform the advection equation are shown.

waves, or (if all oscillations have zero frequency) the composition of a radioactive sample composed of nuclei with different half lives. This formula is analogous to the Fourier synthesis formula, but the analogous method of Fourier analysis, taking the inner product with a mode $e^{i\omega t}$, will not work here since it relies on the orthogonality of the $e^{i\omega t}$, and the functions $e^{\gamma t + i\omega t}$ are very much non-orthogonal, their dot products diverging very strongly [39]. The Laplace transform provides a way to proceed indirectly, never dealing with the mode distribution function $g(\omega, \gamma)$ explicitly. Remarkably, the Laplace transform is in fact the field obtained by considering $g(\omega, \gamma)$ as a distribution of charges and vortices in the $\omega - \gamma$ plane. We can understand this using a useful connection between complex analysis and vector calculus in the plane, which also provides a useful summary for application in later chapters.

Pólya fields

A complex function $f(z)$ can be usefully thought of as a vector field v_f on the plane called the Pólya field [40], given by $v_f(x, y) = \mathrm{Re}(f(z))\mathbf{e}_x - \mathrm{Im}(f(z))\mathbf{e}_y$,

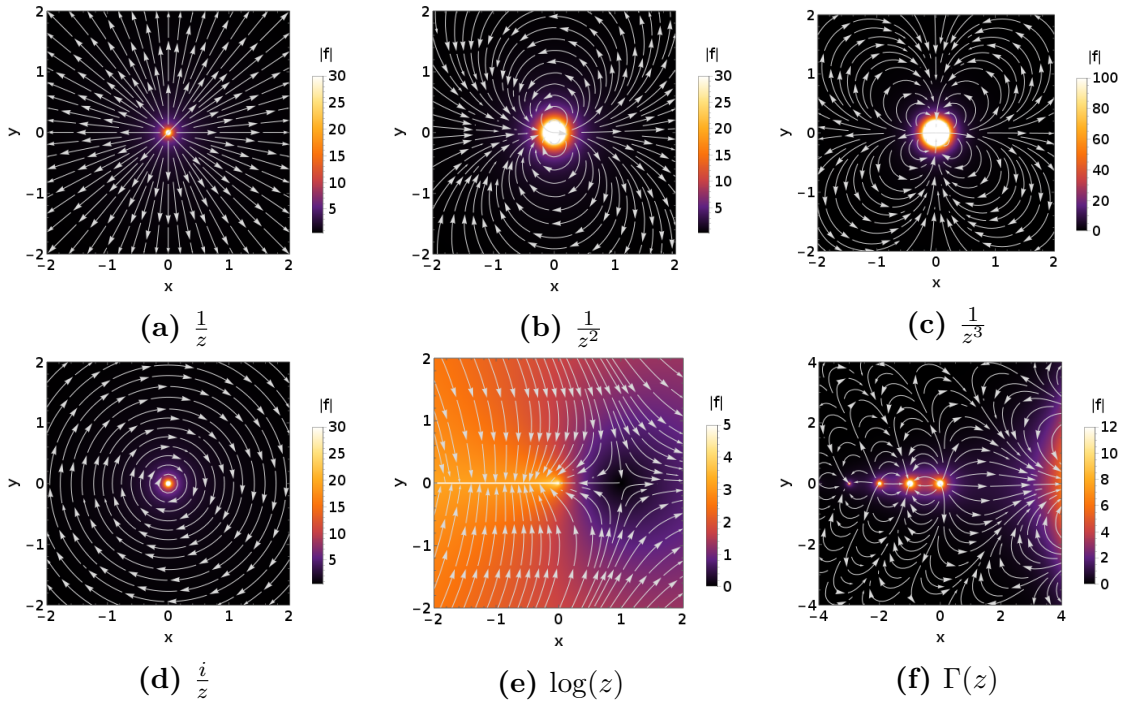

Figure 2.3: A gallery of Pólya plots, showing the Pólya field and the modulus of some complex functions.The Laurent series of a complex function corresponds to a multipole expansion, as the appearance of monopole, dipole and quadrupole fields above illustrates. The Cauchy-Riemann equations are equivalent to the fields having zero divergence and curl away from poles.

where $z = x + iy$. Defined in this way we have the very useful property that the Cauchy-Riemann equations for f simply correspond to v_f having zero divergence and curl (vector fields like this are called harmonic). Further, the contour integral of f around a contour C is simply the flux of v_f out of C plus i times the circulation of v_f around C. Even further, the Laurent series of f corresponds to the multipole expansion of v_f. In this way the residue theorem, that the integral of f around a contour C is equal to $2\pi i$ times the sum of the residues of poles of f inside C, simply reflects Gauss' law and Stokes theorem that the flux out of/circulation around C is determined by the charge/vorticity inside C, and only point charges and point vortices have a net charge/vorticity, not the dipole and higher order terms. Analytic continuation corresponds to thinking of the Pólya field v_f as an incompressible fluid flow and following the stream lines from the region in which we know v_f into the rest of the plane (where possible).

With this in mind, we proceed to the Laplace transform $L(z)$ of the function $u(t)$, defined as

$$L(z) = \int_0^\infty u(t)e^{-zt}\,\mathrm{d}t, \tag{2.28}$$

with the understanding that the integral will only converge for some z and that L will later be analytically continued. Now using our synthesis formula for $u(t)$ in terms of the mode distribution function $g(\omega, \gamma)$, we have

$$L(z) = \int_0^\infty \left(\iint g(\omega,\gamma)e^{(\gamma+i\omega)t}\mathrm{d}\omega\,\mathrm{d}\gamma \right) e^{-zt}\,\mathrm{d}t \tag{2.29}$$

$$= \iint \left(\int_0^\infty e^{(\gamma+i\omega-z)t}\,\mathrm{d}t \right) g(\omega,\gamma)\,\mathrm{d}\omega\,\mathrm{d}\gamma \tag{2.30}$$

which gives, for those values of z for which the bracketed integral converges,

$$L(z) = \iint \frac{g(\omega,\gamma)}{z-(\gamma+i\omega)}\,\mathrm{d}\omega\,\mathrm{d}\gamma. \tag{2.31}$$

This is, apart from a change of notation, exactly Coulomb's law for the electric field in the plane sourced by the real part of $g(\omega, \gamma)$ (that is considering $\mathrm{Re}(g)$ as a distribution of charged wires perpendicular to the plane), together with the analogous law for the determination of the vorticity field from its source (or Ampere's law for currents perpendicular to the plane with density $\mathrm{Im}(g)$).

For example, say the function $u(t)$ we are analyzing is simply e^{at}, so the mode distribution function is $g(\omega, \gamma) = \delta(\omega)\delta(\gamma - a)$ since we have only one component with frequency zero and growth rate a. This corresponds to a point charge at a, and we can calculate directly that the Laplace transform of e^{at} is $L(z) = \frac{1}{z-a}$ which from the Pólya field we know is indeed the field of a point charge at $z = a$.

We can invert the Laplace transform $L(z)$ without calculating $g(\omega, \gamma)$ directly by integrating around a contour C enclosing the region containing sources, that is where $g(\omega, \gamma)$ is non-zero. The inversion is in fact given by the integral

$$I(t) = \frac{1}{2\pi i}\int_C L(z)e^{zt}\,\mathrm{d}z \tag{2.32}$$

$$= \frac{1}{2\pi i}\int_C \left(\iint \frac{g(\omega,\gamma)}{z-(\gamma+i\omega)}\,\mathrm{d}\omega\,\mathrm{d}\gamma \right) e^{zt}\,\mathrm{d}z \tag{2.33}$$

$$= \iint g(\omega,\gamma)\left(\frac{1}{2\pi i}\int_C \frac{e^{zt}}{z-(\gamma+i\omega)}\,\mathrm{d}z \right) \mathrm{d}\omega\,\mathrm{d}\gamma. \tag{2.34}$$

Since the contour C encloses all sources, we can evaluate the inner integral using the residue theorem, obtaining $2\pi i e^{(\gamma+i\omega)t}$, and so

$$I(t) = \iint g(\omega, \gamma) e^{(\gamma+i\omega)t} \, \mathrm{d}\omega \, \mathrm{d}\gamma \tag{2.35}$$

$$= u(t). \tag{2.36}$$

If we are interested in the function $u(t)$ only for $t > 0$, we can deform the contour C into a semicircle whose diameter lies along a vertical line to the right of all the poles of $L(z)$ and then send the radius of the semicircle to infinity off to the left, where $\gamma < 0$ so the factor $e^{\gamma t}$ kills the contribution from the arc of the semicircle, in this way recovering the usual contour used for inverting the Laplace transform. This integral is often evaluated using the residue theorem in any case, which effectively involves bringing back the semicircular arc.

This understanding gives some insight into the calculation and interpretation of Laplace transforms. The most obvious analogy between the Fourier and Laplace transform, that the Laplace transform is simply the Fourier transform for complex frequencies, fails in the sense that the interpretation of the inverse transformation as making up a function from basic mode functions does not at all apply to the usual Laplace inversion integral; the relationship is a little more involved.

2.2 Local methods

2.2.1 The method of characteristics

The method of characteristics allows us to solve partial differential equations by integrating along rays [21], [41], [42]. We give some examples to illustrate the method, which we will need later for solving wave equations in phase space.

Physically the method of characteristics takes advantage of the fact that disturbances in a wave field propagate along definite trajectories, and the evolution of the disturbance depends only on its local environment, not on distant parts of the field. Mathematically the method of characteristics finds these trajectories (called

characteristics or rays) and integrates along them to find the evolution of the wave field. In this way we can solve an equation such as the advection equation

$$\partial_t u + a\partial_x u = 0 \tag{2.37}$$

by specifying a trajectory $X(s)$, where s is a parameter along the trajectory, applying the chain rule to $U(s) = u(s, X(s))$ to give

$$\frac{\mathrm{d}U}{\mathrm{d}s} = \partial_t u + \frac{\mathrm{d}X}{\mathrm{d}s}\partial_x u \tag{2.38}$$

and using the fact that if we choose our trajectory X so that $\frac{\mathrm{d}X}{\mathrm{d}s} = a$, so that we move with a speed a, then the advection equation tells us that $\frac{\mathrm{d}U}{\mathrm{d}s} = 0$ and so at points along our trajectory u is constant. Then the field $u_0(x)$ at time $t = 0$ determines u for all later times, since $X(s) = x_0 + as$ where x_0 is the starting point of our trajectory and $U(0) = u(0, x_0) = u_0(x_0)$ is the value of u at $t = 0$ at the starting point x_0, so from our definition of $U(s)$,

$$u(s, x_0 + as) = u_0(x_0), \tag{2.39}$$

that is the value of u along the trajectory starting at x_0 is just the initial value of u at x_0. This is often enough to solve the equation numerically, giving the values of u along trajectories which we can find numerically. Here we can find $u(x, t)$ explicitly by changing variables, putting $t = s$ and $x = x_0 + as$, to give

$$u(x, t) = u_0(x - at), \tag{2.40}$$

that is the solution is just the initial profile u_0 translating to the right at speed a. The same method goes through if the speed a is allowed to depend on position, time, or even on the value of u (in which case the equation is nonlinear), and if there is a source term on the right hand side (which can also depend on u), that is for an equation like

$$\partial_t u + a(x, t, u)\partial_x u = j(x, t, u), \tag{2.41}$$

the only difference being that the trajectory has to solve $\frac{\mathrm{d}X}{\mathrm{d}s} = a(X(s), s, U(s))$ and U evolves along the trajectory according to $\frac{\mathrm{d}U}{\mathrm{d}s} = j(X(s), s, U(s))$. In two spatial

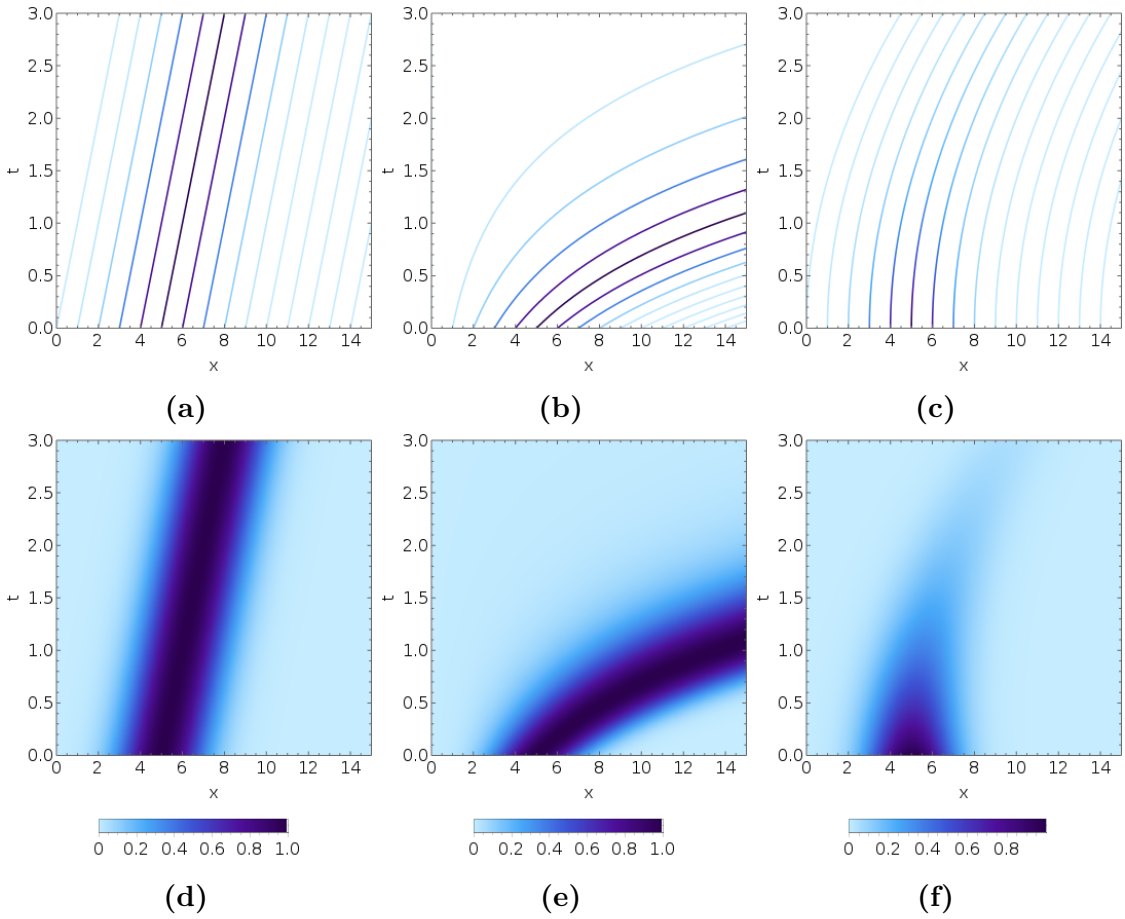

Figure 2.4: Examples of the characteristics and solutions of advection equations with a constant wave speed (a) and (d), a wave speed proportional to x (b) and (e), and a wave speed proportional to t and with damping (c) and (f). The characteristics are coloured according to the value of u along them; together all the characteristics cover the whole plane and reproduce the plots of the solutions below.

dimensions the trajectory is specified by two functions $X(s)$ and $Y(s)$ satisfying analogous equations; it is sometimes useful to include a function multiplying the $\partial_t u$ derivative, in which case we need to include the time $T(s)$ along our trajectory explicitly (this corresponds to the freedom in parameterizing a world-line in relativity [43]).

Figure 2.4 shows the characteristics and the solutions obtained for three example equations. In (a) and (d) the equation solved is $\partial_t u + a\partial_x u = 0$, the case we solved above, so the speed of propagation is constant. In (b) and (e) the equation is $\partial_t + x\partial_x u = 0$, so the speed of propagation is proportional to x, with the characteristics propagating ever faster as they move to the right. In (c) and (f) the

equation is $\partial_t u + t\partial_x u = -u$, so the speed of propagation increases with time and there is a source proportional to $-u$ which leads to damping of the waves. The characteristics are colored according to the value of u along them, so taken together they cover the plane and reproduce the plots of the solutions.

2.2.2 Random characteristics

In applying the method of characteristics intuitively we can imagine following the life of a fluid parcel along its trajectory, with the density of the parcel representing the value of the function along the trajectory. We can further imagine the fluid parcel being made up of many particles, all of which follow the same trajectory, with the value of the function now represented by the density of these particle trajectories, moving from a fluid to a kinetic intuition. We might now ask what happens if these particles can suffer 'collisions' and so change direction at random? In this case the density of these trajectories, these random characteristics, can still satisfy a useful equation. Depending on the nature of the collisions and so of the random characteristics this equation can be for example the telegrapher's equation, the heat equation, or a transport equation [44]–[47].

As an example of these random characteristics, the one-dimensional (1D) wave equation

$$\partial_t^2 u - a^2 \partial_x^2 u = 0 \tag{2.42}$$

has two families of characteristics, one travelling to the right with speed a, one travelling to the left with speed a. This is because it is equivalent to the two independent advection equations $\partial_t f + a\partial_x f = 0$ and $\partial_t g - a\partial_x g = 0$ for $f = \partial_t u - a\partial_x u$, $g = \partial_t u + a\partial_x u$, which we looked at above. We now consider replacing each characteristic by a large number of individual characteristics, with a number proportional to the value of u along the characteristic being replaced. The solution is now obtained as the density of these individual characteristics. Now, if instead of propagating always with their initial velocity, the velocity of a given particle can

change sign in a given time dt with probability bdt, the density of particles no longer satisfies the wave equation, but in fact satisfies the telegrapher's equation [44]

$$\partial_t^2 u - a^2 \partial_x^2 u + b \partial_t u = 0. \tag{2.43}$$

Further, if we consider the limit in which $a \to \infty$ and $b \to \infty$, so the velocity and probability of collision tend to infinity, in such a way that $a^2/2b$ remains a constant D, the random characteristics approach Brownian motions, and their density satisfies the heat equation with diffusivity D. Figure 2.5 shows the random characteristics and the corresponding solutions for the wave equation on the left, in which $b = 0$ and the characteristics are straight lines, the telegrapher's equation in the center, in which the characteristics have Poisson velocity jumps, and the heat equation on the right in the limit in which the random characteristics tend to Brownian motions.

In the example above the characteristics had only two velocities $\pm a$ and switched between them at random. Allowing a distribution of rays in velocity can solve transport equations which describe the evolution of a distribution of particles not just in position but also in velocity, and which, as well as being of considerable practical importance in their own right, provide a very useful stepping stone on the path from particle dynamics to kinetic theory proper. In fact we can illustrate the application of random characteristics to the solution of transport equations using the solution to the telegrapher's equation above and some singular maneuvers to recast the telegrapher's equation for a function $u(x, t)$ of position and time as a transport equation for a function $h(x, v, t)$ of position, velocity and time (admittedly a somewhat degenerate one). First of all the telegrapher's equation can be written as a first order system [48]. Beginning with the telegrapher's equation

$$\partial_t^2 u - a^2 \partial_x^2 u + b \partial_t u = 0 \tag{2.44}$$

we introduce the two quantities $f = \partial_t u - a \partial_x u$ and $g = \partial_t u + a \partial_x u$ (which are the derivatives of u along the trajectories $x = at$ and $x = -at$), in terms of which

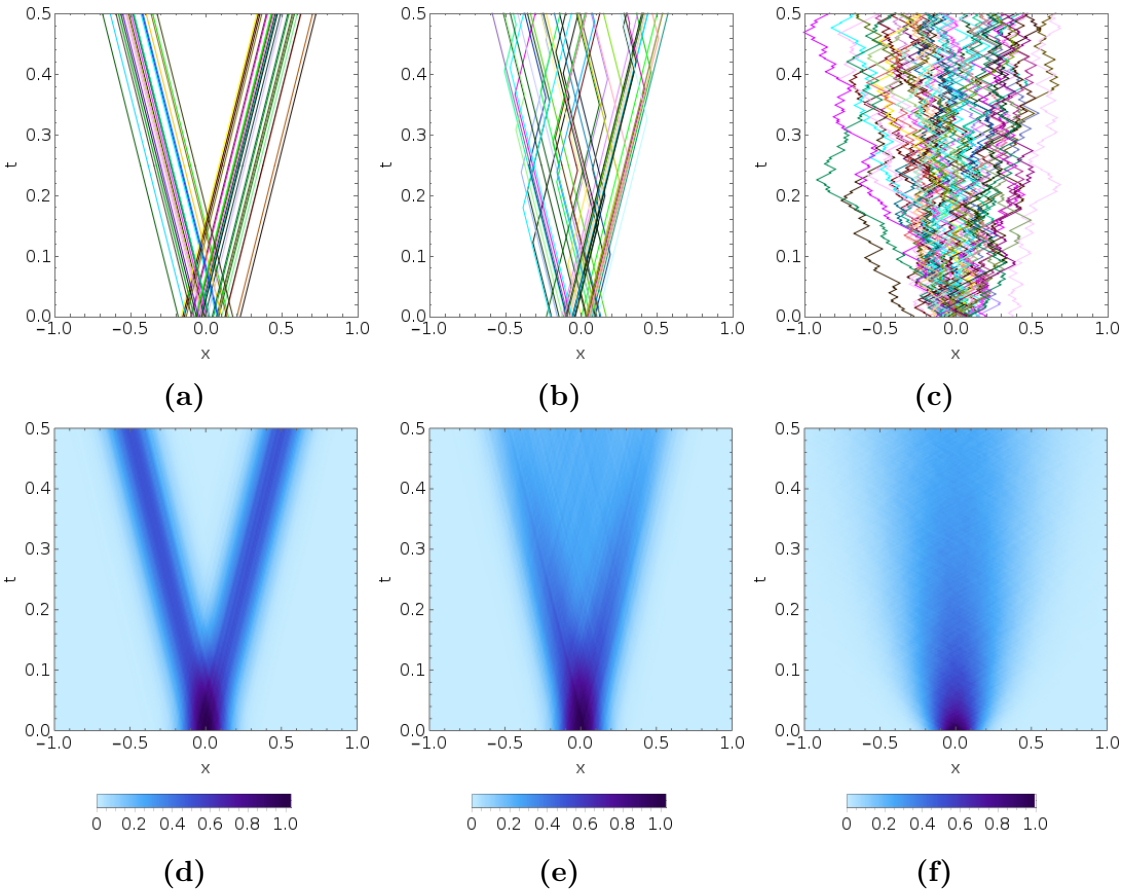

Figure 2.5: The random characteristics (top row) and the corresponding solutions (bottom row) used to solve the wave equation (left), telegrapher's equation (center), and heat equation (right).

the telegrapher's equation reads

$$\partial_t f + a\partial_x f = -\frac{b}{2}(f+g) \tag{2.45}$$

$$\partial_t g - a\partial_x g = -\frac{b}{2}(f+g)\,. \tag{2.46}$$

Already f and g appear related to two species travelling with velocities $\pm a$ (the left hand sides have the form of advections) and interacting with strength proportional to b (the right hand sides represent interactions). We can make contact with transport theory by introducing the velocity coordinate v and the 'distribution function' $h(x,v,t)$ which we postulate to be of the form $h(x,v,t) = f(x,t)\delta(v-a) + g(x,t)\delta(v+a)$, intuitively representing a density of particles f with velocity a and g with a velocity $-a$. The first order system is now equivalent to a single

transport equation for $h(x, v, t)$,

$$\partial_t h + v\partial_x h = \int k(v, v')h(x, v', t)\,\mathrm{d}v', \tag{2.47}$$

where the kernel $k(v, v')$ is given by $\frac{b}{2}(\delta(v - v') + \delta(v + v'))$. The equivalence with the first order system is simply shown by substituting $h = f\delta(v - a) + g\delta(v + a)$ and equating the coefficients of $\delta(v \pm a)$. This equation has the prototypical form of a transport equation, the operator $\partial_t + v\partial_x$ on the left giving free transport in (x, v) space and the integral on the right hand side giving interaction between particles with different velocities in terms of the kernel $k(v, v')$. In fact the $\delta(v - v')$ term in k represents self interaction among particles with the same velocity, giving rise to damping, while the $\delta(v + v')$ term couples particles with opposite velocities, allowing a disturbance initially propagating to the right to develop a left-going component for example, and so the form of k reflects known physical differences between the telegrapher's equation and the wave equation. The key point here was the assumption that h is concentrated at only two velocities $\pm a$; a general transport equation allows $h(x, v, t)$ to be spread across all velocities.

2.3 Summary

In this chapter I have presented essential methods for the study of waves. The Fourier transform was presented along with methods for handling the delta functions and principal value functions that arise when solving wave equations. The Laplace transform was discussed as the field generated by the mode distribution function, allowing its understanding in terms of the Pólya fields associated with complex functions. The method of characteristics, a means of solving wave equations along rays, was described and examples given. The method of random characteristics was presented as a generalization in which the characteristics are allowed to undergo collisions, and a link with transport equations formed. The Fourier transform and method of characteristics form the building blocks for the wavepacket methods developed in the next two chapters.

3 Wavepackets

3.1 Introduction

The description of a wave field in terms of localized wavepackets as opposed to sine waves infinite in extent has a number of intuitive and technical advantages, the exposition of which is the primary purpose of this chapter. The underlying theme is that both physical systems and our descriptions of them naturally display time-varying frequency spectra and their spatial analogues, but despite the almost irresistable intuitive appeal of these concepts they do not sit naturally within a framework based on infinite, periodic waves. In short, our intuitive notion of frequency is not exhausted by its formalization in the Fourier transform. I begin by introducing and illustrating the use of wavepackets by contrast with the Fourier transform, before going on to describe the way in which wavepackets most productively generalize the Fourier transform's happy interaction with differential equations, namely through symbol calculi.

3.2 Time-frequency analysis

By way of introduction we go straight to the founders of two parallel but closely related threads extending the Fourier transform, these two being Gabor and Ville. In a remarkable paper Gabor proposed a very useful extension of the Fourier transform

and introduced a number of concepts of information theory [49]. Gabor makes a strong case for a joint time-frequency description when discussing Fourier's theorem:

> Though mathematically this theorem is above reproach, even experts could not at times conceal an uneasy feeling when it came to the physical interpretation of the results obtained by the Fourier method. After having for the first time obtained the spectrum of a frequency-modulated sine wave, Carson wrote: "The foregoing solutions, though unquestionably mathematically correct, are somewhat difficult to reconcile with our physical intuitions, and our physical concepts of such 'variable frequency' mechanisms as, for example, the siren." The reason is that the Fourier-integral method considers phenomena in an infinite interval, *sub specie aeternitatis*, and this is very far from our everyday point of view. Fourier's theorem makes of description in time and description in spectrum, two mutually exclusive methods. If the term "frequency" is used in the strict mathematical sense which applies only to infinite wave trains, a "changing frequency" becomes a contradiction in terms, as it is a statement involving *both* time and frequency.

The spectrum of the frequency-modulated sine wave is essentially the one discussed in the next chapter which represents the frequency-modulated sine wave as a sum of a carrier and a series of sidebands. Ville in a paper on the analytic signal [50], [51] makes use of a now very popular illustration in terms of music:

> If we consider a fragment [of music] containing many components (which is the least that one should ask) and one note, *la* for example, appears once in the fragment, the harmonic analysis will present us with the amplitude and phase of the corresponding frequency, without locating the time point of the *la*. And yet, it is obvious that in the course of the fragment there will be instants in which the *la* will not be heard. Nevertheless, the representation is mathematically correct, because the phase of the notes near *la* acts to destroy this note by interference when *la* is not heard, and to reinforce it, also by interference, when it is heard; but if there exists in this concept a cleverness which does justice to mathematical analysis, there is also a distortion of reality; in fact, when *la* is not heard, the true reason is that *la is not emitted*.

Ville's distinction between the delicate cancellation by interference and the true reason for our not hearing a sound separates the global and local methods for the study of waves presented in Chapter 2, since the method of characteristics allows us to determine what we hear by tracing back along the characteristics passing

through our present location; we will receive no signal if no sources acted along these characteristics (and there was no free radiation at $t = -\infty$).

In response to these counter-intuitive features of the Fourier transform, a number of time-frequency distributions have been defined, functions which depend on both time and frequency and which roughly speaking are large at times where a particular frequency is present in the signal, providing a description analogous to a musical score [52] rather than a single global description of all frequencies present at any time in a piece of music. These definitions apply just as well to position and wavevector, where rather than notes with different frequencies being played at different times we might think of pulses with different wavelengths centered at different positions. In general a space such as the time-frequency plane or the position-wavevector plane which combines Fourier conjugate coordinates is called a phase space [53], [54]. While Ville is associated with the time-frequency distribution known as the Wigner (or sometimes Wigner-Ville) function [55], Gabor is associated with a time frequency distribution called the windowed Fourier transform [56]. A key difference between the two is that the windowed Fourier transform depends linearly on the field, while the Wigner function depends nonlinearly on the field, leading to some subtle features [57] and "dangerous cross terms" [58]. The Wigner function is closely related to the correlation function type quantities we discuss in Chapter 5 on coherence; we employ the windowed Fourier transform and the related coherent state distribution as our phase space representation. To illustrate the information rendered visible by phase space distributions, Figure 3.1 shows the fields and phase space representations of three functions which all have constant power spectra; a delta function, white noise, and an Airy function. While their power spectra look identical, their phase space representations reflect their radically different behaviors.

3.3 The windowed Fourier transform

The phase space distribution we will use is the coherent state distribution [59]–[61], which is based on the windowed Fourier transform [49], [56]. While the Fourier transform represents a given field as a sum of sine waves of various wavelengths, the

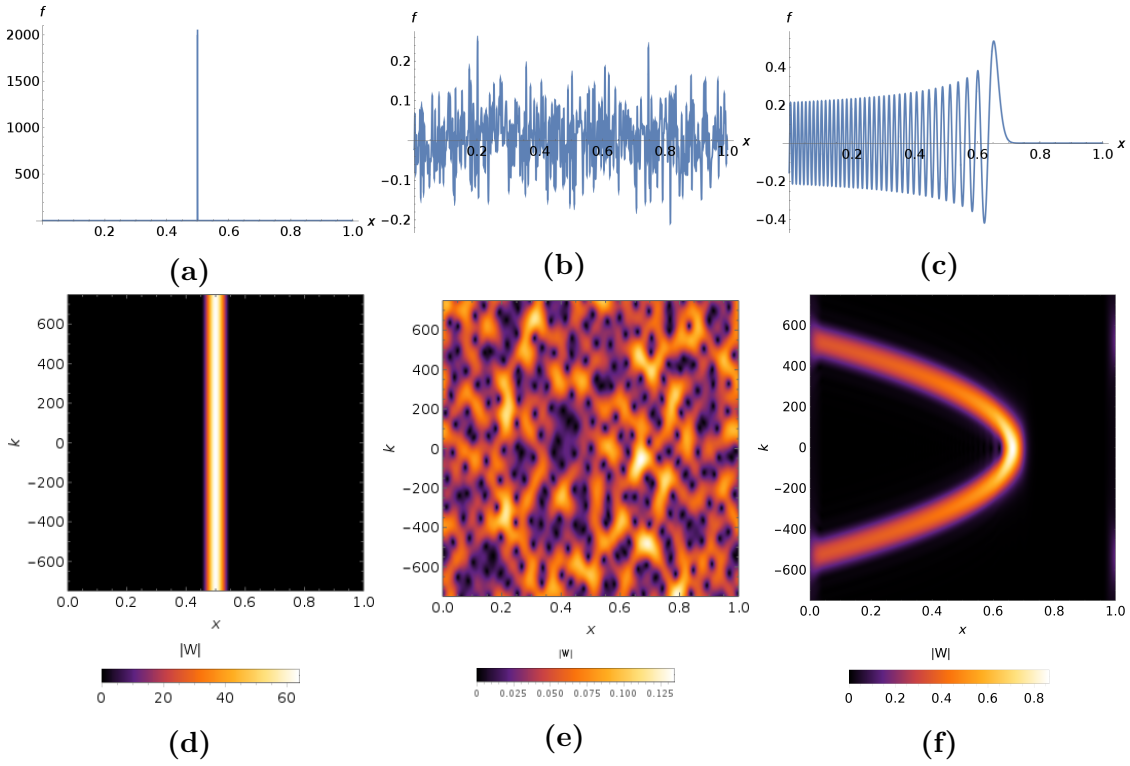

Figure 3.1: Examples of three functions, a delta function (a), white noise (b), and an Airy function (c) and their windowed Fourier transforms (bottom row). All three functions have constant power spectra; the variation of the phase of their Fourier transform leads to radically different behaviors which are reflected in their windowed Fourier transforms.

windowed Fourier transform represents a given field as a sum of wavepackets with various positions and wavelengths. We will use Gaussian wavepackets $f_{xk}(s)$ of the form

$$f_{xk}(s) = (\pi\sigma)^{-\frac{1}{4}} e^{\frac{-(s-x)^2}{2\sigma}} e^{ik(s-x)}, \tag{3.1}$$

so $f_{xk}(s)$ is a wavepacket centered at position x with wavevector k. Here s is the argument of the function f_{xk}, while x and k are labels specifying the wavepacket in question. The parameter σ determines the width of the wavepackets, and has dimensions of [Length]^2. The windowed Fourier transform $W(x,k)$ of a function g is defined [56] as the inner product of the wavepacket f_{xk} and g,

$$W(x,k) = \int_{-\infty}^{\infty} \overline{f_{xk}(s)} g(s)\, \mathrm{d}s. \tag{3.2}$$

The windowed Fourier transform $W(x,k)$ of a function g is a complex quantity, intuitively telling us the amplitude of the wavepacket f_{xk} needed to make up g. Such

an interpretation is justified given the inverse formula [56] for g in terms of $W(x,k)$,

$$g(s) = \frac{1}{2\pi} \iint_{-\infty}^{\infty} W(x,k) f_{xk}(s) \, \mathrm{d}x \, \mathrm{d}k, \tag{3.3}$$

where intuitively we are writing g as a sum of the wavepackets f_{xk}. Figure 3.2 shows an example of a function together with the absolute value and phase of its windowed Fourier transform. The diagonal line in the phase plot (c) results from the competing phases of the two wavepackets in (a), leading to a line of dislocations as discussed in Chapter 5.

The decomposition of a function into wavepackets using the windowed Fourier transform appears closely analogous to the decomposition using an orthogonal basis; we calculate the components by simply taking the inner product with the f_{xk}, and reconstruct the function by adding up the f_{xk} multiplied by the appropriate components. This analogy is surprising in that, unlike an orthogonal basis, the wavepackets f_{xk} are certainly not orthogonal, although their overlap decreases as their labels x and k become more distant, and they are not linearly independent as a basis must be (we can write one f_{xk} as a sum of all the others). In fact this sort of 'overcomplete basis', called a frame, is useful even in finite-dimensional settings. For example in describing crystals with atoms arranged in hexagons it is convenient to use three 'basis vectors' in the plane of the hexagons, rather than the two we could actually have in a basis in the plane. Figure 3.3 shows a basis in the plane (a) together with a frame of three vectors (b) and (c), all in black, along with the components (in blue) of a given vector (in red). While there is a unique set of components (b) with respect to the basis (this being the defining property of a basis [62]), with the frame we can find many different components since the frame is linearly dependent; two such sets are shown in (b) and (c). However there is a unique set of smallest components (which have the smallest summed squares of their lengths), the components we naturally use in describing the hexagonal crystal for example. Calling the frame vectors in Figure 3.3 $\mathbf{f}_1$, $\mathbf{f}_2$, and $\mathbf{f}_3$, it seems perverse to write $2\mathbf{f}_1 + \mathbf{f}_2$ as $102\mathbf{f}_1 + 101\mathbf{f}_2 + 100\mathbf{f}_3$ although they are perfectly equal. Analogously in infinite dimensions the Fourier transform uses a basis of complex exponentials

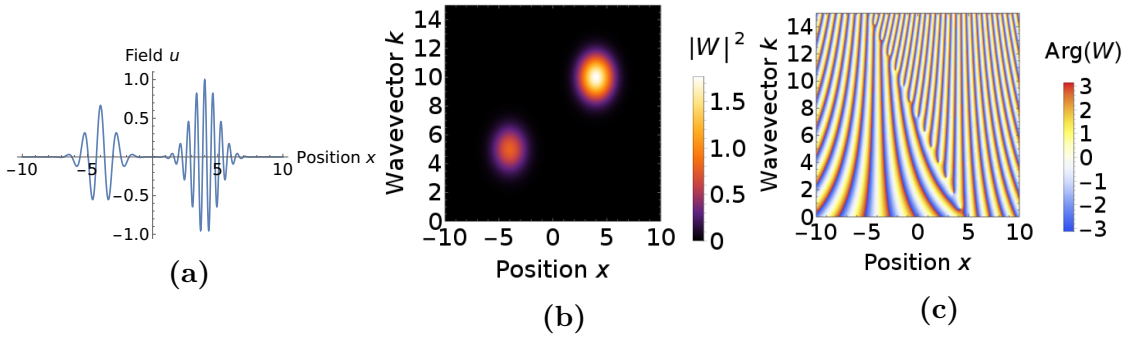

Figure 3.2: An example of a function (a) and the modulus (b) and phase (c) of its windowed Fourier transform. The windowed Fourier transform gives information on both position and wavevector. It is a complex quantity, allowing it to encode the phase of each wavepacket making up a given function.

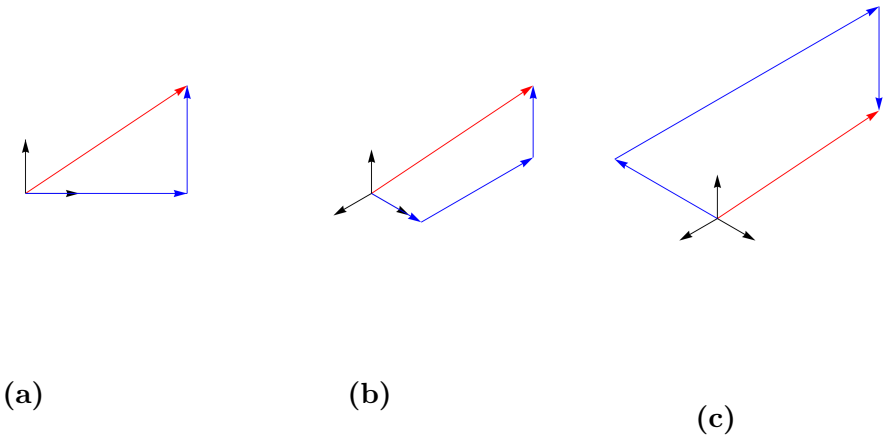

Figure 3.3: The decomposition of a vector $\vec{v}$ (in red) with respect to a basis (a) and a frame (b) and (c). The components (blue) with respect to the basis are unique, while the components with respect to the frame are not, two sets being shown in (b) and (c). However despite the frame being linearly dependent there is a unique smallest set of components, those shown in (b).

e_k, while the windowed Fourier transform uses a frame f_{xk} of wavepackets; while there are many ways to write a function g as a sum of the wavepackets f_{xk}, the windowed Fourier transform has the smallest norm. In fact this minimal property gives the windowed Fourier transform useful robustness properties [56].

3.4 Complex phase space and coherent states

Using a complex phase space with a single complex coordinate $z = x + i\sigma k$ as our position-wavevector phase space allows us to derive simple equations for our phase space distribution by exploiting its analytic properties. Here σ is the window-

width parameter from the definition of the wavepackets f_{xk}; σ has dimensions of [Length]^2, so both x and σk have the dimensions of [Length]. If we use certain rescaled versions of our wavepackets f_{xk}, called coherent states [59], [60], we can derive simple equations using the Wirtinger derivatives $\partial_{\overline{z}} = \frac{1}{2}(\partial_x + (i/\sigma)\partial_k)$ and $\partial_z = \frac{1}{2}(\partial_x - (i/\sigma)\partial_k)$ which are naturally associated with the complex phase space [63]–[65]. The Cauchy-Riemann equations for f to be a holomorphic function of z can be written simply as $\partial_{\overline{z}} f = 0$. The complex structure here is physically natural since in taking the geometrical optics limit of wave equations we obtain ray-tracing equations with a Hamiltonian structure [66], and Hamiltonian structure is intimately tied to complex structure [67]. Here the complex structure reflects not just the Hamiltonian structure of geometrical optics but also the structure of the exact phase space equations through the Wirtinger derivatives and Wick symbol product.

The phase space equations take on a physically transparent form when written in terms of rescaled wavepackets called coherent states ϕ_z, defined in terms of the complex coordinate $z = x + i\sigma k$ as

$$\phi_z(s) = (\pi\sigma)^{-\frac{1}{4}} e^{-\frac{1}{2\sigma}(s^2 - 2sz + \frac{z^2}{2})}. \tag{3.4}$$

Here z is a label for the coherent state, combining the labels x and k into a single complex label, while s is the argument of ϕ_z. Using the fact that $z = x + i\sigma k$ we find that the coherent states ϕ_z and the wavepackets f_{xk} are related according to

$$\phi_z(s) = e^{-\frac{x^2 + \sigma^2 k^2}{4\sigma}} e^{\frac{ixk}{2}} f_{xk}(s), \tag{3.5}$$

so the coherent states ϕ_z are indeed rescaled versions of the Gaussian wavepackets f_{xk}. A number of useful identities involving the coherent states follow from the integral

$$\int_{-\infty}^{\infty} \phi_w(s)\phi_z(s)\,\mathrm{d}s = e^{\frac{wz}{2\sigma}}, \tag{3.6}$$

where z and w are complex numbers labeling the coherent states. From this it follows that the inner product of two coherent states is given by $\phi_w^\dagger \phi_z = e^{\overline{w}z/2\sigma}$, that the squared norm of a coherent state is $|\phi_z|^2 = \phi_z^\dagger \phi_z = e^{\overline{z}z/2\sigma}$, and that the inner product of the Gaussian ϕ_0 with any coherent state is $\phi_0^\dagger \phi_z = 1$.

Just as we can expand any function in terms of the wavepackets f_{xk}, we can also expand any function in terms of coherent states ϕ_z. This is reflected in a formula expressing the identity operator I as a sum of weighted projections onto coherent states. This resolution of the identity is given by

$$I = \frac{i}{4\pi\sigma} \int \mathrm{d}z\, \mathrm{d}\overline{z}\, e^{\frac{-\overline{z}z}{2\sigma}} \phi_z \otimes \phi_z^\dagger. \tag{3.7}$$

Here the $\otimes$ is the tensor product; while ϕ_z is a function, $\phi_z \otimes \phi_z^\dagger$ is an operator (which would be written $|\phi_z\rangle\langle\phi_z|$ in bra-ket notation). The integral is an area integral over the complex plane, where here $\mathrm{d}z\,\mathrm{d}\overline{z}$ is defined in terms of the real and imaginary parts x and k of z as $\mathrm{d}z\,\mathrm{d}\overline{z} = -2i\sigma \mathrm{d}x\,\mathrm{d}k$. Here this is just a notation for an area integral, but the definition was chosen because it is the wedge product $\mathrm{d}z \wedge \mathrm{d}\overline{z}$ for $z = x + i\sigma k$ [68].

3.4.1 Wick symbols of operators

A symbol is a function on phase space associated with a given operator [53]. The concept of a symbol generalizes for example the association between the derivative operator ∂_x and the function ik encountered when using the Fourier transform, or the association between the phase space function p and the operator $-i\partial_x$ encountered when quantizing a classical system. The association between operators such as the derivative and algebraic quantities has a long history, for example Heaviside's operational calculus and 'algebraization' of differential operators [69], [70], which has been formalized using the Laplace transform, and the development of fractional derivatives and integrals [71]. The use of symbols allows us to generalize and extend the common two-step process of studying waves by i) considering a uniform medium, substituting derivatives with $-ik$ and $i\omega$, and finding a dispersion relation and ii) using this (initially global) dispersion relation to treat waves in a nonuniform medium using some sort of eikonal approximation [72]. Using symbols we can treat non-uniform media from the outset, working at once in a space with position and wavevector coordinates, and in so doing avoid some of the divergences associated with geometrical optics and the eikonal approximation which are artifacts of projecting

from phase space into real space [73]. We can also treat cases in which the background medium varies on a scale shorter than the wavelength of the waves, and in which the separation of the two steps is no longer effective and the eikonal approximation breaks down since multiple wavelengths are present at each point in space.

A symbol calculus is a rule for associating operators with their symbols together with a formula for the symbol of the composition of two operators in terms of each of their symbols. This product formula allows us to build up phase space equations from simple components. The product formula of a symbol calculus generalizes the convolution theorem for the Fourier transform. A symbol calculus known as the Weyl symbol calculus, which is naturally associated with the Wigner function, has been widely used in the phase space representation of wave equations [73]–[75]. Here we use the Wick symbol calculus as developed by Berezin [76], [77], which uses the coherent states to associate an operator with a phase space function, its Wick symbol.

With the coherent states ϕ_z in hand the Wick symbol $\mathcal{S}(A)(w,z)$ of an operator A is defined as

$$\mathcal{S}(A)(w,z) = \frac{\phi_w^\dagger A \phi_z}{\phi_w^\dagger \phi_z}, \tag{3.8}$$

an expression which has the form of a 'wavepacket matrix element'. Here the Wick symbol $\mathcal{S}(A)(w,z)$ depends on the two phase space points w and z (each of which encode a real position and wavevector); we obtain a true function on phase space by setting $w = \overline{z}$ to obtain

$$\mathcal{S}(A)(\overline{z},z) = \frac{\phi_z^\dagger A \phi_z}{\phi_z^\dagger \phi_z}. \tag{3.9}$$

For example to calculate the symbol of the second derivative operator we take $A = \partial_x^2$ in equation 3.8. The denominator $\phi_w^\dagger \phi_z$ is exactly the integral in equation 3.6; it is a Gaussian integral which gives $\exp(\frac{wz}{2\sigma})$. Looking at the numerator $\phi_w^\dagger \partial_x^2 \phi_z$, calculating the second derivative we find

$$\partial_x^2 \phi_z(x) = \left(\frac{(x-z)^2 - \sigma}{\sigma^2} \right) \phi_z(x), \tag{3.10}$$

and so the integral for the numerator is a Gaussian integral which can be evaluated to give

$$\phi_{\overline{w}}^{\dagger}\partial_x^2\phi_z = \int_{-\infty}^{\infty} \phi_w(x)\partial_x^2\phi_z(x)\,\mathrm{d}x \tag{3.11}$$

$$= \int_{-\infty}^{\infty} \left(\frac{(x-z)^2-\sigma}{\sigma^2}\right)\phi_w(x)\phi_z(x)\,\mathrm{d}x \tag{3.12}$$

$$= e^{\frac{wz}{2\sigma}}\left(\frac{(w-z)^2}{4\sigma^2}-\frac{1}{2\sigma}\right). \tag{3.13}$$

Combining the numerator and denominator, upon setting $z = x + i\sigma k$ and $w = \overline{z} = x - i\sigma k$ we obtain the symbol $-k^2 - \frac{1}{2\sigma}$ for the second derivative operator.

Table 3.1 shows a table of useful Wick symbols. The symbol of the derivative operator ∂_x is $\mathcal{S}(\partial_x)(w,z) = \frac{z-w}{2\sigma}$, so $\mathcal{S}(\partial_x)(\overline{z},z) = \frac{z-\overline{z}}{2\sigma} = ik$, since $z = x + i\sigma k$. This is in analogy with the Fourier transform, since taking the derivative of a function multiplies its Fourier transform by ik. The symbol of the second derivative operator ∂_x^2 is $-k^2 - \frac{1}{2\sigma}$, which is the $-k^2$ we might expect by analogy with the Fourier transform plus a term which vanishes as $\sigma \to \infty$ (both k^2 and $\frac{1}{2\sigma}$ have dimensions of $1/[\text{Length}]^2$). The symbol ∂_x^n is always $(ik)^n$ plus terms which vanish as $\sigma \to \infty$. Likewise the symbols of multiplication by x and x^2 are given by $\mathcal{S}(x\cdot)(\overline{z},z) = x$ and $\mathcal{S}(x^2\cdot)(\overline{z},z) = x^2 + \frac{\sigma}{2}$. The $\frac{1}{2}$ terms in the symbols of ∂_x^2 and $x^2\cdot$ will give a simple treatment of phase shift at a caustic associated with the Maslov index in the next chapter.

The product formula for the Wick symbol calculus, giving the symbol of the composition $A \circ B$ of two operators A and B in terms of each of their symbols, can be derived inserting the resolution of the identity (3.7) between A and B in the definition of the Wick symbol of $A \circ B$. We define the symbol product $\odot$ by $\mathcal{S}(A) \odot \mathcal{S}(B) = \mathcal{S}(A \circ B)$; it will be our basic working tool for building up phase space equations. The symbol product is given by

$$\mathcal{S}(A) \odot \mathcal{S}(B)(w,z) = \frac{i}{4\pi\sigma}\int \mathrm{d}u\,\mathrm{d}\overline{u}\, e^{\frac{(w-\overline{u})(u-z)}{2\sigma}}\mathcal{S}(A)(w,u)\mathcal{S}(B)(\overline{u},z), \tag{3.14}$$

and in particular

$$\mathcal{S}(A) \odot \mathcal{S}(B)(\overline{z},z) = \frac{i}{4\pi\sigma}\int \mathrm{d}u\,\mathrm{d}\overline{u}\, e^{-\frac{|z-u|^2}{2\sigma}}\mathcal{S}(A)(\overline{z},u)\mathcal{S}(B)(\overline{u},z). \tag{3.15}$$

Operator A	**Definition** $Af(x)$	**Wick Symbol** $\mathcal{S}(A)$
Derivative	$\partial_x f(x)$	ik
Second derivative	$\partial_x^2 f(x)$	$-k^2 - \frac{1}{2\sigma}$
Multiplication by x	$xf(x)$	x
Multiplication by x^2	$x^2 f(x)$	$x^2 + \frac{\sigma}{2}$
Multiplication by e^{iax}	$e^{iax} f(x)$	$e^{\frac{-\sigma a^2}{4}} e^{iax}$
Convolution with e^{-x^2/a^2}	$\int_{-\infty}^{\infty} e^{-(x-y)^2/a^2} f(y)\,\mathrm{d}y$	$2\sqrt{\frac{\pi a^2 \sigma}{a^2+4\sigma}} e^{\frac{-a^2\sigma k^2}{a^2+4\sigma}}$
Integration	$\int_{-\infty}^{\infty} f(x)\,\mathrm{d}x$	$2\sqrt{\pi\sigma} e^{-\sigma k^2}$
Fourier transform ($\sigma = 1$)	$\frac{1}{\sqrt{2\pi}} \int_{-\infty}^{\infty} f(y) e^{-ixy}\,\mathrm{d}y$	$e^{\frac{-(1+i)(x^2+k^2)}{2}}$

Table 3.1: A table of Wick symbols of some common operators. Many of the symbols show analogies with properties of the Fourier transform.

The product formula for $\mathcal{S}(A) \odot \mathcal{S}(B)$ has an asymptotic expansion [77] which is useful when one of the symbols in the product is slowly varying. Intuitively it exploits the factor $e^{\frac{-|z-u|^2}{2\sigma}}$ in the product formula, which acts to localize the integral in the u plane to regions around z, and so we might try to estimate the integral in the product formula purely in terms of the behavior of the integrand near z. The asymptotic expansion of the product formula does just that, and is given by

$$\mathcal{S}(A) \odot \mathcal{S}(B)(\overline{z}, z) \sim \sum_r \frac{2^r \sigma^r}{r!} \partial_z^r \mathcal{S}(A)(\overline{z}, z)\, \partial_{\overline{z}}^r \mathcal{S}(B)(\overline{z}, z) \tag{3.16}$$

$$= \mathcal{S}(A)\mathcal{S}(B) + 2\sigma \partial_z \mathcal{S}(A)\, \partial_{\overline{z}} \mathcal{S}(B) + \ldots \tag{3.17}$$

where the arguments $\overline{z}$, z have been left implicit in the last line. It can be derived by Taylor expanding the symbol $\mathcal{S}(A)$ in u about z and $\mathcal{S}(B)$ in $\overline{u}$ about $\overline{z}$ and carrying out the Gaussian integrals; terms in unequal powers of $u - z$ and $\overline{u} - \overline{z}$ give zero by parity. It initially appears that the rth term in the expansion is of order σ^r, but in fact the derivatives $\partial_{\overline{z}}$ and ∂_z can introduce powers of σ; for example if A and B are both the derivative operator ∂_x then the asymptotic expansion reproduces the symbol

of the second derivative operator $-k^2 - \frac{1}{2\sigma}$ with the $r = 0$ term, k^2, independent of σ and the $r = 1$ term, $\frac{1}{2\sigma}$, of order σ^{-1}. The asymptotic expansion of the product formula is our general purpose tool for short wavelength approximations to treat phenomena such as refraction, photon acceleration, and ponderomotive forces.

3.4.2 Relation to the windowed Fourier transform

The windowed Fourier transform of a function f is related to the symbol S of the operator $f \otimes \phi_0^\dagger$ (we will often abbreviate this operator as $f\phi_0^\dagger$, in bra-ket notation it would be written as $|f\rangle\langle\phi_0|$) according to

$$W(x,k) = e^{\frac{|z|^2}{4\sigma}} e^{\frac{ikx}{2}} S(\overline{z}, z), \tag{3.18}$$

where $z = x + i\sigma k$. This means that we can convert between the windowed Fourier transform and the symbol S simply by multiplying by $e^{\frac{x^2+\sigma^2k^2}{4\sigma}} e^{\frac{ikx}{2}}$. S will be our primary phase space distribution, and has the advantages of satisfying physically transparent equations and being directly related to the windowed Fourier transform which is easy to interpret. From the definition of S we see that it is $\phi_z^\dagger f$, an analytic function of $\overline{z}$, multiplied by a factor $e^{-\frac{\overline{z}z}{2\sigma}}$ which comes from the denominator of equation 3.9, that is $S = e^{-\frac{\overline{z}z}{2\sigma}} F$ where F is an analytic function of $\overline{z}$ which is known as the Bargmann representation of f [78].

The symbol of the operation $f\cdot$ of pointwise multiplication by a function f will be very useful for representing the effect of a background or another field on the waves represented by S, and is equal to a function, independent of f, depending only on w and z multiplied by the windowed Fourier transform of f with a width parameter $\sigma/2$. This is due to a product identity for coherent states,

$$\phi_w^\sigma \phi_z^\sigma = \frac{1}{(2\pi\sigma)^{\frac{1}{4}}} e^{\frac{-(w-z)^2}{8\sigma}} \phi_{(w+z)/2}^{\sigma/2} \tag{3.19}$$

where we have temporarily denoted the coherent state z with window parameter σ as ϕ_z^σ. For a given f the symbol of multiplication by f can be calculated explicitly, for example the symbol of multiplication by e^{iax} is $M_a(w,z) = e^{\frac{-\sigma a^2}{4}} e^{\frac{ia(w+z)}{2}}$. For $w = \overline{z}$ the product identity implies that the symbol of multiplication by f is simply f

smoothed by a Gaussian, as can be verified for $M_a(\overline{z}, z) = e^{\frac{-\sigma a^2}{4}} e^{iax}$. In this way the calculus naturally includes smoothed quantities where required. A further example of this smoothing is that the symbol of convolution with f is the Fourier transform of f smoothed by a Gaussian, as Table 3.1 shows for convolution with a Gaussian.

Products of functions fg frequently arise as couplings in wave equations and give rise to the symbol product $\mathcal{S}(f\cdot) \odot \mathcal{S}(g\phi_0^\dagger)$ (Chapter 4). This product would be treated with the convolution theorem using the Fourier transform, giving a sum over the combinations of wavevectors in f and g. The generalization of the convolution theorem by the symbol product is illustrated by two results, which can be derived either by directly carrying out the integration in the product formula or by using the operator identity $(f\cdot) \circ g\phi_0^\dagger = (fg)\phi_0^\dagger$. If both f and g are complex exponentials, writing M_a for the symbol of multiplication by e^{iax} and H_b for the symbol of $e^{ibx}\phi_0^\dagger$ we have $M_a \odot H_b = H_{a+b}$, which gives rise to the sums of wavevectors from the convolution theorem for the Fourier transform. If both f and g are Gaussian wavepackets with positions x_1 and x_2 and wavevectors k_1 and k_2 respectively, then $\mathcal{S}(f\cdot) \odot \mathcal{S}(g\phi_0^\dagger)$ is (after multiplying by $e^{\frac{|z|^2}{4\sigma}} e^{\frac{ikx}{2}}$ to get the effect of the coupling on the windowed Fourier transform) a Gaussian centered at wavevector $k = k_1 + k_2$, the sum of the two wavevectors, and position $x = \frac{x_1+x_2}{2}$, the average of the two positions, with an amplitude depending on $e^{\frac{-(x_1-x_2)^2}{c}}$ (where c is a constant related to σ) and so decaying rapidly with the distance between the wavepackets. In this way the product term gives a coupling nonlocal in wavevector but still localized in position, and so physically waves are only affected by the part of the medium they are propagating in.

3.4.3 Extension to several variables

The theory presented above generalizes to cover functions of several variables in a straightforward way using products of single variable coherent states [53], [77]. In particular to analyze functions of two variables x and t we use wavepackets $f_{xkt\omega}$ which are now wavepackets localized in space-time formed from products of the one-dimensional wavepackets above with widths σ_x and σ_t. The phase space now has two complex coordinates which it is convenient to label as $\tau = t + i\sigma_t\omega$ and

$\chi = x + i\sigma_x k$. The coherent states and Wick symbols are defined as before, and the resolution of the identity and Wick symbol product formula go through similarly [77].

3.4.4 Interpretation of the equation for the Wick symbol

If u is a field satisfying a wave equation, the equation of motion for the Wick symbol S of $u\phi_0^\dagger$ immediately displays the group velocity v_g of the waves along with the rates of change of frequency v_ω and wavevector v_k and the dispersion relation D (where the actual dispersion relation is given by $D = 0$). In fact the equation of motion for the Wick symbol takes the form, in terms of the complex velocities $v_\tau = 1 - i\sigma_t v_\omega$ and $v_\chi = v_g - i\sigma_x v_k$,

$$v_\tau \partial_{\overline{\tau}} S + v_\chi \partial_{\overline{\chi}} S + iDS = 0. \tag{3.20}$$

This equation is in the form of a complex advection equation, with a source term iDS proportional to the dispersion relation which drives rapid oscillations in regions of phase space away from the dispersion surface. In case of nonlocal effects in phase space the equation gains an integral source term on the right hand side. In cases which give rise to damping D becomes complex and leads to the damping of the phase space distribution; this occurs without introducing imaginary frequencies. The reason the equation can be interpreted in this way is that due to the analytic properties of S it can be solved along complex characteristics, as will be discussed in Chapter 4. The physically transparent form of the equation of motion is a further reason for the use of the complex phase space along with the Wick symbol and Wirtinger derivatives $\partial_{\overline{\tau}}$ and $\partial_{\overline{\chi}}$.

3.5 Summary

In this chapter I have presented tools for working with wavepackets. The windowed Fourier transform was presented as a phase space distribution which encodes information on the position, wavevector and phase of the wavepackets making up a field. A complex phase space combining the position x and wavevector k into a single complex coordinate $z = x + i\sigma k$ was introduced, and coherent states labelled

by z were introduced as rescaled wavepackets with useful analytic properties. In terms of the coherent states the Wick symbol of an operator was defined as a wavepacket matrix element, associating the operator with a function on the complex phase space. The relationship between the windowed Fourier transform of a function f and the Wick symbol of some operators related to f was given, and the Wick symbols of some operators useful for the treatment of wave equations were presented in preparation for the next chapter. Finally the form of the equation for the Wick symbol of the operator $u\phi_0^\dagger$ as a complex advection equation was discussed, the derivation and extension of which will be taken up in the next chapter.

4

Phase space representation of wave equations

The phase space representation of a wave equation is an equation of motion for the wave field's distribution in position, wavevector and frequency. It has been applied, for example, in condensed matter to describe thermal conduction as the propagation of phonons in a temperature gradient [79], in the statistical description of waves in a turbulent plasma [80], [81], and in the (non-statistical) description of classical wave propagation and geometrical optics [72], [73], [75], [80]. Having chosen a particular phase space representation of the physical fields (for example the Wigner [55], [57], [58], wavelet [82], [83] or coherent state [49], [60] distributions), beginning with wave equations describing the system we can derive equations describing the evolution of the phase space distribution [73]. Here it has been found useful to proceed indirectly by rewriting the classical field equations as equivalent operator equations in order to make use of powerful mathematical tools known as symbol calculi, of which the Wick symbol calculus presented in Chapter 3 is one example, which associate operators and functions on phase space [53]. For example when using the Wigner function as the phase space distribution, this method generalizes the case familiar from quantum mechanics in which the Schrödinger equation for the wave function is rewritten as the Von Neumann equation for the density operator, which

in turn is rewritten using the Weyl symbol calculus [53], [84] as the Wigner-Moyal equation for the Wigner function [85].

Reference [73] systematically derives phase space representations for wave equations using the Weyl symbol calculus, using both the Wigner function and coherent state distribution as phase space distributions. In addition, reference [86] contains a wealth of information on wavepacket methods including material on coherent states. Gaussian wavepackets have been widely used to study the semiclassical approximation of the Schrödinger equation [87]–[89] and many of the techniques and intuitions developed apply to other wave equations [90]. Coherent states have been used to derive uniform semiclassical approximations of wave equations from a phase space path integral [91], [92], and the Bargmann representation [78] (equal up to a factor to the coherent state distribution) has been applied to develop uniform phase space WKB methods [93], [94]. Wave kinetic equations describing the evolution of a distribution of waves in position and wavevector are widely employed [22], [79], [81], [95]–[97] and have been studied using the Wigner function [98]–[100] along with the Weyl symbol calculus [73]–[75] as well as the windowed Fourier transform [101]–[103]. Quasiparticle based numerical methods have been used to study wave propagation [104]–[106] and in plasma physics [107]–[114]. References [115]–[117] give detailed asymptotic analysis and physical interpretation for kinetic equations governing gravity waves, and in particular give as the essential distinction between an ensemble of particles and of wavepackets that "the energy transfer between a discrete set of wave groups depends not only on the momentum and position of the wave groups but also on their relative phases" [116], a property transparently encoded by the coherent state distribution. The case for a joint time-frequency perspective is made in, for example, [49], [50], [52], [56]. While it does not deal explicitly with phase space distributions, Synge's work on rays and waves provides very useful background and a powerful motivation for thinking in terms of wavepacket trajectories, [118]–[120] and in particular his letter on water waves and hydrons [121], see also [68], [122].

The Wick symbol calculus allows us to derive phase space representations of wave equations which bring physically intuitive concepts to the fore. Here we apply the method to five examples chosen to display physically interesting phenomena in a simple context. First of all an oscillator with varying frequency is studied in phase space, allowing a detailed presentation of the use of the exact product formula for rapidly varying phenomena and the asymptotic expansion of the product formula for slowly varying phenomena. Following this a model equation for wave propagation in a medium allows us to study the frequency and wavevector shifts resulting from a medium which varies in space and time, the harmonic generation which can result when the medium varies on a scale shorter than the wavelength of the waves, as well as the effect of sources and dispersion. We then treat the nonlinear Schrödinger equation to demonstrate how the method neatly handles group velocity, dispersion, nonlinear frequency shifts, and ponderomotive forces. Next we give an solution of a mode conversion problem by solving the corresponding complex phase space equation along rays. Finally the Vlasov equation is studied to illustrate how the Wick symbol method naturally treats kinetic frequency, the Fourier conjugate of velocity, and phase mixing, making contact with some modern developments in the study of Landau damping [123], [124].

For ease of reference we collect here some of our notations. Our convention for dealing with frequency ω and wavevector k is to use plane waves of the form $e^{i(kx+\omega t)}$, which removes some minus signs from the basic formulae of the Wick symbol calculus [53]. For functions and operators we use a notation [56] in which functions are written as f, corresponding to $|f\rangle$ in bra-ket notation, and dual vectors of functions are written as $f^\dagger$, corresponding to $\langle f|$. Operators of the form $f \otimes g^\dagger$, where $\otimes$ is the tensor product, will often be written simply as $fg^\dagger$, corresponding to $|f\rangle\langle g|$. The composition of two operators A and B will be written as $A \circ B$, the symbol of an operator A as $\mathcal{S}(A)$, and the symbol product as $\odot$, so the symbol $\mathcal{S}(A \circ B)$ is given by $\mathcal{S}(A) \odot \mathcal{S}(B)$.

4.1 Oscillator with varying frequency

In order to introduce the Wick symbol calculus method for deriving the phase space representation of a given differential equation, we look at the simple case of a first order oscillator with a varying frequency. First of all we consider an oscillator with a linearly increasing frequency, before treating an oscillator with an oscillating frequency as in frequency modulation and in the quote from Gabor in Chapter 3. These examples clearly demonstrate the sense in which the asymptotic expansion of the Wick symbol product formula treats locally varying frequencies, and illustrate the key methods which we will then use to study wave equations.

As the equation for an oscillator with a varying frequency we take the first order equation

$$\partial_t u - i\,(a + g(t))\,u = 0, \tag{4.1}$$

which as we will see describes an oscillator with frequency a which is being varied as $g(t)$. First order oscillators of this sort are in fact a very useful building block from which to make up more complicated equations. The (second order) harmonic oscillator equation can be written as a system of two uncoupled first order oscillator equations, one with positive and one with negative frequency. Further, this form of the equations is physically very helpful since if we weakly couple two harmonic oscillators, in this representation the positive frequency modes of each oscillator interact largely among themselves, and so too for the negative frequency modes, so the system of coupled harmonic oscillators may be treated approximately as two systems of coupled first order oscillators (this forms the basis of coupled mode theory [125]).

4.1.1 Linear chirp

Taking $g(t) = bt$ in the oscillator equation (4.1) we obtain the equation of motion

$$\partial_t u - i(a + bt)u = 0, \tag{4.2}$$

an equation readily solved to give the solution (with $u(0) = 1$)

$$u(t) = e^{i(at+\frac{b}{2}t^2)}. \tag{4.3}$$

This solution is an oscillation with frequency $a + bt$ varying linearly in time, that is a linear chirp, as can be verified by calculating the windowed Fourier transform directly or in this case by taking the derivative of the phase. In order to apply the Wick symbol calculus to derive the phase space representation of this equation, we first rewrite it as an operator equation equivalent to (4.2). Introducing the operator $u \otimes \phi_0^\dagger$ (which we will abbreviate as $u\phi_0^\dagger$) the symbol of which is related to the windowed Fourier transform of u as described in Chapter 3, the operator equation

$$\partial_t \circ u\phi_0^\dagger - iau\phi_0^\dagger - ibt \circ u\phi_0^\dagger = 0 \tag{4.4}$$

is equivalent to equation (4.2), in the sense that whenever one holds the other does. Here $\circ$ denotes the composition of operators, and the t in the last term on the right hand side stands for the operation of pointwise multiplication by t. We can show this equivalence by calculating the action of the operators in the equation on a given function f; an operator is zero if it gives zero when acting on all functions. In the bra-ket notation $u\phi_0^\dagger = |u\rangle\langle\phi_0|$ and we have post multiplied equation (4.2) by $\langle\phi_0|$. The second step is to take the symbol of the operators on each side of equation (4.2). Using the symbols of the derivative and multiplication operators from Chapter 3 and the fact that the symbol of the composition of two operators is the symbol product $\odot$ of their symbols, we obtain (in terms of $\tau = t + i\sigma\omega$)

$$\frac{\tau - \overline{\tau}}{2\sigma} \odot S - iaS - ib\frac{\tau + \overline{\tau}}{2} \odot S = 0, \tag{4.5}$$

where S is the symbol of $u\phi_0^\dagger$. Now calculating the symbol products, either directly or using the asymptotic expansion of the product which here terminates and is exact, we obtain as our phase space equation

$$(1 - i\sigma b)\partial_{\overline{\tau}} S + i(\omega - a - bt)S = 0. \tag{4.6}$$

One can verify that the phase space distribution S corresponding to the solution u satisfies this equation exactly. The form of this equation is a one dimensional

version of the form given in Chapter 3, with the complex velocity $1 - i\sigma b$ giving the correct rate of change of frequency b, and the local dispersion relation giving the correct relation $\omega = a + bt$. Although we defer full discussion until the section on mode conversion below, the reason these interpretations are possible is because the equation (4.6) can be solved exactly using the complex method of characteristics. By analogy with the real method of characteristics (Chapter 2) but using the complex variable $\overline{\tau} = t - i\sigma\omega$ instead of a real variable x, the values of S can be found along characteristic curves $\overline{T}(s)$, here complex, determined by the differential equation $\mathrm{d}\overline{T}/\mathrm{d}s = 1 - i\sigma b$. The characteristics are thus given by $\overline{T}(s) = s - i\sigma\left(\omega_0 + bs\right)$, where the characteristics are assumed to begin at $t = 0$ and ω_0 is the initial frequency of the characteristic. Looking at the real and imaginary parts of $\overline{T}(s)$, along a characteristic the time is s and the frequency is $\omega_0 + bs$. Considering the characteristic starting at $\omega_0 = a$ gives agreement with the interpretation in terms of the local dispersion relation. The fact that the phase space equation is local in phase space suggests that a phase space equation which has the form (4.6), even with coefficients in the complex velocity and local dispersion relation that depend on time and frequency, can be understood in terms of the local complex velocity and dispersion relation, as we will see in detail in the next section on an oscillator with oscillating frequency.

4.1.2 Oscillating frequency

Taking $g(t) = b\cos(ct)$ in equation (4.1) we have an oscillator with an oscillating frequency, exactly as in the quote from Gabor in Chapter 3. The equation of motion in this case is then

$$\partial_t u - i(a + b\cos(ct))u = 0, \tag{4.7}$$

whose solution with $u(0) = 1$ is

$$u(t) = e^{i(at + \frac{b}{c}\sin(ct))}. \tag{4.8}$$

Figure 4.1 shows the solution $u(t)$ along with its power spectrum and windowed

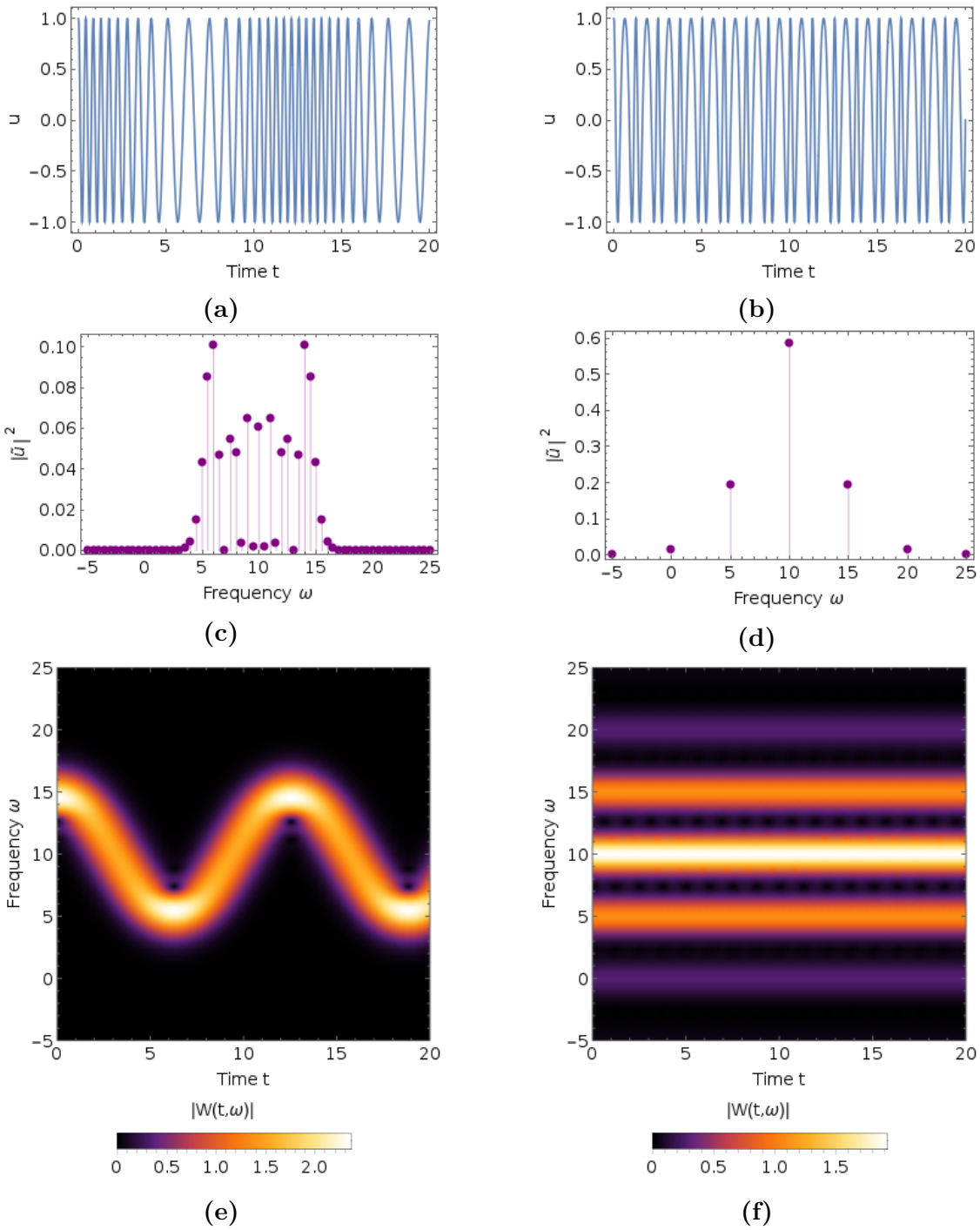

Figure 4.1: The displacement (top), power spectrum (middle), and windowed Fourier transform (bottom) of an oscillator whose frequency is varied slowly (a) and rapidly (b). The Wick symbol equation is satisfied exactly for both cases, including (b) which shows mode coupling nonlocal in phase space, but the asymptotic expansion of the symbol product and the resulting local behavior in phase space holds only for a slowly varying frequency (a).

Fourier transform for the cases in which the oscillator's frequency is varied slowly (a) and rapidly (b). The Wick symbol equation which will be derived is satisfied exactly in both cases. The asymptotic expansion of the product formula is only valid for a slowly varying frequency, in which case the distribution flows along complex characteristics, while for a rapidly varying frequency it can be coupled into sidebands non-locally in frequency by the exact integral form of the product formula.

Using a Bessel function identity we can expand u in harmonics,

$$u(t) = \sum_{n=-\infty}^{\infty} J_n(b/c) e^{i(a+nc)t}, \tag{4.9}$$

exhibiting u as the sum of the fundamental frequency a together with sidebands separated from a by multiples of c. Writing the $\cos(ct)$ as a sum of complex exponentials, we can write the equivalent operator equation as

$$\partial_t \circ u\phi_0^\dagger - iau\phi_0^\dagger - \frac{ib}{2}\left(e^{ict} \circ u\phi_0^\dagger + e^{-ict} \circ u\phi_0^\dagger\right) = 0, \tag{4.10}$$

which upon taking the symbol of each operator gives the phase space equation

$$\partial_{\overline{\tau}} S + i(\omega - a)S = \frac{ib}{2}\left(M_c \odot S + M_{-c} \odot S\right), \tag{4.11}$$

where M_c denotes the symbol of pointwise multiplication by e^{ict}. We can verify the correctness of this equation as well as its expansion for slowly varying frequency using the properties of the symbols M_c and the symbols H_c of the operators $e^{ict}\phi_0^\dagger$, in terms of which (using the fact that the taking the symbol is a linear operation) we can expand the symbol S as

$$S = \sum_{n=-\infty}^{\infty} J_n(b/c) H_{a+nc}. \tag{4.12}$$

As discussed in Section 3.4.2, the symbols M_c and H_c satisfy

$$M_a \odot H_b = H_{a+b}, \tag{4.13}$$

and taking the required derivatives we find that

$$\partial_{\overline{\tau}} H_a = i(a - \omega)H_a. \tag{4.14}$$

Using this derivative identity term by term on S we see that the left hand side of the phase space equation is given by

$$(\partial_{\overline{\tau}} + i(\omega - a))S = \sum_{n=-\infty}^{\infty} incJ_n(b/c)H_{a+nc}. \tag{4.15}$$

Likewise the symbol product identity gives for the right hand side of the phase space equation, upon operating term by term and relabelling the terms in the sum,

$$\frac{ib}{2}(M_c + M_{-c}) \odot S = \frac{ib}{2} \sum_{n=-\infty}^{\infty} \left(J_{n-1}(b/c) + J_{n+1}(b/c)\right) H_{a+nc}. \tag{4.16}$$

It now follows that the left and right hand sides of the phase space equation are equal using the Bessel function identity

$$J_{n-1}(x) + J_{n+1}(x) = \frac{2n}{x} J_n(x). \tag{4.17}$$

This method of demonstrating that the phase space equation holds, by expanding in terms of the symbols of harmonics H_c, does not really use the time-frequency capabilities of the Wick symbol calculus; beyond showing the correctness of the phase space equation, the main point here is that the symbol calculus provides identities to treat those cases which can be well treated using the convolution theorem and the Fourier transform. But a real advantage comes in using the asymptotic expansion of the product formula to find an approximate equation in cases in which the frequency is slowly varying (conditions for which we derive below). Using the fact from Section 3.4.2 that

$$M_c(w, z) = e^{\frac{-\sigma c^2}{4}} e^{\frac{ic(w+z)}{2}}, \tag{4.18}$$

applying the asymptotic expansion of the product formula we derive as our approximate phase space equation

$$\left(1 + i\sigma bce^{\frac{-\sigma c^2}{4}} \sin(ct)\right) \partial_{\overline{\tau}} S + i\left(\omega - a - be^{\frac{-\sigma c^2}{4}} \cos(ct)\right) S = 0. \tag{4.19}$$

Interpreted by comparing this equation locally with the phase space equation for the oscillator with a linear chirp, we would read this equation as saying that the local frequency of the oscillator is given by $a + be^{\frac{-\sigma c^2}{4}} \cos(ct)$ and that the rate of change

of the frequency is $-bce^{\frac{-\sigma c^2}{4}}\sin(ct)$, statements which are at least consistent. The factor $\exp(\frac{-\sigma c^2}{4})$ in the local frequency, not obvious from equation of motion, results from windowing with a width $\sqrt{\sigma}$; it is shown below that it improves the accuracy of the approximation. We can find the conditions under which this equation holds using the asymptotic expansion of $M_a \odot H_b$, which we can study very explicitly. Calculating the ratio of the approximate and exact expressions for $M_a \odot H_b$, we obtain

$$\frac{M_a H_b + 2\sigma\partial_\tau M_a \partial_{\overline{\tau}} H_b}{H_{a+b}} = e^{\frac{\sigma a^2}{4}} e^{-\sigma a(\omega - b)} \left(1 + \sigma a(\omega - b)\right), \tag{4.20}$$

and so the approximation for $M_a \odot H_b$ will be a good one if the right hand side of this equation is close to one. This will indeed be the case if

$$\sigma a^2 \ll 1 \tag{4.21}$$

and

$$|\sigma a\,(\omega - b)\,| \ll 1. \tag{4.22}$$

The first of these is a condition that the function e^{iat} which M_a represents multiplication by is slowly varying on the scale of $\sqrt{\sigma}$, as we might have guessed since we are looking for a 'slowly varying' type of condition. The second requires that we are in a part of phase space not too distant from b; so long as the phase space distribution is small outside of this region, the approximation will be a good one (we have calculated the fractional error here).

Since we can derive the asymptotic expansion of the phase space equation by applying the asymptotic expansion of $M_c \odot H_{a+nc}$ to each harmonic in S, for the approximate phase space equation to hold we require the approximation of $M_c \odot H_{a+nc}$ to be good for all harmonics $a + nc$ with significant amplitude. The first condition above here requires $\sigma c^2 \ll 1$, or that $\cos(ct)$ is slowly varying. In this case we can show using the properties of Bessel functions [126] that the spectrum of harmonics is small outside of the band $c \pm b$; for this reason the second condition above here requires that

$$\sigma cb \ll 1, \tag{4.23}$$

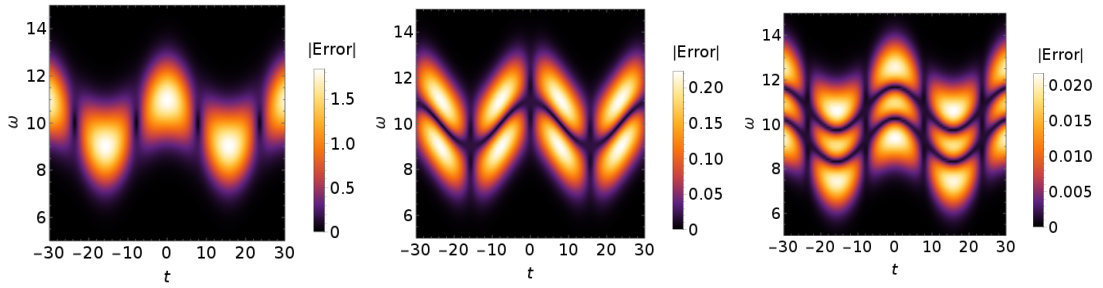

(a) **(b)** **(c)**

Figure 4.2: The error in the approximate phase space equation for a frequency modulated oscillator for (a) the approximation in which the symbol from the frequency modulation is neglected, (b) the zeroth order approximation in which only the local dispersion relation term is used, and (c) the first order approximation in which the complex velocity term representing the rate of change of the frequency is included. The approximation is considerably improved as each physical effect is taken into account.

since in this case the second condition will hold for all significant harmonics in S. This condition can be read as a condition on b, the amplitude in the swing of the frequency of the oscillator; it is reasonable that we require a restriction on b since by increasing it we can make the frequency of the oscillator vary arbitrarily rapidly.

To check the validity of the approximate phase space equation 4.19 numerically, I have calculated the left hand side of the approximate phase space equation (which should be approximately equal to zero) for varying degrees of approximation. Fig 4.2 shows the absolute value of the error, multiplied by the factor converting from symbols to windowed Fourier transforms for ease of interpretation, for three degrees of approximation, (a) neglecting the terms from the M_c completely on the grounds that for small b, $bM_c \odot S \sim 0$, (b) including only the zeroth order approximations $M_c \odot S \sim M_c S$ which give the local dispersion relation, and (c) including also the first order approximation terms $M_c \odot S \sim M_c S + 2\sigma\partial_\tau M_c \partial_{\overline{\tau}} S$ which give the complex velocities. The plots shown are for $a = 10$, $b = 1$, $c = 0.2$, with $\sigma = 1$, so the smallness parameters calculated above are $\sigma c^2 = 0.04$ and $\sigma cb = 0.2$. The scale of the error in going from (a) through (c) decreases roughly by a factor of 10. It is interesting to note that in case we set the $e^{-\sigma c^2/4}$ in the local dispersion relation to one the error in plot (c) almost doubles, so the Gaussian smoothing involved in the symbols of pointwise multiplication improves the approximation significantly [127].

In the preceding paragraphs we used detailed knowledge of the behaviour of the symbols relating to harmonics to verify the equations and their approximation; this should not give the impression that the expansion of solutions in terms of harmonics is required for the application of the Wick symbol method. In fact from here we will take symbols as our primary tool, the expansion in harmonics here having served only to demonstrate their properties. Exploiting the fact that symbols allow us to work with time and frequency at once, the asymptotic expansion of the product formula sums up how the contrivance of interfering harmonics can give rise to purely local phenomena in phase space, and even gives us equations governing them.

4.2 Wave propagation in a medium

As a model equation for wave propagation in a medium we will take

$$\partial_t u + a\partial_x u - igu = j, \tag{4.24}$$

where $u(x,t)$ is our wave field, $g(x,t)$ is a function characterizing the response of the medium, a is a constant, and $j(x,t)$ is some given source function. This is the differential equation corresponding to a model dispersion relation proposed by Schuster [128] and studied by Brillouin and Sommerfeld [129], here with the medium allowed to depend on position and time. For $g = 0$ the equation reduces to the advection equation; the term igu represents the linear response of the medium to the wave field. In order to apply the Wick symbol calculus we first rewrite this equation as an operator equation,

$$\partial_t \circ u\phi_0^\dagger + a\partial_x \circ u\phi_0^\dagger - ig \circ u\phi_0^\dagger = j\phi_0^\dagger. \tag{4.25}$$

Now we can translate the operator equation into a phase space equation using the Wick symbol calculus

$$\frac{\tau - \overline{\tau}}{2\sigma_t} \odot S + a\frac{\chi - \overline{\chi}}{2\sigma_x} \odot S - iG \odot S = S_j, \tag{4.26}$$

where S is the symbol of $u\phi_0^\dagger$, G is the symbol of pointwise multiplication by g and S_j is the symbol of $j\phi_0^\dagger$. Evaluating the symbol products from the derivatives gives

$$\partial_{\overline{\tau}} S + a\partial_{\overline{\chi}} S + i(\omega + ka)S = iG \odot S + S_j. \tag{4.27}$$

Derivative terms like $\partial_t u$ in the wave equation give terms $\partial_{\overline{\tau}} S + i\omega S$ in the phase space equation; this rule can be quickly applied and (purely formally) resembles the rule $\partial_t \to \partial_t + i\omega$ encountered when making slowly varying envelope approximations [130].

4.2.1 Wave propagating in a linear gradient

The equation for a pulse in a medium undergoing a linear shift in frequency and wavevector can be solved exactly, and its phase space representation verifies the interpretation of Wick symbol equations in terms of complex velocities. Taking the medium function in (4.24) as $g(x,t) = bt + cx$ gives the equation of motion

$$\partial_t u + a\partial_x u - i(bt + cx)u = 0, \tag{4.28}$$

where a, b and c are constants. The phase space representation of this equation is

$$(1 - ib)\partial_{\overline{\tau}} S + (a - ic)\partial_{\overline{\chi}} S + i(\omega + ka - bt - cx)S = 0. \tag{4.29}$$

Using the method of characteristics we can solve for u to give

$$u(x,t) = u_0(x - at)e^{i\left(cxt + (b-ac)\frac{t^2}{2}\right)}, \tag{4.30}$$

where $u_0(x)$ gives the initial profile of u. The phase space distribution of this u can be calculated exactly if u_0 is a Gaussian (it is then a Gaussian integral in x and t) and it can be verified that it satisfies the phase space equation. In this case we can also calculate the local frequency Ω and wavevector K defined in terms of the derivatives of the phase ϕ of u, $\Omega = \partial_t \phi$ and $K = \partial_x \phi$ (these are the definitions appropriate for our sign convention for frequency and wavevector). We obtain $K = ct$ and so $(\partial_t + a\partial_x)K = c$, and $\Omega = cx + (b - ac)t$, so $(\partial_t + a\partial_x)\Omega = b$. In this way we see that the solution indeed describes a pulse propagating with speed a whose wavevector changes at a rate c and whose frequency changes at a rate b (in the frame of the pulse), verifying the interpretation of the Wick symbol equation in terms of complex velocities.

4.2.2 Slowly varying medium

In a slowly varying medium we can expand the symbol product $G \odot S$ using the asymptotic expansion of the product formula to give

$$(1 - 2i\sigma_t \partial_\tau G)\, \partial_{\overline{\tau}} S + (a - 2i\sigma_x \partial_\chi G)\, \partial_{\overline{\chi}} S + i\,(\omega + ka - G)\, S = S_j. \tag{4.31}$$

Using the interpretation of Wick symbol of equations in terms of complex velocities, we see that a time variation in the medium causes a frequency shift at the rate $\partial_t G$, while a spatial variation in the medium causes a shift in wavevector at the rate $\partial_x G$ (the single variable symbol G is simply g smoothed by a Gaussian and is independent of ω and k, so $\partial_\tau G = \frac{1}{2}\partial_t g$ and $\partial_\chi G = \frac{1}{2}\partial_x G$). The frequency shift is what would be called photon acceleration in the context of laser plasma interaction [131], while the wavevector shift is the 1D version of refraction. The dispersion relation shows that in the medium the waves locally satisfy $\omega + ka - G = 0$.

4.2.3 Rapidly varying medium

If the medium varies on a scale shorter than the wavelength of the waves described by u, the asymptotic expansion of the product formula will not be valid. This is the situation in Raman backscatter for example, in which light is scattered from a Langmuir wave with approximately twice the wavevector, and so half the wavelength, of the light [132]. In this case the exact formula for the symbol product allows us to obtain a phase space equation describing the resulting phenomena which are nonlocal in phase space (this is to be contrasted to the fluid-like flow of the phase space distribution in a slowly varying medium). Setting the source term j to zero for now, using the exact form of the product formula we obtain for our phase space equation in a rapidly varying medium

$$\partial_{\overline{\tau}} S + a\partial_{\overline{\chi}} S + i(\omega + ka)S = \frac{-1}{(4\pi)^2 \sigma_t \sigma_x} \int \mathrm{d}u\, \mathrm{d}\overline{u}\, G(\overline{z}, u) S(\overline{u}, z). \tag{4.32}$$

In this equation z and u stand for pairs of coordinates (τ, χ), so the integral is over time, frequency, position, and wavevector. Given the relation discussed in Section 3.4.2 of the symbol G to the windowed Fourier transform of the medium

function g, the integral term from the product formula gives the coupling between the waves and medium according to the sum of wavevectors which is often derived using the convolution theorem for the Fourier transform. Here the coupling is localized in space and time, allowing us to see for example that in regions where there is no medium the propagation proceeds as in vacuum. For example if g is a Gaussian wavepacket representing a localized disturbance in the medium, the Gaussian example in Section 3.4.2 shows that the effect of g on the phase space distribution is exponentially small away from the position of the disturbance.

Figure 4.3 shows snapshots of the fields solving equation (4.24) for a medium function $g(x,t) = 10 + 5\cos(cx)$ for $c = 0.5$ (left column) and $c = 5$ (right column), corresponding to a slowly varying and rapidly varying medium respectively, along with their position-wavevector distributions and their frequency-position-wavevector distributions. For the slowly varying medium, the white surface in (e) shows the local dispersion surface as given by the asymptotic expansion of the product formula. The phase space distribution lies on the local dispersion surface. For the rapidly varying medium (f) sidebands are produced away from the dispersion surface, generated by the coupling from the integral form of the product formula which is nonlocal in wavevector.

4.2.4 Sources

The source term j in the wave equation gives rise to a source term S_j in the complex wave space equation which can pump a part of phase space which does not satisfy the dispersion relation of the waves. Physically the equation tells us that a source, such as an antenna, with a given frequency and wavevector here pumps waves with that same frequency and wavevector. This is relevant for example in waveguides driven off resonance and in the study of nonlinear wave processes in which waves off the dispersion surface can be driven nonlinearly [133]. The simple handling of the source term results from the linearity of the windowed Fourier transform in the wave field; when employing the Weyl symbol calculus

and Wigner function the treatment of sources require the symbol of the inverse of the operator acting on the wave field u [73], [75].

4.2.5 Dispersive medium

If the medium does not respond instantaneously to the field it will in general be dispersive and absorptive [129], [134]. In this case the term igu is replaced by $ir * u$ where $r(t)$ is a function describing the ringing down of the medium as it responds to a delta function excitation and $*$ denotes convolution in time. The Wick symbol handles this case naturally since the symbol of convolution with r is simply the Fourier transform of r smoothed by a Gaussian in frequency. Denoting this symbol by R, generically R will have a real and imaginary part, $R = D + iA$, responsible for dispersion and absorption. The Wick symbol equation for the field is then

$$((1 - \partial_\omega D) - i\partial_\omega A)\,\partial_{\overline{\tau}} S + a\partial_{\overline{\chi}} S + i(\omega + ka - D - iA) = 0. \tag{4.33}$$

Reading off the complex velocities (first dividing through to make the rate of change of time equal to 1), we obtain the correct group velocity of $a/(1 - \partial_\omega D)$ and a frequency shift at a rate $\partial_\omega A/(\sigma_t(1 - \partial_\omega D))$. Looking at the dispersion relation, D modifies the dispersion relation while A has an imaginary coefficient and so contributes damping, as expected.

4.3 Nonlinear Schrödinger equation

4.3.1 Phase space representation

The nonlinear Schrödinger equation is very popular, perhaps due to its diverse physical applications and rich mathematical properties [135], [136]. It has many remarkable solutions of interest in plasma physics including various species of soliton as well as self-focusing and filamenting pulses [137]–[139]. The Wick symbol method allows us to derive a phase space representation of the nonlinear Schrödinger equation which illustrates dispersion, group velocity, and nonlinear frequency shifts. The asymptotic expansion of the product formula naturally gives rise

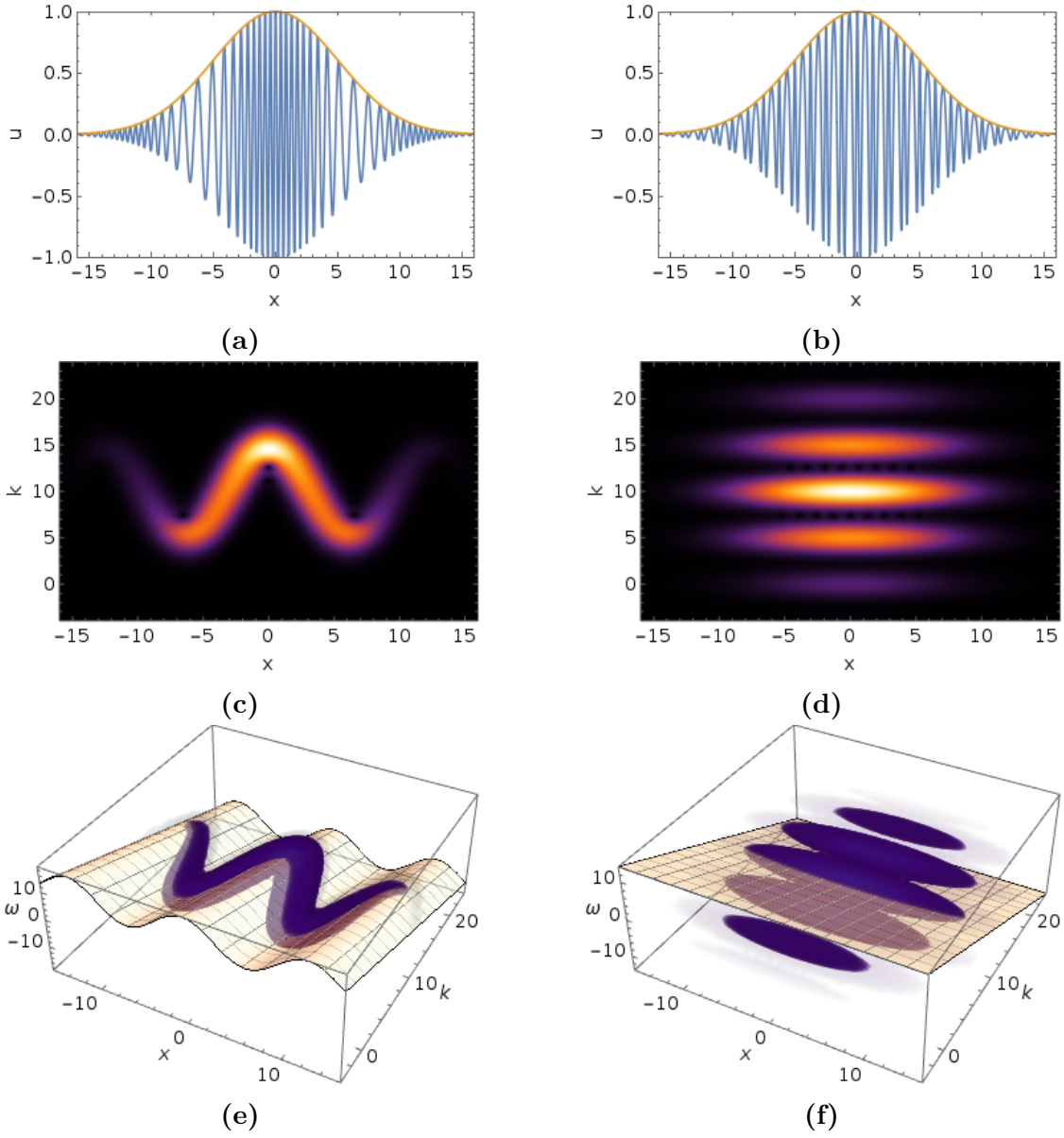

Figure 4.3: Snapshots of the fields (top row), position-wavevector phase space distributions (middle row) and position-wavevector-frequency distributions (bottom row) for a pulse moving a slowly varying (left column) and rapidly varying (right column) sinusoidal density profile. The complex phase space equation is satisfied in both cases. In the slowly varying case the pulse is constrained to flow on the local dispersion surface which reflects the varying density, the white surface in (e), as described by the asymptotic expansion of the product formula. In the rapidly varying case sidebands are produced which lie away from the dispersion surface (f), requiring the exact integral form of the product formula which couples distant points in frequency and wavevector while maintaining locality in position and time.

to a ponderomotive force in the phase space equation. The nonlinear Schrödinger equation can be written in the form

$$i\partial_t u + \frac{a}{2}\partial_x^2 u + b|u|^2 u = 0. \tag{4.34}$$

To obtain a phase space representation we first rewrite it as an operator equation

$$i\partial_t \circ u\phi_0^\dagger + \frac{a}{2}\partial_x^2 \circ u\phi_0^\dagger + b|u|^2 \circ u\phi_0^\dagger = 0, \tag{4.35}$$

where the operator $b|u|^2$ is pointwise multiplication by $b|u|^2$. Now we obtain a phase space equation by taking the symbol,

$$i\frac{\tau - \overline{\tau}}{2\sigma_t} \odot S + \frac{a}{2}\left(\frac{(\chi - \overline{\chi})^2}{4\sigma_x^2} - \frac{1}{2\sigma_x}\right) \odot S + bS_{|u|^2} \odot S = 0, \tag{4.36}$$

where $S_{|u|^2}$ is the symbol of pointwise multiplication by $|u|^2$. Using the asymptotic expansion of the product formula, we obtain

$$\left(1 - 2i\sigma_t b\partial_\tau S_{|u|^2}\right)\partial_{\overline{\tau}} S + \left(ka - 2ib\sigma_x \partial_\chi S_{|u|^2}\right)\partial_{\overline{\chi}} S + i\left(\omega + \frac{ak^2}{2} - bS_{|u|^2}\right) S = 0. \tag{4.37}$$

The physical information in this phase space equation can be extracted using the interpretation of Wick symbol equations in terms of complex velocities. The quantity $S_{|u|^2}$ is simply $|u|^2$ smoothed by the Gaussian ϕ_0, the smoothed envelope of the wave field. So the term in $\partial_{\overline{\tau}} S$ tells us that if the smoothed envelope is changing in time, the frequency of the wave is shifted at a rate $\partial_t S_{|u|^2}$. The term in $\partial_{\overline{\chi}} S$ tells us that the group velocity is ka, the correct group velocity, and that if the smoothed envelope is changing in space the wavevector is shifted at a rate $\partial_x S_{|u|^2}$. These envelope gradient forces are ponderomotive forces, and their appearance within the Wick symbol method, including the smoothing of the envelope, is entirely natural. Looking at the dispersion relation we can read off the usual dispersion relation for the Schrödinger equation (allowing for the present sign convention) together with a nonlinear frequency shift $-bS_{|u|^2}$.

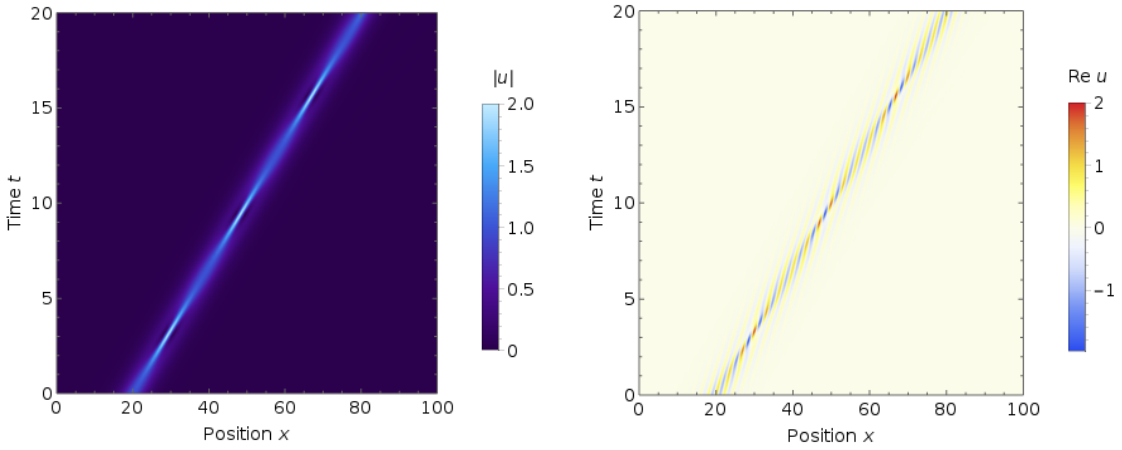

Figure 4.4: Space-time plots of the absolute value (a) and real part (b) of the field u as a single soliton propagates. Due to the nonlinearity the envelope in (a) oscillates and the pulse does not disperse. Dispersion manifests itself in (b) as the wave crests moving with respect to the envelope.

4.3.2 Phase space description of solitons

To verify the phase space representation of the nonlinear Schrödinger equation derived above and to demonstrate the utility of the phase space point of view, I present the phase space representation of a numerical solution of the nonlinear Schrödinger equation exhibiting a single soliton. The initial profile of the pulse is taken as $u_0(x) = \mathrm{sech}(x/2)\exp(3ix)$, chosen since $u_0(x) = \mathrm{sech}(x)\exp(3ix)$ would have given rise to a soliton which simply translated with an unchanging envelope. The numerical solution was found using a pseudospectral method in Mathematica's NDSolve function.

Fig. 4.4 shows space-time plots of the absolute value and real part of the field. The pulse does not disperse and oscillates in profile. For the linear Schrödinger equation ($b = 0$) the pulse would disperse as it propagates. We can understand the mechanism by which the nonlinear term prevents the pulse from dispersing using the phase space description above.

Fig. 4.5 shows snapshots of the position-wavevector phase space distribution of the soliton as it propagates. The initial distribution is centered at $x = 0$, $k = 3$. As time passes it propagates to the right and swirls around clockwise. This behavior

is explained by the phase space velocities calculated for the nonlinear Schrödinger equation. Without the nonlinearity the velocity field is a shear flow in the x direction caused by the dispersion, reflecting the fact that here higher k parts of the pulse propagate faster. The nonlinearity introduces a k component in the velocity field which acts to move parts of the pulse where the gradient of the envelope is large up and down in phase space. In particular the front of the pulse is moved downwards to a slower moving part of the shear flow, allowing it to be overtaken by the rest of the pulse, while the back of the pulse is moved upwards in k to a faster moving part of the flow. In this way the pulse stays together rather than dispersing, the envelope oscillating during the course of each overturning of the pulse in phase space. Early wave kinetic simulations of the nonlinear Schrödinger equation observed a vortex motion of the computational particles [140]. As the pulse overturns two dislocations (discussed in Chapter 5) form in the phase (d,f), visible as zeros in the amplitude distributions (c,e). The plots of the phase have been masked according to the amplitude of the distribution, since the phase is best determined numerically where the amplitude is large.

Figure 4.6 shows (in orange) a snapshot of the distribution of the soliton in position, wavevector and frequency at time $t = 3$ when its amplitude is large. Also shown is the local dispersion surface (blue). The center of the pulse is shifted down in frequency to lie on the local dispersion surface, verifying the nonlinear dispersion relation.

4.4 Mode conversion

Mode conversion is a process in which one type of wave in a varying medium is partially converted into another type of wave at a point where their local dispersion surfaces meet [141], [142]. Here we treat a widely applicable mode conversion equation [143] using the physically intuitive method of tracing a ray through the mode conversion point and integrating along the ray to find how the field amplitude and phase changes along it. In particular this gives both the reflection coefficient and the phase change of the field during the mode conversion process. Mode conversion

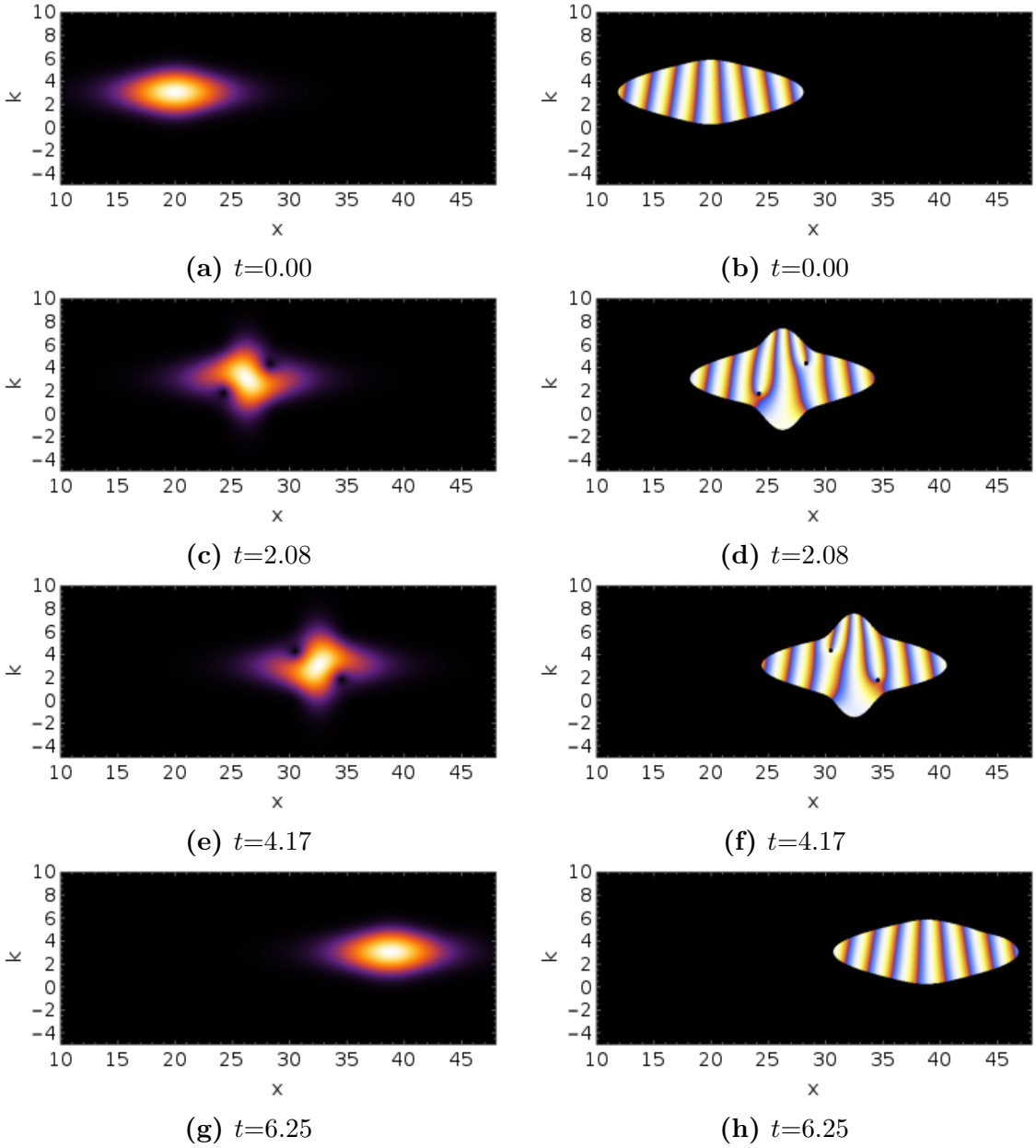

(a) t=0.00 **(b)** t=0.00

(c) t=2.08 **(d)** t=2.08

(e) t=4.17 **(f)** t=4.17

(g) t=6.25 **(h)** t=6.25

Figure 4.5: Snapshots of the absolute value (left column) and phase (right column) of the position-wavevector phase space distribution during the propagation of a soliton. The ponderomotive force combines with the shear flow in phase space to cause the pulse to overturn in phase space, preventing it from dispersing. During the overturning dislocations form in the phase of the distribution, the black holes in (d) and (f).

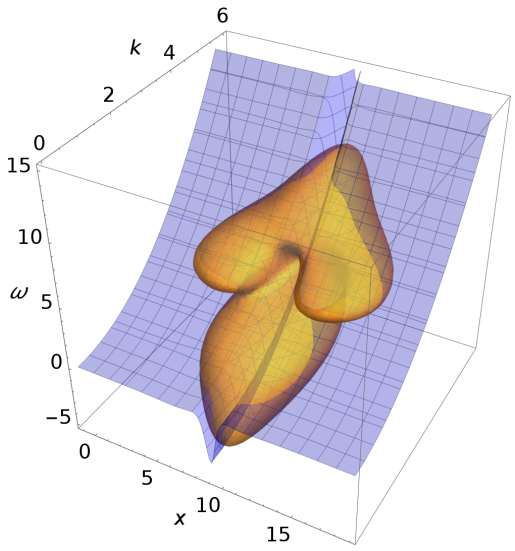

Figure 4.6: The position-wavevector-frequency ($xk\omega$) distribution of the soliton (orange) as its amplitude peaks. The local dispersion surface (blue) is shifted downwards where the envelope is largest, in accordance with the complex phase space equation.

has been extensively studied in phase space using the Wigner function, Weyl symbol calculus, and metaplectic transformations [75], [144]–[146].

In [143] by considering two first order equations for fields representing the two modes involved in the mode conversion process, after eliminating one of the fields and changing variables a mode conversion equation of the following form is obtained

$$\frac{a}{2}\partial_x^2 u - \left(c + \frac{b}{2}x^2\right) u = 0. \tag{4.38}$$

Here a and b are real constants and c is a complex constant. For real c this equation is the time independent Schrödinger equation for the harmonic oscillator, the problem for which Schrödinger initially introduced the coherent states [147], [148] and which has been extensively studied using complex methods [73], [78], [149], [150]. Here we will study a version of this equation which includes time dependence explicitly,

$$i\partial_t u + \frac{a}{2}\partial_x^2 u - \left(c + \frac{b}{2}x^2\right) u = 0. \tag{4.39}$$

In case u depends on time as $e^{\beta t}$ for some (possibly complex) β this equation reduces to the time-independent version with a different constant c. Applying the method as above, using the symbols for the second derivative operator ∂_x^2 and the operation

of multiplication by x^2, we obtain the phase space equation

$$\partial_{\overline{\tau}} S + i(x\sigma_x b - ika)\partial_{\overline{\chi}} S \\ +i(\omega + c + \frac{ak^2 + bx^2}{2} + \frac{a}{4\sigma_x} + \frac{b\sigma_x}{4})S - \frac{i}{2}(a - b\sigma_x^2)\partial_{\overline{\chi}}^2 S = 0. \tag{4.40}$$

A judicious choice of σ_x can now remove the term in $\partial_{\overline{\chi}}^2 S$ [73]; setting $\sigma_x = \sqrt{\frac{a}{b}}$ gives the exact equation

$$\partial_{\overline{\tau}} S + i\sqrt{ab}\overline{\chi}\partial_{\overline{\chi}} S + i(\omega + c + \frac{b}{2}\chi\overline{\chi} + \frac{\sqrt{ab}}{2})S = 0. \tag{4.41}$$

Reading off the complex velocities, we see that the x velocity is ak, which is the correct group velocity coming from the dispersive $\frac{a}{2}\partial_x^2 u$ term in the wave equation 4.39, while the k velocity is $-bx$, as we would expect considering the potential term $\frac{b}{2}x^2 u$ in equation 4.39. The local dispersion relation gives the real part of the frequency as $\mathrm{Re}(c) + \frac{b}{2}x^2 + \frac{a}{2}k^2 + \frac{\sqrt{ab}}{2}$, while the imaginary part of the frequency is $\mathrm{Im}(c)$. These facts together suggest wavepackets moving along elliptical trajectories in phase space, damping at a rate $\mathrm{Im}(c)$. In fact we can solve the equation exactly by integrating along rays in phase space using a complex method of characteristics, verifying this behaviour.

The success of the method of characteristics in this case depends on the analytic properties of the functions involved, and so the solution is easiest in terms of the analytic function F which S is proportional to (Section 3.4.2). The function F satisfies

$$S = e^{-\frac{\chi\overline{\chi}}{2\sigma_x} - \frac{\tau\overline{\tau}}{2\sigma_t}} F, \tag{4.42}$$

and in terms of F the phase space equation reads

$$\partial_{\overline{\tau}} F + i\sqrt{ab}\overline{\chi}\partial_{\overline{\chi}} F + \left(\frac{-\overline{\tau}}{2\sigma_t} + i\left(c + \frac{\sqrt{ab}}{2}\right)\right) F = 0. \tag{4.43}$$

This equation can now be solved by using a complex version of the method of characteristics, finding complex trajectories in phase space along which the evolution of F is particularly simple. Formally we can simply proceed by analogy with the real case presented in Chapter 2, but the fact that this works is surprising in that the

derivatives $\partial_{\overline{\chi}}$ and $\partial_{\overline{\tau}}$ are in fact sums of partial derivatives ∂_x, ∂_t, ∂_k and ∂_ω, and the 'velocities' multiplying them are complex and so products such as $v\partial_{\overline{\chi}}$ with v a 'complex velocity' contain cross terms. The reason that the method works is that F is an analytic function of $\overline{\tau}$ and $\overline{\chi}$, which means that $\partial_\tau F = 0$ and $\partial_\chi F = 0$. This means that in applying the chain rule we find that $\mathrm{d}F = \partial_\tau F\,\mathrm{d}\tau + \partial_{\overline{\tau}} F\,\mathrm{d}\overline{\tau} + \partial_\chi F\,\mathrm{d}\chi + \partial_{\overline{\chi}} F\,\mathrm{d}\overline{\chi}$ reduces to $\mathrm{d}F = \partial_{\overline{\chi}} F\,\mathrm{d}\overline{\chi} + \partial_{\overline{\tau}} F\,\mathrm{d}\overline{\tau}$, so by choosing appropriate complex trajectories we can reproduce equations involving only F, $\partial_{\overline{\chi}} F$ and $\partial_{\overline{\tau}} F$ such as equation 4.43. Put shortly, the chain rule is the basis of the method of characteristics, and the analyticity of F allow us to simplify the chain rule and so apply the same reasoning as for the real method of characteristics. With this understanding, proceeding by analogy with the real method of characteristics we introduce the complex trajectories $\overline{X}(s)$ and $\overline{T}(s)$ depending on a parameter s, along with the function $\phi(s)$ defined by $\phi(s) = F(X(s), T(s))$, satisfying the ordinary differential equations

$$\frac{\mathrm{d}\overline{T}(s)}{\mathrm{d}s} = 1 \tag{4.44}$$

$$\frac{\mathrm{d}\overline{X}(s)}{\mathrm{d}s} = i\sqrt{ab}\,\overline{X}(s) \tag{4.45}$$

$$\frac{\mathrm{d}\phi(s)}{\mathrm{d}s} = \left(\frac{\overline{T}(s)}{2\sigma_t} - i\left(c + \frac{\sqrt{ab}}{2}\right)\right)\phi(s). \tag{4.46}$$

These equations can be integrated to give

$$\overline{T}(s) = \overline{\tau}_0 + s \tag{4.47}$$

$$\overline{X}(s) = \overline{\chi}_0 e^{i\sqrt{ab}\,s} \tag{4.48}$$

$$\phi(s) = \phi_0 \exp\left(\frac{\overline{\tau}_0 s + s^2/2}{2\sigma_t} - is\left(c + \frac{\sqrt{ab}}{2}\right)\right), \tag{4.49}$$

where $\overline{\tau}_0$ and $\overline{\chi}_0$ are our chosen initial values for $\overline{X}(0)$ and $\overline{T}(0)$, giving the initial position, wavevector, time and frequency for our phase space trajectory, and $\phi_0 = F(\overline{\chi}_0, \overline{\tau}_0)$ from the definition of ϕ. The phase space trajectories describe ellipses in the position-wavevector plane, or an elliptical helix in a space of position, wavevector and time (here the frequency is unchanged along a characteristic). Now substituting our solutions for $\phi(s)$, $\overline{X}(s)$ and $\overline{T}(s)$ into the definition $\phi(s) =$

$F(\overline{X}(s), \overline{T}(s))$ we obtain

$$F(\overline{\tau}_0 + s, \overline{\chi}_0 e^{i\sqrt{ab}\,s}) = F(\overline{\tau}_0, \overline{\chi}_0) \exp\left(\frac{\overline{\tau}_0 s + s^2/2}{2\sigma_t} - is\left(c + \frac{\sqrt{ab}}{2}\right)\right). \tag{4.50}$$

This equation gives the value of F at any point along the elliptical helix trajectory starting at $\overline{\chi}_0$ and $\overline{\tau}_0$.

To obtain the phase and amplitude of the field it is convenient to convert back from F to the windowed Fourier transform W. This is a matter of multiplying by the appropriate factor; from the definitions

$$S = e^{-\frac{\chi\overline{\chi}}{2\sigma_x} - \frac{\tau\overline{\tau}}{2\sigma_t}} F \tag{4.51}$$

$$W = e^{\frac{\chi\overline{\chi}}{4\sigma_x} + \frac{\tau\overline{\tau}}{4\sigma_t}} e^{\frac{i}{2}(kx+\omega t)} S \tag{4.52}$$

and so

$$F = e^{\frac{\chi\overline{\chi}}{4\sigma_x} + \frac{\tau\overline{\tau}}{4\sigma_t}} e^{-\frac{i}{2}(kx+\omega t)} W, \tag{4.53}$$

which upon substitution gives

$$\frac{W(t_0 + s - i\sigma_t\omega_0, (x_0 - i\sigma_x k_0)e^{i\sqrt{ab}\,s})}{W(t_0 - i\sigma_t\omega_0, x_0 - i\sigma_x k_0)} =$$
$$\exp\left(i\left(-x_0 k_0 \sin^2(\sqrt{ab}\,s) + \frac{k_0^2\sigma_x^2 - x_0^2}{4\sigma_x}\sin(2\sqrt{ab}\,s) - s\left(c + \frac{\sqrt{ab}}{2}\right)\right)\right). \tag{4.54}$$

This expression gives us the evolution of the phase and amplitude at all points along a ray starting at an arbitrary point in phase space. In particular for determining the phase and amplitude change during the mode conversion process we can pick a ray which begins at $x = 0$ with some given wavevector $k = k_0$, and which after a time $t = \pi/\sqrt{ab}$ has returned to $x = 0$ but now with $k = -k_0$; the ray has thus been reflected. Calling W at the ray's starting position W_{in} and W at the ray's finishing position, after being reflected, W_{out}, we have putting $x_0 = 0$, $s = \pi/\sqrt{ab}$ in equation (4.54)

$$\frac{W_{\text{out}}}{W_{\text{in}}} = \exp\left(\frac{-ic\pi}{\sqrt{ab}} - \frac{i\pi}{2}\right). \tag{4.55}$$

So the change in amplitude during the process is given by

$$\frac{|W_{\text{out}}|}{|W_{\text{in}}|} = \exp\left(\frac{\pi \operatorname{Im}(c)}{\sqrt{ab}}\right) \tag{4.56}$$

and the change in phase by

$$\arg\left(\frac{W_{\text{out}}}{W_{\text{in}}}\right) = -\frac{\pi \operatorname{Re}(c)}{\sqrt{ab}} - \frac{\pi}{2}. \tag{4.57}$$

The change in amplitude (4.56) agrees with the energy transmission coefficient in [143], with the parameters corresponding according to $a = 2$, $b = \frac{1}{2}$, $c = \frac{-i\eta_0}{ag-bf} - \frac{1}{2}$, and accounting for the energy here being given by $|W|^2$. The first term in the change in phase (4.57) is due to the evolution under $\operatorname{Re}(c)$ for a time $t = \pi/\sqrt{ab}$, but the $-\pi/2$ term is a phase shift due to the ray passing through a turning point, a Maslov phase [151]. The Maslov phase here accumulates continuously along the ray and results from the 1/2 terms which appear in the symbols of ∂_x^2 and $x^2\cdot$; we do not need to separately consider the Maslov index of the ray [151]. Littlejohn discusses this continuous change of phase associated with the Maslov index when using coherent states [86]. It is interesting to note that Maslov [152] in deriving a stationary phase estimate for the Fourier transform, now a common strategy for deriving these phase shifts, in fact replaces the problem with finding the evolution of the integrand according to the Schrödinger equation for the harmonic oscillator after a quarter period (which is related to the Fourier transform), and even carries out the approximation using classical trajectories in phase space.

Equation (4.54) gives not just the phase and amplitude change after reflection but throughout the process; along a ray starting at $x = 0$, $k = k_0$ at $t_0 = 0$, we obtain

$$\frac{W(s - i\sigma_t\omega_0, (x_0 - i\sigma_x k_0)e^{i\sqrt{ab}\,s})}{W(i\sigma_t\omega_0, x_0 - i\sigma_x k_0)} = \exp i\left(\frac{k_0^2\sigma_x}{4}\sin(2\sqrt{ab}\,s) - s\left(c + \frac{\sqrt{ab}}{2}\right)\right). \tag{4.58}$$

These expressions can be tested on a numerical solution of the wave equation.

4.4.1 Numerical solution

By solving the wave equation (4.39) numerically we can verify both the overall damping and phase shifts caused by the mode conversion process as well as the evolution of the amplitude and phase during the process. Figure 4.7 shows snapshots of the position-wavevector phase space distributions and the real part of the field at times before, half way through, and after the mode conversion, along with the evolution in time of the phase and the amplitude at the center of the pulse as it is reflected. Three cases are shown corresponding to different initial widths of the pulse. The left column uses a pulse with width equal to one; it is proportional to one of the wavepackets f_{xk} used in our phase space representation. The center column corresponds to a longer initial pulse, the right to a shorter. In all cases the overall amplitude and phase shifts are given by the analytic expressions. For the initial width of one the evolution of the phase and the amplitude goes exactly as the evolution along a ray. For the longer pulse, the amplitude increases then decreases during the process as the wavepackets initially spread in position give rise to a range of wavevectors all located at the reflection point. For the shorter pulse, the initial wide range of wavevectors are each reflected at a different point, leading to a reduced amplitude at the reflection point. The point is that our equations hold along a given ray, and that the evolution of a complete pulse is to be understood in terms of the evolution of its constituent wavepackets along their respective rays. It so happens in this problem that the amplitude and phase change of all wavepackets is the same after a time $\pi/\sqrt{ab}$, so in this case the simple formulae apply for the phase and amplitude change of any pulse. In a linear potential, studied below, this is no longer true, but the method still allows us to calculate and understand the behaviour of pulses as they are reflected and damped.

4.4.2 Linear potential

The phase space equation can be solved in the same way if there is a linear term in the potential, either directly or by completing the square and changing coordinates. In this way we can treat the turning point of a wave in a linear potential, described by

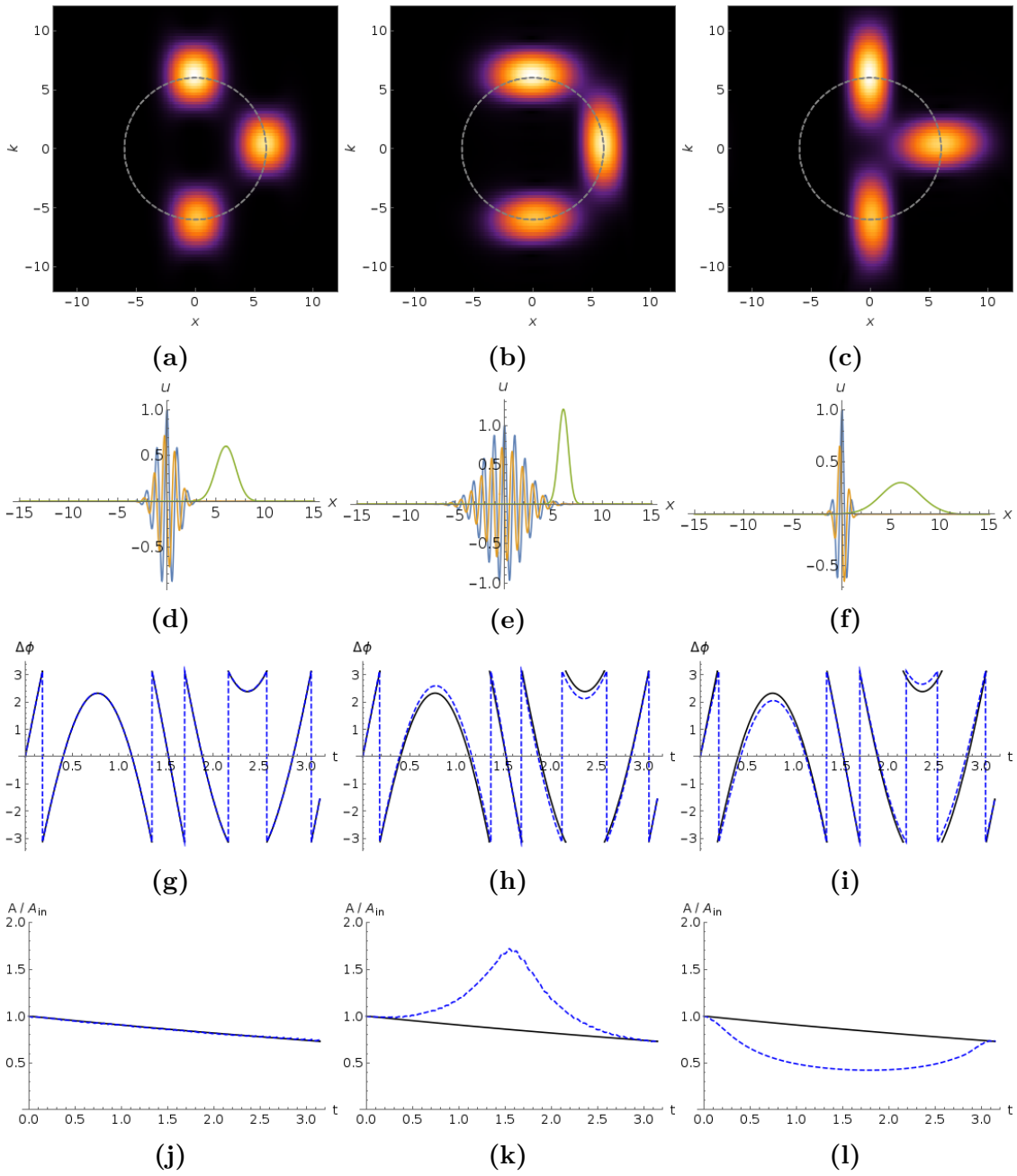

Figure 4.7: Snapshots of the position-wavevector distribution (top row) and field (second row) at times before, halfway through, and after the mode conversion process from numerical solutions for three pulses of different lengths. The third and fourth rows show the evolution of the phase and amplitude respectively during the mode conversion process, with the black solid lines showing the theoretical curve for a single wavepacket, the blue dashed lines the amplitude and phase at the center of the pulse in the numerical solutions. In accordance with the phase space equations all the pulses undergo the same total change in phase and amplitude during the process, but the different ranges of wavepackets in the pulses alter the evolution during the process.

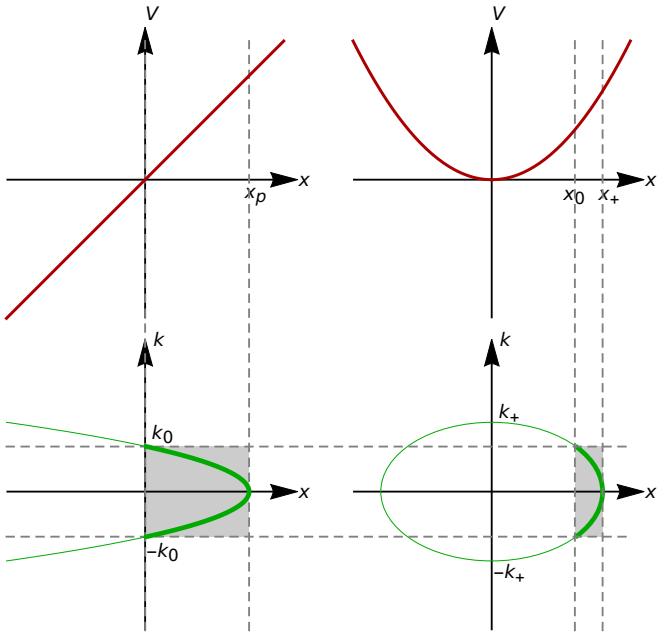

Figure 4.8: The geometry involved in studying mode conversion in a linear potential (left column) as a limit of mode conversion in a parabolic potential (right column). The top row show the potentials in each case along with the limits of the pulse's travel during the process, while the bottom row show the corresponding segments of the phase space rays, parabolic for linear potential and elliptical for the quadratic potential. In the limit the highlighted portion the phase space ellipse moves out to infinity on the right and approaches a parabolic shape.

the Airy equation, as a limit of the solution above. In this limit the elliptical phase space trajectories above become parabolas [87], and for real c the approximation reflects the fact that near its turning points a Hermite function behaves like Airy function. More complicated mode conversion processes can often be described as a succession of these simpler mode conversion processes [143], [153]. Our equation (4.54) can be applied to this problem using a change of variables and a limit to approach the linear potential. The wave equation in this case is

$$i\partial_t u + \frac{a}{2}\partial_x^2 u - (c + \frac{b}{2}x^2 + dx)u = 0, \tag{4.59}$$

where we have a linear potential of slope d together a potential bx^2 which we will send to zero, taking the limit $b \to 0$. Completing the square in the potential we can write this equation as

$$i\partial_t u + \frac{a}{2}\partial_x^2 u - \left(\left(c - \frac{d}{2b^2}\right) + \frac{b}{2}\left(x + \frac{d}{b}\right)^2 + dx\right) u = 0, \tag{4.60}$$

which with a shift of coordinates $x \to x + \frac{d}{b}$ and a shift of the constant $c \to c - \frac{d}{2b^2}$ is exactly our equation (4.39). Figure 4.8 shows the geometry in phase space associated with this limit. The left column shows the linear potential (top) and associated parabolic phase space trajectory (bottom), where we consider a ray starting at $x = 0$, $k = k_0$, and which turns around at a position x_p. The right column shows the quadratic potential (top) and phase space ellipse (bottom), where the ray begins at $x = x_0 = \frac{b}{d}$, $k = k_0$, and turns around at x_+, and when traced back to $x = 0$ has a wavevector of k_+. The shaded portions of phase space correspond to each other in the limit $b \to 0$. As $b \to 0$, the shaded part of the phase space ellipse moves out to infinity, with $x_0 = \frac{d}{b}$ and x_+ both moving to infinity but in the limit separated by x_p.

To apply our ray equation (4.54), we need only integrate along the ray starting at (x_0, k_0) and take the limit as $b \to 0$. Using the fact that all points (x, k) on the phase space ellipse have the same value of $x^2 + \sigma^2 k^2$, we can determine x_+ and k_+, the extremities of the ellipse, from the starting point (x_0, k_0). Then the solution for the trajectory determines the time s_{int} taken to traverse the portion of the ray indicated; one can show that in the limit $b \to 0$ this time is $s_{\text{int}} = \frac{2k_0}{d}$. Using this expression in equation (4.54) and taking the limit $b \to 0$ gives

$$\frac{W_{\text{out}}}{W_{\text{in}}} = \exp\left(-i\left(\frac{2ck_0}{d} + \frac{ak_0^3}{3d}\right)\right). \tag{4.61}$$

The first term in the exponent physically represents the phase and damping due to c acting for the time $s_{\text{int}} = 2k_0/d$, while the second term represents the phase one would obtain from integrating the phase accumulated taking account of the changing wavevector. Figure 4.9 show the phase shift and amplitude change from this formula (solid line) along with points giving the phase and amplitude shifts from numerical solutions for pulses with initial wavevector k_0. The agreement here is good; for shorter pulses dispersion leads to a reduction in the amplitude at the center of the pulse after reflection as its constituent wavepackets have dispersed, an effect understood by considering the range of wavepackets present in the pulse.

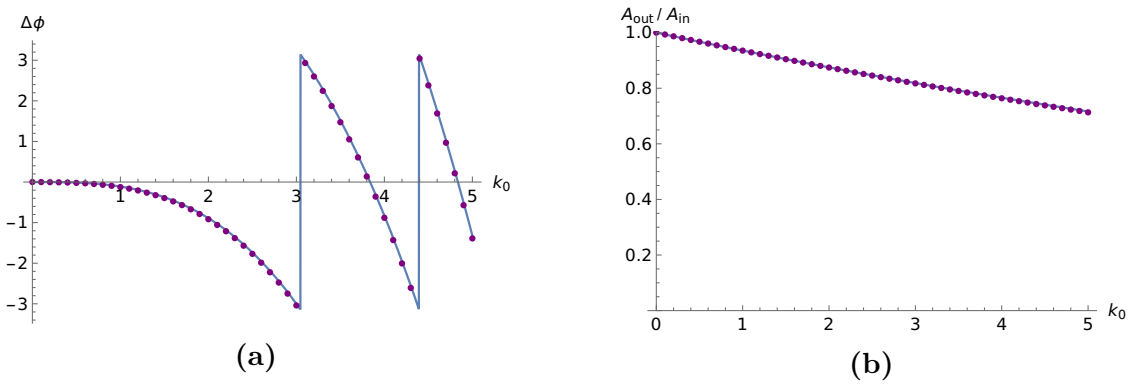

Figure 4.9: The phase (a) and amplitude (b) changes of a pulse undergoing mode conversion in a linear potential. The dots show results from numerical solution of the wave equation, the solid line the theoretical curve obtained from the limit of the quadratic potential solution.

4.5 Vlasov equation

The Vlasov equation is a plasma kinetic equation describing the evolution of a particle distribution function $f(x, v, t)$ in a space of position, velocity and time [139], [154]. Here we give the phase space representation of the Vlasov equation in a simplified physical situation (an unmagnetized plasma in one spatial dimension) to illustrate how the phase space description is a convenient setting for some phenomena encountered in some modern developments in the study of nonlinear Landau damping [123], [124]. The phenomenon of Landau damping, the collisionless damping of Langmuir waves, has greatly stimulated mathematical physics, through Landau's initial paper [14] as well as for example the introduction of the singular Case-Van Kampen modes [155], [156] and recent work on nonlinear Landau damping [157]. Among many popular physical interpretations of Landau damping I mention two; i) that particles with a velocity near the phase velocity of the Langmuir wave can interact with the wave and in the presence of a velocity gradient can extract energy from the wave, damping it, or give energy to the wave, amplifying it [158]; and ii) that the development of fine scale structure in the velocity dependence of the particle distribution function $f(x, v, t)$ leads to the averaging out of the density perturbation [123], being obtained from f by integrating over v, this effect being called phase mixing.

In [123] equations are derived for the evolution of the particle distribution function f in kinetic frequency s, the Fourier conjugate of the velocity coordinate v, considering the Vlasov equation for a magnetized plasma containing density gradients. The equations describe the interplay between phase mixing, the development of fine structure in velocity, and its opposite effect anti-phase mixing, in which fine scale structure in velocity is unwound causing the development of structure in position space. The formalism of [123] has been applied to the one-spatial-dimension Vlasov-Poisson system [124]. The equations are derived using a Hermite expansion of the distribution function in velocity [159]–[163]; the kinetic frequency s appears as the square root of the Hermite index. Using the Wick symbol calculus we can derive equations for the evolution of f as a function of position x, wavevector k, time t, frequency ω, velocity v and kinetic frequency s. The interpretation of the symbol equation using complex velocities gives the effects of phase mixing and anti-phase mixing, identified in [123] as propagation in kinetic frequency s with velocity proportional to the wavevector k. The exact form of the product formula gives a term allowing the field E to couple the phase mixing and anti-phase mixing parts of phase space as discussed in [123], a term proportional to the kinetic frequency s and hence more effective for large s.

The Vlasov equation for the distribution function $f(x, v, t)$ in this case is given by

$$\partial_t f + v\partial_x f + E\partial_v f = 0, \tag{4.62}$$

where the charge and mass of the particles have been set equal to one. Introducing the complex coordinates $\chi = x + ik$, $\tau = t + i\omega$, and $\nu = v + is$ (suppressing the width parameters σ_x, σ_t, σ_v for clarity), the equation for the symbol S of $f\phi_0^\dagger$ is

$$\partial_{\overline{\tau}} S + v\partial_{\overline{\chi}} S + ik\partial_{\overline{\nu}} S + i(\omega + kv)S = -i(s\mathcal{E}) \odot S, \tag{4.63}$$

where $\mathcal{E}$ is the symbol of multiplication by E, related to the windowed Fourier transform of E. Reading off the complex velocities, this equation tells us that S propagates in position x with velocity v. The term $ik\partial_{\overline{\nu}} S$ tells us that the kinetic frequency s shifts at a rate $-k$. Phase mixing is the shift to shorter velocity

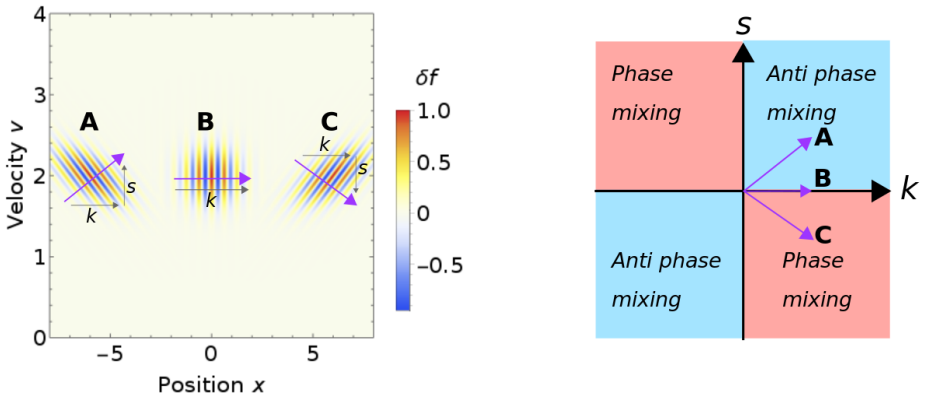

Figure 4.10: The evolution of a perturbation of the distribution function f through three consecutive stages A, B and C. The perturbation is shown in the position-velocity (x-v) phase space in (a) as it evolves in the shear flow in phase space. The evolution of the perturbation in kinetic frequency - wavevector space (s-k) is shown in (b) . As the relative sign of k and s change, the perturbation passes from an anti-phase mixing to a phase mixing part of the phase space.

scales, anti-phase mixing to larger. The kinetic frequency s can be negative, so the condition for phase mixing is not that $k < 0$ but that the wavevector k and kinetic frequency s have opposite signs, while anti-phase mixing will occur if they have the same sign. This can be understood by considering the effect of the shear flow in the space x and v on a wavepacket with given k and s. Figure 4.10 shows the evolution of a perturbation of the distribution function in the shear flow in phase space at three successive instants. Initially the perturbation has $k > 0$ and $s > 0$, and the shear acts to reduce s in magnitude, so we have anti-phase mixing. Once s changes sign the shear acts to increase it in magnitude, so we have phase mixing. The term on the right hand side couples waves with the same x, v and s but different k, since E is independent of v so $\mathcal{E}$ is independent of v and s. It is proportional to kinetic frequency s and so more effective for large s, that is in parts of phase space corresponding to shorter scale variations in velocity. Coupling between modes with opposite signs of k gives coupling between phase mixing and anti-phase mixing modes (since s is unchanged) [123].

The field E is sourced by the charge density of the particles described by f. It can also contain external contributions from fields already in the plasma. In

case E is a sum of the self-generated field E_1 and a large scale time independent external field E_2, we can expand the term in $\mathcal{E}_2$ to give

$$\partial_{\overline{\tau}} S + (v + 2is\partial_{\chi}\mathcal{E}_2)\partial_{\overline{\chi}} S + (\mathcal{E}_2 + ik)\partial_{\overline{\nu}} S + i(\omega + kv + s\mathcal{E}_2)S = -i(s\mathcal{E}_1) \odot S. \tag{4.64}$$

Again looking at the complex velocities, one effect of the external field is to increase the velocity at a rate $\mathcal{E}_2$, which is correct given that the charge and mass of the particles have been set equal to one. However it also shifts the wavevector k at a rate $-s\partial_x\mathcal{E}_2$. The mechanism is similar to the one in Figure 4.10, since an electric field gradient causes a shear in velocity. This effect is of interest since it is proportional to kinetic frequency s, and so becomes stronger as phase mixing progresses, and shifts the wavevector k and so could move the pulse into an anti-phase mixing part of phase space if it changes the sign of k.

4.5.1 Relation to Hermite expansions

Expansions in terms of Hermite functions have been widely used in kinetic theory [159]–[163]. Hermite polynomials are naturally well suited to kinetic problems since they are orthogonal with respect to a Gaussian weight function, such as the Maxwellian velocity distribution. In fact Hermite functions are also very closely related to the coherent states and Wick symbols above [53]; this can be understood since the Hermite functions are eigenfunctions of the Fourier transform [164], that is they generalize the property that 'the Fourier transform of a Gaussian is a Gaussian,' and this together with their tie to the Gaussian weight function via the Hermite polynomials makes them uniquely adapted to the windowed Fourier transform. The Wick symbol method can be used to derive a hierarchy of equations for Hermite coefficients as used in [123] by treating x and t as parameters and applying the symbol method only to the velocity coordinate. Here I illustrate the method by deriving a hierarchy of equations for time-frequency symbols from the time-frequency-position-wavevector symbol equation for the advection equation.

The definition of Hermite function most suited to our present conventions is

$$H_n(x) = \frac{1}{(\pi\sigma)^{1/4}} e^{\frac{-x^2}{2\sigma}} h_n\left(\frac{x}{\sqrt{\sigma}}\right), \tag{4.65}$$

where $h_n(x)$ is the n^{th} Physicists' Hermite polynomial (for example $h_0(x) = 1$, $h_1(x) = 2x$, $h_3(x) = -2 + 4x^2$). Note that H_n depends on σ though as with the coherent states ϕ_z we do not indicate this unless necessary. The Hermite functions so defined satisfy the identity

$$\int \phi_z(x) H_n(x)\,\mathrm{d}x = \left(\frac{z}{\sqrt{\sigma}}\right)^n, \tag{4.66}$$

and so $\phi_z^\dagger H_n = (\overline{z}/\sqrt{\sigma})^n$; in this representation the Hermite functions act as the monomials [53]. Defining A_n as the symbol of the operator $H_n\phi_0^\dagger$, and now taking $\sigma = 1$ for clarity, we have

$$A_n(\overline{z}, z) = e^{\frac{-z\overline{z}}{2}} \overline{z}^n. \tag{4.67}$$

Due to the simple form of the A_n, taking their $\partial_{\overline{z}}$ derivatives leads to useful identities for the A_n which are equivalent to Hermite function identities, such as

$$(\partial_{\overline{z}} + ik)A_n = nA_{n-1} - \frac{1}{2}A_{n+1}, \tag{4.68}$$

and

$$(\partial_{\overline{z}} + x)A_n = nA_{n-1} + \frac{1}{2}A_{n+1}, \tag{4.69}$$

which are equivalent to two recurrence relations for Hermite functions [165]. Expanding a given symbol S in terms of the A_n is equivalent to a Taylor series expansion of the analytic function F for which $S = e^{\frac{-\overline{z}z}{2}} F$ (Section 3.4.2), since

$$\begin{aligned} S(\overline{z}, z) &= e^{\frac{-\overline{z}z}{2}} F(\overline{z}) && (4.70)\\ &= e^{\frac{-\overline{z}z}{2}} \left(a_0 + a_1\overline{z} + \frac{a_2}{2!}\overline{z}^2 + \dots\right) && (4.71)\\ &= a_0 e^{\frac{-\overline{z}z}{2}} + a_1 e^{\frac{-\overline{z}z}{2}}\overline{z} + \frac{a_2}{2!} e^{\frac{-\overline{z}z}{2}}\overline{z}^2 + \dots && (4.72)\\ &= a_0 A_0 + a_1 A_1 + \frac{a_2}{2!}A_2 + \dots, && (4.73) \end{aligned}$$

where the a_n are the Taylor coefficients of F. Using this series expansion together with the derivative identities allows us to convert a given symbol equation for S into a hierarchy of equations for the a_n, as we now demonstrate for the advection equation. Taking $g(x,t) = 0$ in the equation (4.24) for a wave in a medium gives the phase space representation of the advection equation $\partial_t u + c\partial_x u$ as

$$\partial_{\overline{\tau}} S + c\partial_{\overline{\chi}} S + i(\omega + kc)S = 0. \tag{4.74}$$

Now we expand S as a series in $A_n(\overline{\chi}, \chi)$, with coefficients $a_n(\overline{\tau}, \tau)$ depending on τ,

$$S(\overline{\tau}, \tau, \overline{\chi}, \chi) = \sum_{n=0}^{\infty} \frac{a_n(\overline{\tau}, \tau)}{n!} A_n(\overline{\chi}, \chi), \tag{4.75}$$

in terms of which

$$\partial_{\overline{\tau}} S + c\partial_{\overline{\chi}} S + i(\omega + kc)S = \sum_{n=0}^{\infty} \frac{1}{n!}(\partial_{\overline{\tau}} a_n + i\omega a_n)A_n + c\sum_{n=0}^{\infty} \frac{a_n}{n!}(\partial_{\overline{\chi}} + ik)A_n \tag{4.76}$$

$$= \sum_{n=0}^{\infty} \frac{1}{n!}(\partial_{\overline{\tau}} a_n + i\omega a_n)A_n + c\sum_{n=0}^{\infty} \frac{a_n}{n!}(nA_{n-1} - \frac{1}{2}A_{n+1}) \tag{4.77}$$

$$= \sum_{n=0}^{\infty} \frac{1}{n!}\left(\partial_{\overline{\tau}} a_n + i\omega a_n + c\left(a_{n+1} - \frac{n}{2}a_{n-1}\right)\right)A_n \tag{4.78}$$

where we have applied the derivative identity (4.68) and relabelled terms in the sum, with the convention that $a_{-1} = 0$. Now since the A_n are proportional to $\overline{\chi}^n$, we can equate each coefficient of $\overline{\chi}^n$ to zero to give the hierarchy of equations

$$\partial_{\overline{\tau}} a_n + i\omega a_n + c\left(a_{n+1} - \frac{n}{2}a_{n-1}\right) = 0 \tag{4.79}$$

for $n = 0, 1, 2, 3, \ldots$ for the symbols a_n which depend only on time and frequency. In this way the symbol method is most naturally related to hierarchies of equations for Hermite function coefficients, which we would be led to simply by considering Taylor series.

4.6 Summary

In this chapter I have derived new complex phase space representations of wave equations using the Wick symbol calculus. The study of an oscillator with varying

frequency illustrated the process by which an equation of motion is translated into an equivalent operator equation, the symbol of which gives the phase space representation. The use of the exact integral form of the product formula was shown to give coupling between frequency sidebands, and the way in which the asymptotic expansion of the product formula gave a local description in terms of complex velocities studied in detail. The phase space representation of a wave equation for wave propagation in a medium was derived, illustrating how the asymptotic expansion of the product formula treated frequency and wavevector shifts while the exact product formula gave coupling nonlocal in frequency and wavevector but localized in position and time. Dispersion and sources were also treated. A phase space representation of the nonlinear Schrödinger equation was derived with a ponderomotive force term which naturally included the smoothing of the wave envelope, and a numerical solution analyzed to explain soliton propagation as an overturning in phase space driven by a ponderomotive force. A mode conversion problem was solved by integrating the phase space equation along complex characteristics, with the amplitude and phase of the pulse studied throughout the interaction and compared with a numerical solution. A complex phase space representation of the Vlasov equation including both velocity and kinetic frequency coordinates was derived, and an interpretation of phase mixing and anti-phase mixing given in this framework. The application of the method to derive hierarchies of equations for Hermite function coefficients using Taylor series in z was derived. In the next chapter the structure of incoherent fields will be studied in terms of their complex phase space distributions.

5

Coherence and phase dislocations

The phase space representation of plasma waves has strong historical ties with incoherent wave fields and random phase approximations. Quasilinear theories of weak turbulence and wave kinetics [81] employ a position-wavevector phase space representation of an incoherent wave field as a 'sea of quasiparticles,' with a real and positive distribution function analogous to the particle distribution function $f(x, v, t)$ for a distribution of particles in kinetic theory. The theory and examples of previous chapters make no assumptions on the coherence of the wave field, but it is of interest to see how incoherent fields are represented in this framework both because of the historical ties to incoherence and because the complex phase space description gives a useful characterization of incoherence in terms of phase dislocations, zeros in the distribution caused by intersections in contours of the distribution's phase. I begin by presenting some quantitative measures of coherence and their relation to the windowed Fourier transform.

5.1 Coherence

I begin with some conventional measures of coherence for later theoretical comparison and numerical computation. To fix ideas, Figure 5.1 shows four fields which we would intuitively consider as a) coherent, b) incoherent, c) partially coherent, and

d) coherent on the left, becoming gradually more incoherent to the right. These judgements reflect an intuitive definition of incoherence as 'messiness' or irregularity, present in b) but missing in a), as well as the possibility of different degrees of coherence c) which can even be localized as in d). The definitions that follow try to make precise these judgements. I will present a degree of coherence function [166] and in terms of it a coherence length which reflects roughly 'how long the field remains in step with itself'. These are global quantities, which can be localized using a windowing technique (much as in the windowed Fourier transform). Both of these quantities are derived from the autocorrelation of the field, and take advantage of the fact that the sort of field we would like to call coherent overlaps well with itself when translated by an appropriate distance. I then discuss another quantity, the entropy of the field [167], which can be thought of as a more discriminating version of the time-bandwidth product of the field which appears in traditional uncertainty relations, and which can also distinguish coherent from incoherent pulses.

5.1.1 Coherence length

The correlation $C_{fg}(\tau)$ between two functions f and g is defined as

$$C_{fg}(\tau) = \int_{-\infty}^{\infty} \overline{f}(t) g(t-\tau)\,\mathrm{d}t, \tag{5.1}$$

and the autocorrelation $A_f(\tau)$ of a function f as the correlation of f with itself, $C_{ff}(\tau)$, and so

$$A_f(\tau) = \int_{-\infty}^{\infty} \overline{f}(t) f(t-\tau)\,\mathrm{d}t. \tag{5.2}$$

The correlation is a sort of sliding dot product, giving the overlap between two functions subject to a relative delay τ. The correlation C_{ff} is related up to a minus sign in the definition to the convolution with f and g, and so interacts well with the Fourier transform via the convolution theorem.

The degree of coherence function $g_f(\tau)$ is defined as a normalized autocorrelation,

$$g_f(\tau) = \frac{A_f(\tau)}{|f|^2} \tag{5.3}$$

$$= \frac{\int_{-\infty}^{\infty} \overline{f}(t) f(t-\tau)\,\mathrm{d}t}{\int_{-\infty}^{\infty} \overline{f}(t) f(t)\,\mathrm{d}t} \tag{5.4}$$

and is useful for the definition of coherence properties since it is independent of the amplitude of f (in the sense that multiplying f by a constant does not change g_f) and g is dimensionless. The whole function g can be of interest, but we can define a summary parameter as the norm of g (suppressing the subscript f), the coherence time t_c

$$t_{\mathrm{c}} = \int_{-\infty}^{\infty} |g(\tau)|^2 \, \mathrm{d}\tau. \tag{5.5}$$

So defined the coherence time t_{c} has dimensions of time (from the $\mathrm{d}\tau$ in the integral), and is the norm of the degree of coherence function. Both the degree of coherence $g_f(\tau)$ and the coherence time t_{c} can be localized by windowing; we simply multiply f by a window centered at some time t_0 and calculate $g_f(\tau)$ and t_{c} as above, obtaining $g_f(\tau)$ and t_{c} as functions of t_0. This localization will be used in Chapter 7 to study the local coherence properties of the waves produced in a beam plasma instability.

Taking for example $f(t) = e^{-t^2/2a^2} e^{ibt}$, we can calculate t_{c} explicitly to give $\sqrt{2\pi}a$. Note that t_{c} is determined here by the envelope width a, so that a very short pulse which we might rightly think of as very coherent can have a short coherence length on account of being a short pulse.

5.1.2 Entropy

The entropy of a field is a measure of how densely packed it is in phase space; it was defined in quantum mechanics inspired by the definition of entropy in information theory and statistical mechanics [167]. The entropy as defined below is naturally a phase space quantity, depending on position and wavevector. It is useful here because, like the bandwidth or time-bandwidth product, a large entropy can be a sign of incoherence. However it can also result from a chirp for example. Inspired by quantum mechanics, the definition of the entropy is motivated by considering $|f(x)|^2$ and $|\tilde{f}(k)|^2$ as probability distributions and by the definition of the entropy in statistical mechanics and information theory as $S = -\int p(x) \log(p(x)) \, \mathrm{d}x$. These considerations serve only as motivation here; there is nothing intrinsically quantum mechanical or probabilistic in the definition, which simply associates a number

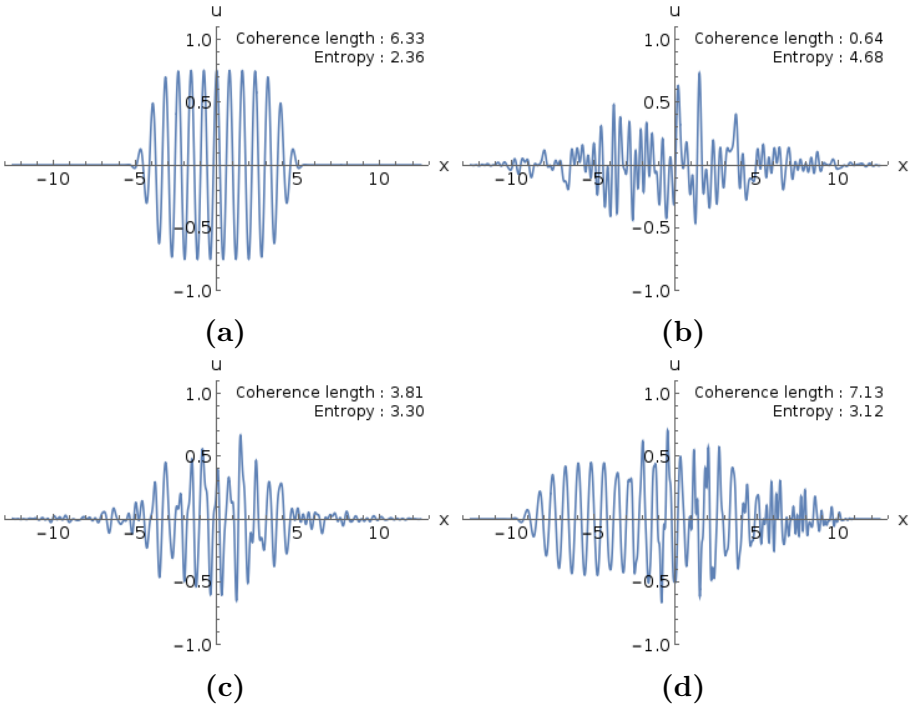

Figure 5.1: Example pulses to demonstrate the coherence length and field entropy. Both of these are global quantities, the single numbers shown associated with the whole field plotted, but local versions can be defined to treat the spatially varying coherence of pulse (d) for example.

called the entropy with a given field. The entropy of a field f which is normalized so that $|f|^2 = 1$ is then defined [167] as

$$H = H_x + H_k \tag{5.6}$$

$$= -\int_{-\infty}^{\infty} |f(x)|^2 \log(|f(x)|^2)\,\mathrm{d}x - \int_{-\infty}^{\infty} |\tilde{f}(k)|^2 \log(|\tilde{f}(k)|^2)\,\mathrm{d}k, \tag{5.7}$$

where $\tilde{f}(k)$ is the Fourier transform of f, which is here for convenience normalized as $\tilde{f}(k) = \frac{1}{\sqrt{2\pi}} \int e^{-ikx} f(x)\,\mathrm{d}x$. While each term can become arbitrarily large and negative, corresponding to taking f as a delta function $\delta(x)$ (no uncertainty in x) or a complex exponential e^{ikx} (no uncertainty in k), their sum is bounded below; this is an 'uncertainty principle' [167], and is given by

$$H \geq 1 + \log \pi. \tag{5.8}$$

A similar inequality holds in more than one dimension or if the normalization $|f|^2 = 1$ is not assumed. The entropy will here be a useful addition to the coherence

length since a short coherent pulse has a short coherence length by virtue of being short but still has a low entropy.

5.2 Phase dislocations

The windowed Fourier transform of an incoherent wave field has a structure dictated by the presence of phase dislocations, points at which the phase of the complex phase space distribution cannot be defined, causing the presence of zeros in the phase space distribution. These zeros have been studied extensively in wave trains in real space [168], in the phase space representation of a white noise field [169], and in quantum chaos [170]. Here I give examples to illustrate that the density of phase dislocations is related to the coherence of the wave field. The precise location of the dislocations depends on the realization of the incoherent wave field, and hence upon ensemble averaging the structure of the distribution is washed out to give a smooth phase space distribution.

Figure 5.2 shows the field together with the modulus and phase of its x-k phase space distribution for four pulses formed from the same wavepackets, centered at $x = 0$ with wavevectors between $k = 2$ and $k = 20$. The top row (a-c) show a completely coherent pulse with all of the wavepackets added with the same phase, with each row having progressively more randomized phases; the bottom row shows an incoherent pulse for which the wavepackets were given totally random phases. As the pulse becomes more incoherent, more and more zeros in the phase space distribution appear, which are located at positions where different contours of the phase intersect. Even a pulse which has totally random phases, which does not have nicely behaved phase fronts in real space, has well defined phase fronts in its x-k distribution, except at phase dislocations where the phase fronts intersect. In this way even random phase waves, very irregular in real space (analogous to an amorphous solid), are fairly regular when their complex phase space distributions are considered (analogous to a crystal with dislocations) [169].

Ensemble averages are often employed when deriving a wave kinetic equation. This is absolutely not forced on us here; the complex phase space description applies

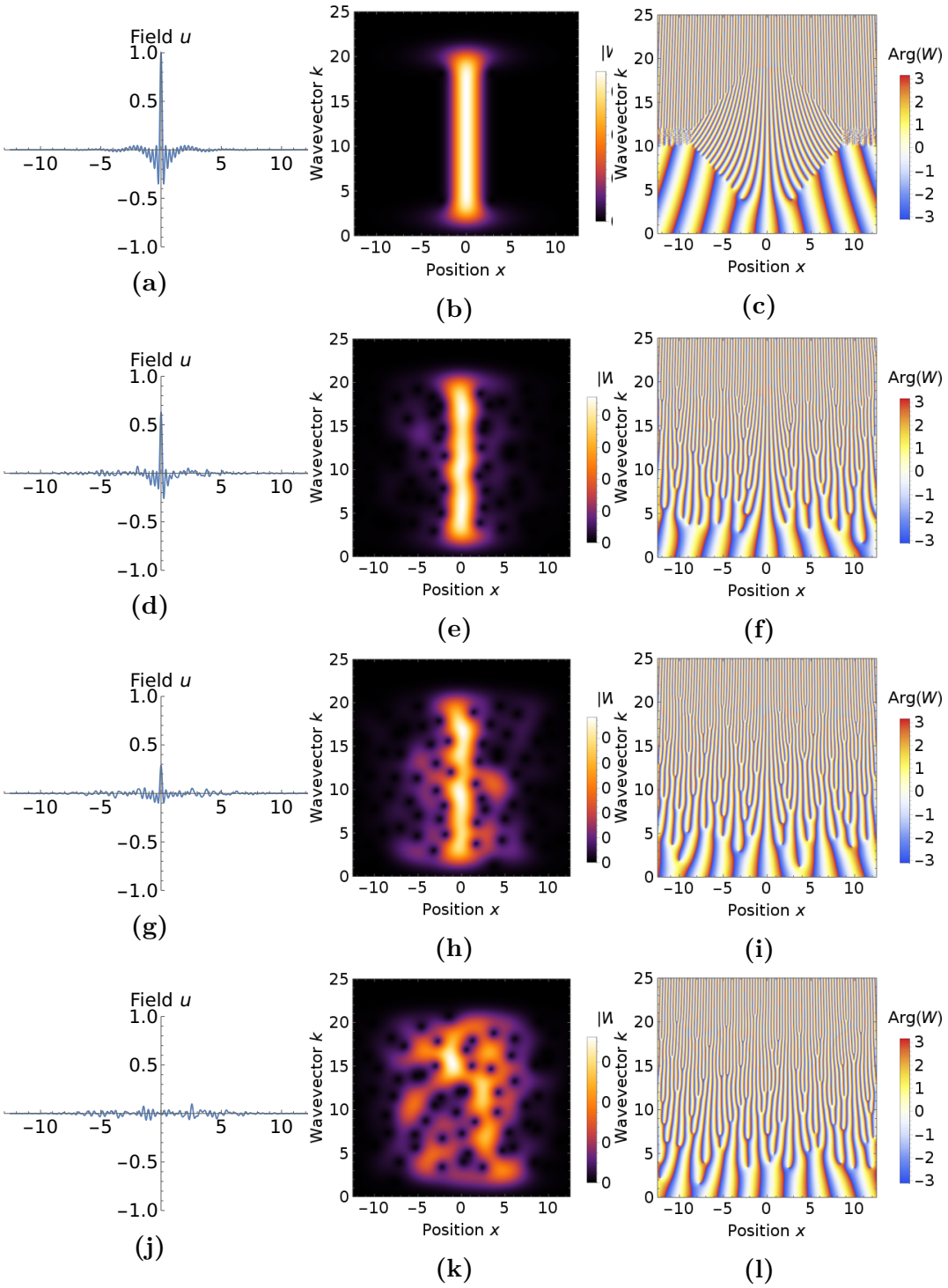

Figure 5.2: Plots of the field together with the modulus and phase of its x-k phase space distribution for pulses of varying coherence. The randomization of the pulses' phases (see text) increases going from the top row to the bottom row. The holes in the pulses' phase space distributions (middle column) result from phase dislocations where contours of their phase intersect (right column).

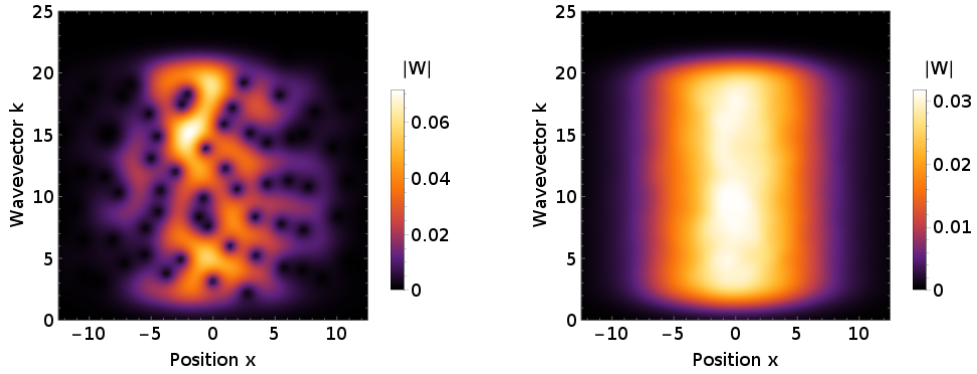

(a) $N = 1$ **(b)** $N = 500$

Figure 5.3: The effect of ensemble averaging on the modulus of the phase space distribution. The ensemble here consists of pulses made up of a sum of wavepackets with randomly assigned phases. The absolute value of the phase space distribution for a single field is shown in (a), the ensemble average of the absolute values of the phase space distributions of 500 fields in (b). The dislocation structure of the phase space distribution is washed out by the average, leaving a smooth distribution.

perfectly well to a single instance of a wave field, coherent or incoherent, and in fact gives an interesting picture of the phase space structure of a given incoherent wave field. However it may be of interest to see how the complex phase space distribution of an incoherent field, structured and non-uniform in phase space as we saw above, is related to the smooth and broad distribution in x-k space often associated with incoherent waves. We can calculate the ensemble average of the modulus of the phase space distribution over and ensemble of the random phase pulses used above. Figure 5.3 shows the result of such an average for ensemble of 500 fields. The ensemble average causes the amplitude of the phase space distribution to be reduced and it becomes very smooth; this is because the phase dislocations in each element of the ensemble are in different places. It is the smoothed out phase space distribution which is most closely analogous to the position-velocity distributions of particles in kinetic theory and which is often considered in wave kinetics.

5.3 Coherence and phase dislocations

The relationship between dislocations and coherence can be made more precise by relating the number of dislocations in a given phase space distribution to the

coherence properties of the field, in particular the coherence length and field entropy discussed above. The number of dislocations in a given phase space distribution is a dimensionless quantity, so on dimensional grounds we might guess that it is related to the field entropy, also a dimensionless quantity. Likewise the number of dislocations per unit length, or dislocation density d, has the dimensions of $[\text{Length}]^{-1}$ and so we might expect it to be related to the coherence length L according to $dL = \text{constant}$.

5.3.1 Counting dislocations with image analysis

In order to test the relationship between phase dislocations and coherence we need to be able to count the number of dislocations in a given phase space distribution. I have automated this process using image analysis, allowing large samples to be tested quickly. Figure 5.4 illustrates the steps in the image analysis pipeline. Beginning with a given field, the position-wavevector distribution is calculated, compressed to take only the values zero or one based on a threshold and the connectedness of the thresholded regions, split into components which are then filtered by size to exclude the large components in the background, these filtered components finally representing the dislocations which are then counted. The automated procedure agrees well with the count one would make by eye, and while there are cases in which two nearby dislocations may be counted as one, and the count depends to some extent on the thresholds chosen, the conclusions below are insensitive to these details. The number of dislocations also depends on the window width parameter σ used in numerically calculating the windowed Fourier transform, but for a wide range of σ the later judgements about coherence are unchanged.

5.3.2 Correlation between phase dislocations and coherence

Bandwidth of random phase waves

As a first test of the relationship between the number of dislocations and the coherence properties of the field, I have calculated the dislocation count, coherence length, and field entropy for a collection of fields made up from random phase waves with varying bandwidths. Figure 5.5 shows some representative examples

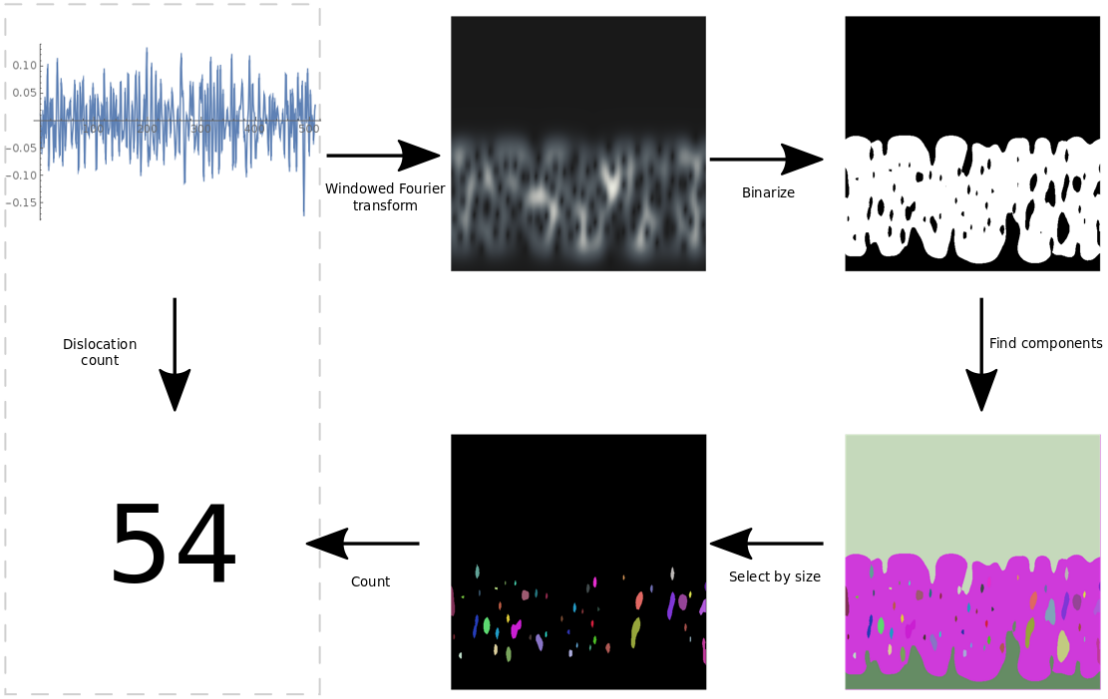

Figure 5.4: An illustration of the image analysis pipeline used to count the number of dislocations in a given phase space distribution. The windowed Fourier transform of the field is computed analytically, before the resulting distribution is binarized to take only the values zero and one based on its amplitude and connectedness properties. This image is then broken into components, which are filtered by size to exclude the background and finally counted to give the number of dislocations. This pipeline allows the test of the relationship between phase dislocations and coherence properties.

of these fields; they are homogeneous in position and become more irregular as the bandwidth is increased, as is to be expected.

Figure 5.6 shows the correlation between the number of dislocations and the coherence length (a) and field entropy (b). The coherence length decreases with the number of dislocations, so here the number of dislocations gives a good indication of the degree of coherence of the field. The entropy increases with the number of dislocations, once again indicating that the number of dislocations is correlated with the degree of coherence of the field. The coherence length varies as the reciprocal of the dislocation count, as might be expected by a dimensional argument since the fields in this case are homogeneous so the dislocation density is proportional to the dislocation count. Since the windowed Fourier transform depends locally on the

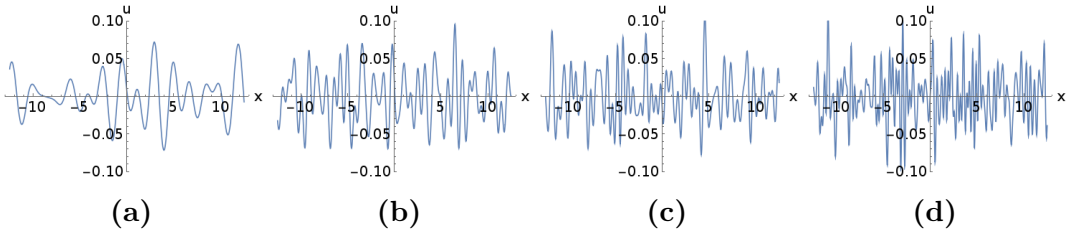

Figure 5.5: Examples of the fields made up of random phase waves of varying bandwidths (a-d) used to test the relationship between phase dislocations and coherence.

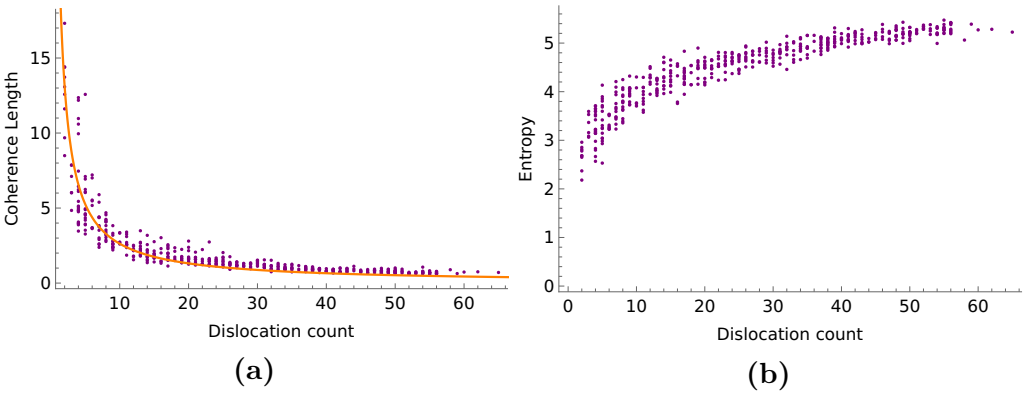

Figure 5.6: Plots showing how the coherence length (a) and the field entropy (b) are correlated with the number of dislocations in the phase space distribution for a collection of homogeneous random phase fields of varying bandwidth. The correlation length decreases with the number of phase dislocations, while the entropy increases, showing that the number of phase dislocations gives a good measure of the degree of incoherence of the field. The orange curve shows a $1/x$ fit as might be expected on dimensional grounds.

field, it is likely that the local density of dislocations determines the local coherence length; this is supported by the fact the Fourier transform in k of the modulus of the windowed Fourier transform is related to a local autocorrelation function [73].

Degree of phase randomization

To further understand the relationship between phase dislocations and coherence I considered a collection of fields made up by adding together the same set of waves but with the random phases added to each, the phases being drawn from $[-m\pi, m\pi]$ with m a parameter between zero and one. Each field thus had the same bandwidth and varied from completely in phase, for $m = 0$, to completely random phase, for $m = 1$. Figure 5.7 shows some examples of the fields in this collection; with no phase randomization the waves give a short coherent pulse, and as the phase

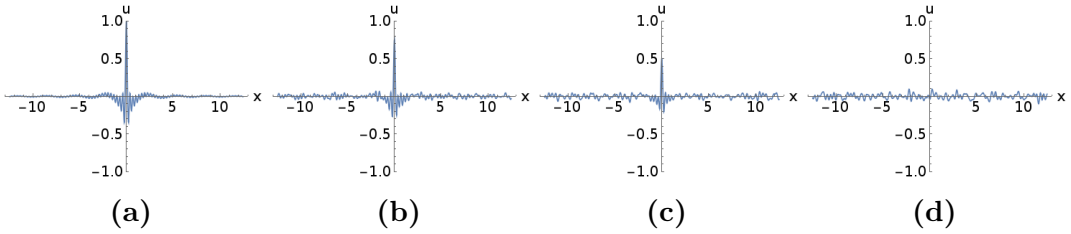

Figure 5.7: Examples of the fields made up of random phase waves of varying degrees of phase randomization (a-d) used to test the relationship between phase dislocations and coherence.

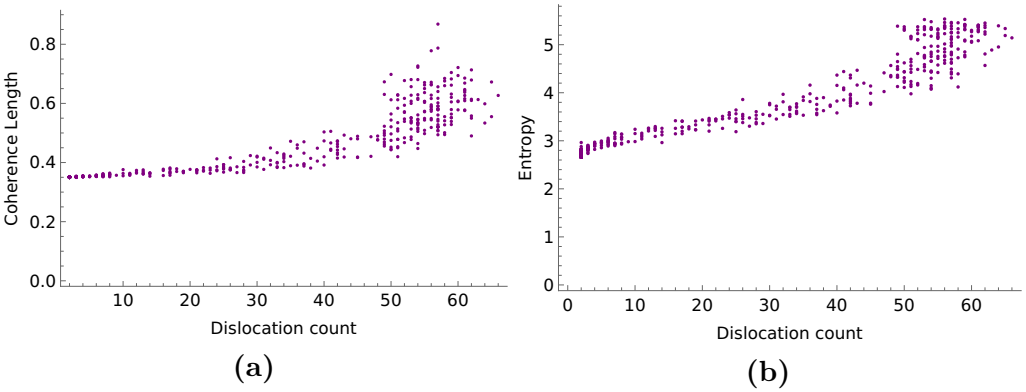

Figure 5.8: The correlation between the dislocation count and the coherence length (a) and field entropy (b) in a collection of fields of varying degrees of phase randomization. In this case the entropy increases with the dislocation count, reflecting the tie between phase dislocations and incoherence. For these fields the coherence length in fact increases as the phases become more randomized, since the fields with ordered phases are short pulses.

randomization increases the pulse is spread out and becomes less coherent.

Figure 5.8 shows the relationship between the dislocation count and the coherence length and entropy, as in the Figure 5.6 but here for a physically different collection of fields. Once again the entropy increases with the dislocation count, consistent again with a high dislocation count indicating incoherence. But in this case the coherence length increases with the dislocation count. This is due to the coherence length being short even when the phases are not randomized at all because in this case the field has the form of a short pulse. So this increase of coherence length with dislocation count does not reflect a breakdown of the relation between phase dislocations and incoherence, but rather the inappropriateness of the coherence length as a measure of the coherence of a short pulse.

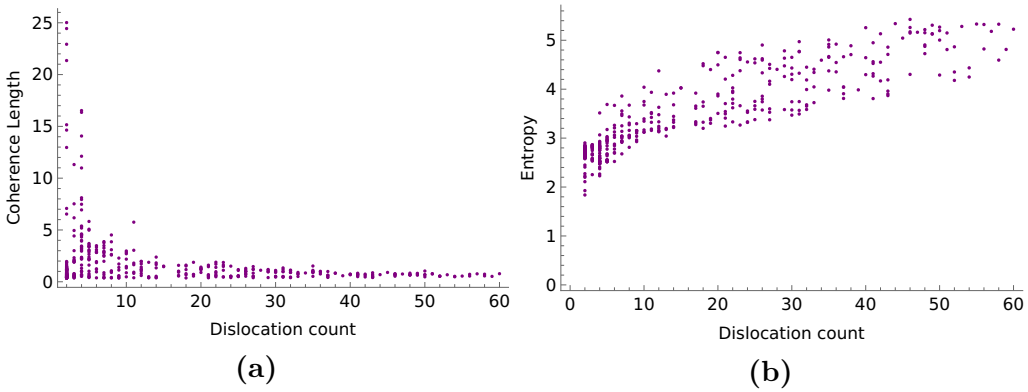

(a) (b)

Figure 5.9: The correlation between the coherence length (a) and field entropy (b) with the number of phase dislocations for a collection of pulses of varying bandwidth and phase randomization. While the coherence length is short for short coherent pulses with few dislocations, the entropy and dislocation count are correlated even in this very diverse collection of fields.

Bandwidth and degree of randomization

As a final test of the relationship between dislocations and coherence I considered a collection of fields of both varying bandwidth and varying degree of coherence, each as in the previous two examples. This collection of fields contained very diverse pulses, including short coherent pulses of varying lengths with no phase randomization and varying bandwidth, as well as partially coherent pulses of varying duration and coherence length.

Figure 5.9 shows the relationship between the dislocation count and the coherence length and the field entropy for this collection of pulses. The entropy is still strongly correlated with the dislocation count, even for this very diverse collection of fields. The coherence length is no longer as closely connected with the dislocation count, with short coherence lengths present at essentially all dislocation counts. This reflects the fact that in this collection there are both short coherent pulses and homogeneous wide bandwidth random phase fields, both of which have short coherence lengths, but the short coherent pulses, as we saw above, have very few phase dislocations while the wide bandwidth random phase fields have many.

It seems intuitively reasonable that the field entropy is so closely related to the number of phase dislocations, since the field entropy measures how densely the field is packed in phase space, with a large entropy indicating that the field is more

spread out in phase space than is required by the uncertainty principle (as expressed by the lower bound on the entropy discussed above), and the presence of holes in the phase space distribution necessarily spreads it out over phase space. In this connection it is worth noting that the integral of the modulus squared of the phase space distribution over phase space $\iint |W(x,k)|^2 \,\mathrm{d}x\,\mathrm{d}k$ is equal to a constant times the norm of the field $\int |f(x)|^2 \,\mathrm{d}x$ [56], so as we consider randomizing the phases of the waves in f we leave the 'energy' of W in phase space unchanged. The presence of many dislocations is a clearer signal of incoherence than a large bandwidth, large entropy, or short coherence length, since these can all be associated with coherent fields (short or chirped pulses for example). In this way the density of phase dislocations appears to map our intuitions on coherence quite closely.

5.4 Summary

In this chapter I have studied the relationship between dislocations in phase space distributions, zeros associated with intersecting contours of the distributions' phase, and the coherence properties of fields. The dislocation structure was shown to be washed out by an ensemble average, giving a smooth phase space distribution as often associated with incoherent fields. An image analysis pipeline for counting the dislocations in a given phase space distribution was developed, allowing the study of the relationship between phase dislocations and the entropy and coherence length of the field. The field entropy was found to be correlated with the number of phase dislocations for a wide range of fields, including homogeneous random phase waves and short coherent pulses. The density of dislocations was discussed as an effective formalization of the intuitive notion of partial coherence. In Chapter 7 the phase dislocations in plasma waves from simulations of beam plasma instability will be studied numerically. The next chapter presents instability calculations in preparation for these simulations.

6 Instabilities

6.1 Introduction

In the following two chapters I study the instability of crossing electron beams in a plasma, with a view to both applying the theory developed in the previous chapters and to understanding a potential scheme for plasma heating using crossing electron beams. As we will see the electron beams produce waves in the plasma as they become unstable, and the phase space representation of these waves gives insight into this heating process.

Plasma heating by electron beams is the subject of intense study due to its varied applications, such as warm dense matter production [171], laboratory astrophysics [172], and magnetic and inertial confinement fusion [173], [174], and the insights into fundamental plasma theory it provides. These electron beams can be produced by the absorption of a high power laser pulse by an overdense material [175]. While beam electrons may give up their energy simply by colliding with particles in the plasma [176]–[179], the collective process of beam-plasma instability, in which the beam electrons act together to drive plasma waves, can also efficiently extract energy from the beam [18]. Further, this collisionless stopping process may be effective even for relativistic electron beams whose collisional stopping length is much longer than the target. On a coarse level, we might expect collisionless stopping (a

collective effect) to be relevant for plasmas with a large plasma parameter [139]. Even for densities well above solid density the plasma parameter may be large at sufficiently high temperatures. In particular, the plasma parameter is large for the conditions in the hot spot of an inertial confinement fusion isobaric compression, but not in the dense fuel layer surrounding the hot spot (due to the relatively low temperature of the dense fuel). Representative inertial confinement hot spot and fuel parameters may be found in [180]–[182].

An analytic treatment of the collective stopping of a single relativistic electron beam was given in [183], calculating the parameters which favor collective stopping and examining strategies to localize the energy deposition. Other studies include theoretical treatments of beam-plasma instabilities [184], [185], collective stopping of electron beams [97], [186], [187], Vlasov-Poisson simulations of collective heating [188] and ion-acoustic wave decay [189], as well as experiments on nonlinear coupling between plasma waves [190] and on plasma heating by counter-propagating laser-generated electron beams [191], [192]. Recent reviews of laser-plasma interaction [193] and fast electron transport [179] contain much detailed information together with further references. In this chapter I begin by presenting some general methods for the understanding of instabilities before applying these methods to study the instability of crossing electron beams in a plasma.

6.2 Methods

6.2.1 Complex dispersion surface

As a preliminary definition we will call a wave unstable if it grows exponentially in time. We saw in Chapter 1 that when analyzing functions which grow exponentially we use the Laplace transform rather than the Fourier transform, and we saw some of the resulting complexity. However for synthesizing solutions of linear(ized) wave equations we can employ the principle of superposition to add together any solutions, exponentially growing or otherwise. When studying stable waves we write one of

the solutions constructed from superpositions of plane waves (in space and time) as

$$u(x,t) = \int_D g(s) e^{i(-\omega t + kx)} \, \mathrm{d}s, \tag{6.1}$$

where D is the dispersion surface. Taking the advection equation as an example, D is determined by substituting a plane wave $e^{i(-\omega t+kx)}$ into the advection equation $\partial_t u + a\partial_x u = 0$, giving the condition

$$\omega - ka = 0, \tag{6.2}$$

so here D is the line $\omega = ka$ in (ω, k) space. For the purposes of constructing a solution by superposition we do not need to introduce the Fourier transform explicitly; we simply argue that (6.1) is a solution since it is a sum of solutions $e^{i(-\omega t+kx)}$. The integral is really a 1D integral along the dispersion surface here, rather than a 2D integral across the entire ω-k plane as a Fourier transform of a function of two variables would ordinarily be (as we saw in Chapter 2, this is in fact because the Fourier transform contains a delta function restricting it to the dispersion surface). For example if we parameterize D as $(\omega, k) = (as, s)$ and use $g(s) = e^{-s^2/2}$, our solution is

$$u(x,t) = \int e^{-s^2/2} e^{i(-ast+sx)} \, \mathrm{d}s \tag{6.3}$$

$$= \sqrt{2\pi} e^{-(x-at)^2/2}, \tag{6.4}$$

that is a Gaussian translating to the right at speed a. Figure 6.1 (a) shows the dispersion surface $\omega = ka$ as a purple line, along with the function $g(s)$, plotted as a 2D distribution confined to the dispersion surface.

Now we can construct a more general solution by noting that $e^{i(-\omega t+kx)}$ is a solution whenever $\omega = ka$, even if ω and k are complex. Since we are here only interested in synthesizing a solution we do not need to introduce the Laplace transform explicitly (but see Chapter 2), simply applying the principle of superposition. In this case our solution is

$$u(x,t) = \int_{D_c} g(s) e^{i(-\omega t + kx)} \, \mathrm{d}s, \tag{6.5}$$

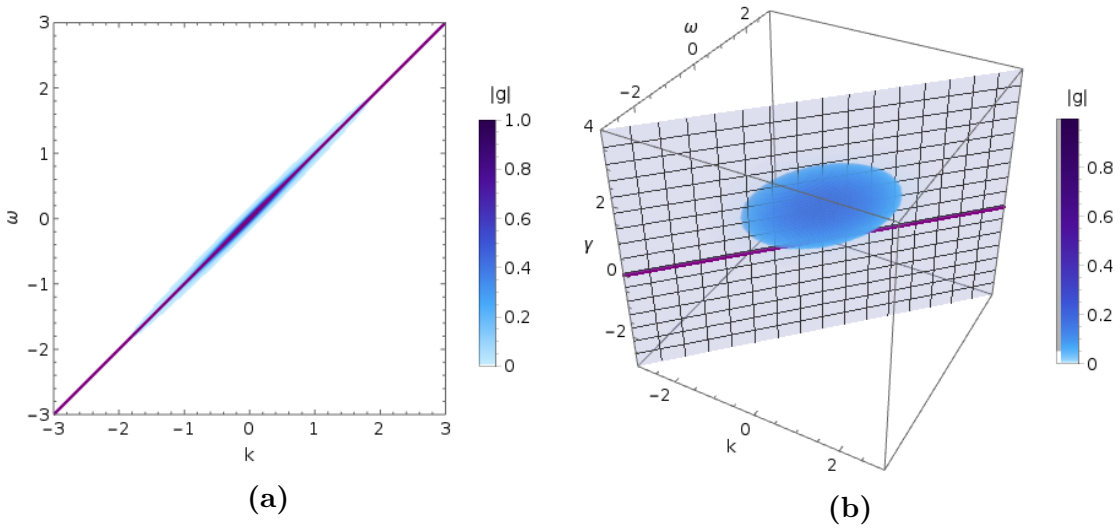

Figure 6.1: The real (a) and complex (b) dispersion surfaces for the advection equation $\partial_t u + a\partial_x u = 0$, here with $a = 1$. In this case the dispersion surfaces are give by $\omega = ak$. The distribution of waves indicated in blue on the real dispersion surface superpose to give a translating Gaussian, while the distribution of waves on the complex dispersion surface gives a translating exponential.

where D_c is now a surface in the four (real) dimensional space of (Ω, K), complex frequencies Ω and complex wavevectors K, defined by $\Omega - Ka = 0$, a surface which we will call the complex dispersion surface. For the advection equation D_c is two dimensional, a two dimensional surface in $\mathbb{C}^2$. For example if we parameterize D_c as $(\Omega, K) = (a(\alpha + i\beta), \alpha + i\beta)$ and take $g(\alpha, \beta) = e^{-(\alpha^2+(\beta-1)^2)/2}$, then our solution constructed as a superposition is

$$u(x,t) = \int e^{-(\alpha^2+(\beta-1)^2)/2} e^{i(-a(\alpha+i\beta)t+(\alpha+i\beta)x)} \, \mathrm{d}\alpha \mathrm{d}\beta \tag{6.6}$$

$$= 2\pi e^{at-x}. \tag{6.7}$$

The solution $2\pi e^{at-x}$ is simply an exponential translating to the right at speed a. Figure 6.1 (b) shows the complex dispersion surface together with the distribution $g(\alpha, \beta)$ which gave the translating exponential by superposition. The surface is really a surface in the four dimensional space of complex frequencies and wavevectors Ω and K, or if we introduce their real and imaginary parts according to $\Omega = \omega + i\gamma$, $K = k + i\kappa$, the space of $(\omega, \gamma, k, \kappa)$. We have plotted the surface in (ω, γ, k) space, with different values of κ specifying different curves lying in the plotted surface. In particular we have indicated the curve $\kappa = 0$ by the purple line. One

often restricts waves to have $\kappa = 0$ since if $\kappa \neq 0$ the wave grows exponentially in space, however these modes are required for example for studying waves at surfaces [194] or distinguishing between convective and absolute instabilities [195], [196]. In this case the curve $\kappa = 0$ lies entirely in the plane $\gamma = 0$, and in fact coincides with the real dispersion curve plotted in Figure 6.1 (a). In the next section this will not be the case; there are solutions with $\gamma \neq 0$, $\kappa = 0$ which are bounded in space but grow exponentially in time.

6.2.2 Model equations

In order to study the physics of instabilities most simply and to introduce the method which I will later apply to beam plasma instabilities, I present a model set of equations which describe two interacting systems each described by a single function. These equations are equivalent to the weak coupling dispersion relation given in [195]. Electron beams are described at least by their density and velocity, two degrees of freedom, and the additional degrees of freedom give additional branches which do not participate in the instability. The model equations are

$$\partial_t f + a\partial_x f = cg \tag{6.8}$$

$$\partial_t g + b\partial_x g = cf, \tag{6.9}$$

where f describes a system travelling with velocity a, g describes a system travelling with velocity b, and the systems interact with a strength proportional to c (roughly analogous to the charge of the particles in a beam). The strategy is to find the complex dispersion surface, just as we did above for the advection equation. Trying a solution $f = Ae^{i(-\Omega t + Kx)}$, $g = Be^{i(-\Omega t + Kx)}$, where Ω and K are the complex frequency and wavevector, or in matrix form $[f, g] = [A, B]e^{i(-\Omega t + Kx)}$, we obtain

$$\begin{bmatrix} -i(\Omega - Ka) & c \\ c & -i(\Omega - Kb) \end{bmatrix} \begin{bmatrix} A \\ B \end{bmatrix} = 0 \tag{6.10}$$

For a non-zero solution for $[A, B]$ we require $\det(M) = 0$, where M is the matrix multiplying $[A, B]$ in equation (6.10), a condition giving a quadratic equation in

Ω and K which can be solved to give $\Omega = \Omega_\pm$ with

$$\Omega_\pm = \frac{K(a+b) \pm \sqrt{K^2(a-b)^2 - 4c^2}}{2}. \tag{6.11}$$

This equation explicitly gives us the complex dispersion surface, with the $\pm$ giving two branches of the dispersion surface, corresponding to the two degrees of freedom f and g. It applies for complex K, and will in general give a complex Ω. To look for spatially bounded instabilities we consider real K, that is set $\kappa = 0$, in which case we have an instability (a solution with $\gamma > 0$) if $|k| < |2c/(a-b)|$, or for all k if $b = a$. If $b = a$, that is both systems move with the same velocity, then $\Omega = ka \pm \sqrt{-c^2}$, so we have an instability with growth rate $\gamma = |c|$ for all k. If $b = -a$, so the systems travel with the same speed but in opposite directions, we have $\Omega = \pm\sqrt{K^2a^2 - c^2}$, so considering modes with $\kappa = \mathrm{Im}(K) = 0$, we have an instability if $|c| > |ka|$, in which case ω is purely imaginary. Figures 6.2 and 6.3 show the frequency and growth rate curves and the complex dispersion surfaces for the systems with $a = 1$, $b = 1$ and $a = 1$, $b = -1$.

Having found the complex dispersion surface from the condition $\det(M) = 0$, we can continue to find the solutions for the amplitudes A and B corresponding to each point on the dispersion surface. For a solution the vector $[A, B]$ must be an eigenvector of M with eigenvalue zero. The vector $[A, B]$ corresponding to a given mode on the dispersion surface is called the polarization vector of the mode, since in solving Maxwell's equations by these methods it indeed gives the optical polarization. A little algebra gives the polarization vectors $P_\pm$ corresponding to the two branches $\Omega_\pm$ as

$$P_\pm = \begin{bmatrix} i\left(\frac{K(b-a)}{2c} \pm \sqrt{\frac{K^2(b-a)^2}{4c^2} - 1}\right) \\ 1 \end{bmatrix}. \tag{6.12}$$

The polarizations are determined only up to an overall constant factor (so long as the zero of the dispersion they correspond to is a single root, else only the subspace they span is determined). In case the systems have the same velocity, that is $a = b$, the $P_\pm$ simplify considerably, giving $P_\pm = [\pm 1, 1]$, and so the modulus of the amplitude of oscillation of f and g is always the same, and for the growing

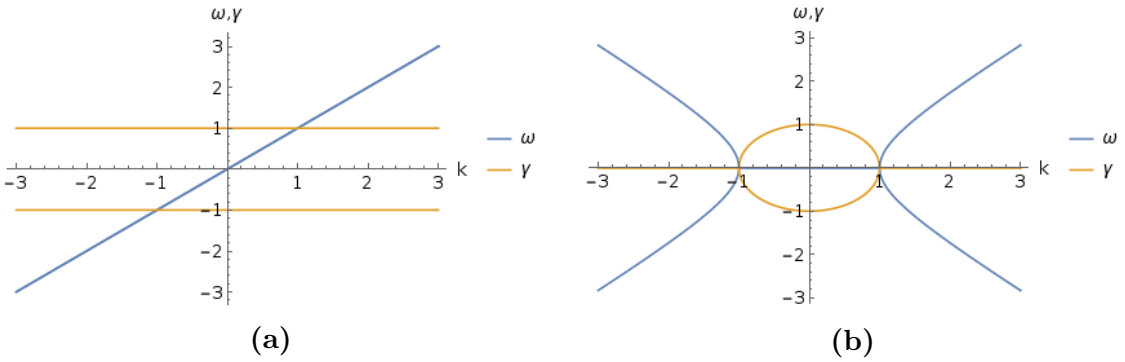

Figure 6.2: The frequencies and growth rates for the model equations for two systems travelling (a) with the same velocity ($a = 1$, $b = 1$) and (b) with opposite velocities ($a = 1$, $b = -1$). For systems with the same velocity the growth rate of the instability is the same for all wavevectors k, while for systems with opposite velocities there is only instability in a band of wavevectors centered at zero.

solution they are in phase, while for the decaying solution they are π out of phase. This can be understood physically, since in this case the disturbances in f and g have the same size and $f = \pm g$ the model equations reduce to $\partial_f + a\partial_x f = \pm cf$, describing translation together with an exponential growth at rate $\pm c$.

While both of these cases give rise to instabilities, they are physically very different kinds of instability. When the two systems travel at the same velocity a, the unstable region is convected with the systems at speed a, and so appears to move past a stationary observer as it grows. When the two systems travel with opposite velocities, $b = -a$, the unstable region remains fixed in space as it grows. Considering a plasma device of a finite size, the first behavior is well suited to the amplification of a pulse, with the input pulse travelling through the device and increasing in amplitude before leaving the device. The second behavior can lead to the disruption of the device, since an initial disturbance remains in the device while increasing in amplitude. For this reason it is useful to distinguish between the first behavior, in which the amplitude of the disturbance ultimately tends to zero at any point in space, called a convective instability, and the second, in which the amplitude of the disturbance grows exponentially in time at all points in space, called an absolute instability [195], [196]. The theory of convective and absolute instabilities was developed in the context of electron beam instabilities [195]. This classification

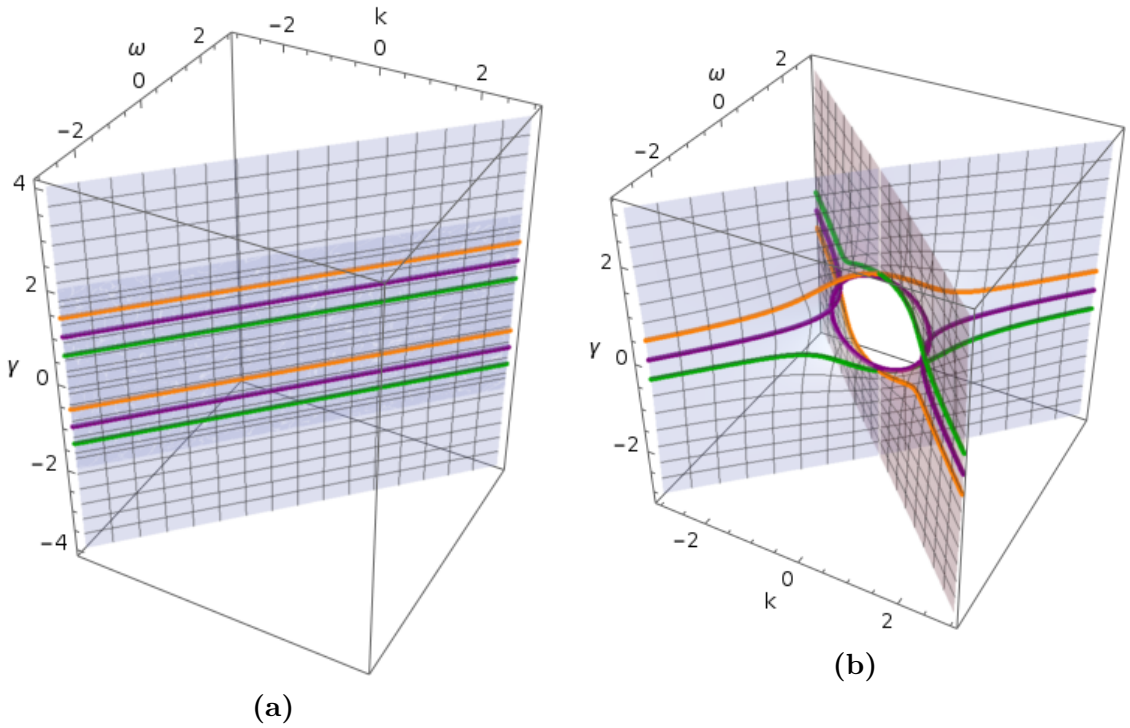

Figure 6.3: The complex dispersion surfaces corresponding to the model equation solutions shown in Figure 6.2. The purple curve shows the $\kappa = 0$ curve of modes with zero spatial growth rate, while the orange and green curves show modes with $\kappa = \pm 0.1$. The system in (b) shows an absolute instability, while (a) gives rise to a convective instability.

depends on the frame we use (a convective instability will be absolute in a frame moving with the pulse), but it is useful in as much as a plasma device or particular region of space singles out a frame we are interested in. Figure 6.4 shows numerical solutions of the model equations for the parameters $a = 1$, $b = -1$, $c = 1$ in (a), and $a = 1$, $b = 1$, $c = 1$ in (b), illustrating these behaviors, with the plot (c) of the amplitudes at a given point in space as a function of time highlighting the distinction between the absolute instability in (a) and the convective instability in (b).

6.3 Beam plasma instabilities

A beam of particles travelling through a plasma can under appropriate conditions become unstable, producing Langmuir waves in the plasma. In fact as we saw in Chapter 1 some of the earliest plasma experiments were Langmuir and Tonks' experiments on the production of Langmuir waves in a plasma as an electron beam

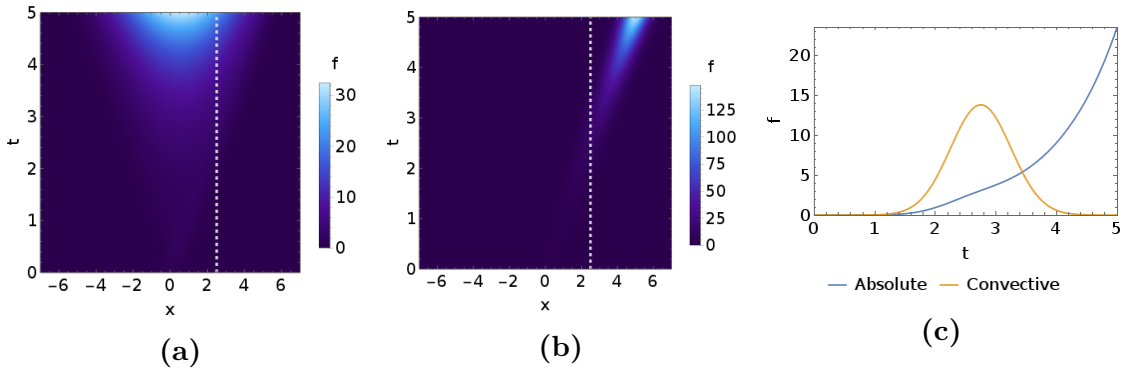

Figure 6.4: The development of (a) an absolute instability and (b) a convective instability, solutions of the equations $\partial_t f + a\partial_x f = cg$, $\partial_t g + b\partial_x g = cf$. The field amplitudes at the position marked by the dashed lines in (a) and (b) are shown together in (c).

became unstable in a plasma. The subject of beam plasma instability has been a constant source of stimulation for the development of plasma theory.

6.3.1 Heuristics

Transverse and longitudinal relativistic masses

As a beam of electrons becomes unstable the density in the beam, initially uniform, becomes perturbed. The electrons can bunch longitudinally, breaking the beam up along its length, transversely, breaking the beam across its breadth into filaments, or at some intermediate angle. We calculate the growth rate of these various modes of instability below, but a simple physical argument based on relativistic masses can give us some intuition for how the electron beams of different energies will behave. The acceleration of a relativistic electron is in general not parallel to the force on it [43], but in case the force is either parallel or perpendicular to the electron's velocity, the force and acceleration are indeed proportional but with different factors of proportionality in each case. These factors are understandably called the transverse and longitudinal relativistic mass, given by the expressions

$$m_\perp = \gamma m_0 \qquad\qquad m_\parallel = \gamma^3 m_0, \tag{6.13}$$

where m_0 is the electron's rest mass and $\gamma = 1/\sqrt{1 - v^2/c^2}$ is the electron's gamma factor with v being the electron's velocity. These formulae tell us not just that a faster moving electron is harder to accelerate, but that as the electron velocity

increases the electron becomes proportionally harder to accelerate parallel to its motion than perpendicular to its motion. Thinking of the motions of the electrons in a beam that breaks up longitudinally, the necessary accelerations are parallel to the electrons' motion, while for the beam to filament the necessary motions are perpendicular to the electrons' motion. Thus because the longitudinal relativistic mass increases faster than the transverse relativistic mass with γ, if there is an instability at all a lower energy electron beam will tend to break up longitudinally, with higher energy beams tending toward filamentation [185].

Shear fluid flow analogy

The next chapter will study the evolution of beam plasma instabilities in detail, but there is a very useful analogy with fluid mechanics which can give some intuition. The Vlasov equation for the plasma electron distribution function is given by

$$\partial_t f + v\partial_x f + E\partial_v f = 0, \tag{6.14}$$

where the charge and mass have been set to one. This has the form of a fluid equation in (x, v) space with velocity field (v, E). The x component of the velocity is always given by v, so we have at all times a shear flow in the phase space (x, v). This shear describes the 'free streaming' motion of the particles and is useful to have in mind when looking at phase space plots (from Vlasov or particle-in-cell simulations for example). The v component of the velocity is given by the electric field E. Since the electric field acts equally on particles of all velocities, this effectively introduces a nonlocality in the velocity dimension (this nonlocality can be seen explicitly in the form of the charge density $\rho = q \int f \, \mathrm{d}v$).

Based on this fluid analogy it seems plausible that beams in plasmas can be unstable, since shear flows in fluids are well known sources of instability (for example the Kelvin-Helmholtz instability). The quirk is that the beam and background plasma are separated in velocity, and so in an ordinary (local) fluid would not be able to influence each other (since only neighboring fluid elements can act on each other in an ordinary fluid). But the nonlocality in velocity allows a perturbation in

the beam to influence the background via the electric field. Further, considering the effect of a given electric field on the phase space velocity (v, E) of particles in the beam and background, since the beam is faster than the background a given E can change the direction of (v, E) much more for background particles owing to their small v; in this way a small bunching in the beam can give rise to a significant perturbation in the background.

6.3.2 Multiple relativistic fluids

To calculate the growth rate of the instability of two beams crossing in a plasma I will model each beam as well as the background plasma electrons and ions as a relativistic fluid [197]. This is a simplification of the fully kinetic description of the plasma particles employed in the later simulations, but it gives a useful first look at the physics and is helpful in informing the set-up of the numerical work. In fact the consideration of many beams described as fluids is more general than it may first appear, and can give not just intuition but even quantitative results on the fully kinetic description of a plasma. While I do not pursue this here, using a large number of beams finely spaced in velocity Dawson has derived the Landau damping rate [198]. Intuitively the description emphasizes the very many degrees of freedom in the kinetic description and prepares us to think of phase mixing and anti-phase mixing as the 'constituent beams' of the plasma falling in and out of step.

The equations of motion for a charged relativistic fluid [197] are the continuity and momentum equations for the number density n and velocity v,

$$\partial_t n + \vec{\nabla} \cdot (n\vec{v}) = 0 \tag{6.15}$$

$$(\partial_t + \vec{v} \cdot \vec{\nabla})\gamma\vec{v} = \frac{q}{m}(\vec{E} + \vec{v} \times \vec{B}) \tag{6.16}$$

where $\gamma = (1 - v^2/c^2)^{-1/2}$ is the relativistic gamma factor, q is the charge of the particles, m their mass, and $\vec{E}$ and $\vec{B}$ the electric and magnetic fields. The continuity equation expresses conservation of particle number, the momentum equation conservation of momentum. Note that we have four scalar equations for

the four fields n and the components of $\vec{v}$. The fields $\vec{E}$ and $\vec{B}$ can be prescribed or supplemented with Maxwell's equations to determine their evolution,

$$\vec{\nabla} \cdot \vec{E} = \frac{1}{\epsilon_0}\rho \tag{6.17}$$

$$\vec{\nabla} \times \vec{B} - \frac{1}{c^2}\partial_t \vec{E} = \mu_0 \vec{J} \tag{6.18}$$

$$\vec{\nabla} \times \vec{E} + \partial_t \vec{B} = 0 \tag{6.19}$$

$$\vec{\nabla} \cdot \vec{B} = 0. \tag{6.20}$$

The first and last of Maxwell's equations above are constraints in the sense that if they hold at some time and charge is conserved then they hold at all later times. The two evolution equations give six scalar equations for the six components of $\vec{E}$ and $\vec{B}$. Here, dealing with a single fluid, the charge and current densities ρ and $\vec{J}$ are given by $\rho = qn$ and $\vec{J} = qn\vec{v}$.

The growth rates for the instability of a system of charged relativistic fluids can be derived by linearizing the relativistic fluid equations, a technique which can be automated using a computer algebra system, before applying the methods for studying instabilities for linear equations presented in the previous section. The method thus proceeds in two stages: i) linearize the fluid equations using an expansion in the amplitude of the waves; and ii) look for solutions proportional to $e^{i(-\omega t+kx)}$ and so find the dispersion surface (D_c from the previous section).

The first step, linearization, consists of making an expansion of each field F of the form $F = F_0 + \epsilon F_1 + \epsilon^2 F_2 \ldots$, where F_0 is the equilibrium value of F and ϵ is a small parameter reflecting the assumed smallness of the wave amplitude. We will keep only terms up to order ϵ and hope that the approximation gets better for small ϵ; this kind of expansion is called asymptotic [31], [199] and can be compared with a convergent Taylor series in which we usually think of improving accuracy by summing higher and higher ordered terms. The difference is between approximating the relativistic energy as $E = \gamma mc^2 \sim mc^2 + \frac{1}{2}mv^2$ and noting that this approximation becomes better as v/c becomes smaller and smaller and expanding E as $E = mc^2 + \frac{1}{2}v^2 + \frac{3m}{8c^2}v^4 + \frac{5m}{16c^4}v^6 + \ldots$ and noting that this expression will be close to E if we include enough terms for any $v/c < 1$. This example

also illustrates the point that the first terms of an asymptotic series often have a direct physical interpretation, here as rest energy and kinetic energy, or in a plasma perhaps in terms of interactions between wave species for example. The F_0 can depend on position and time but we take them as constant here, describing waves in a uniform plasma. Our expansion is then

$$n = n_0 + \epsilon n_1 \tag{6.21}$$

$$\vec{v} = \vec{v_0} + \epsilon \vec{v_1} \tag{6.22}$$

$$\vec{E} = 0 + \epsilon \vec{E_1} \tag{6.23}$$

$$\vec{B} = 0 + \epsilon \vec{B_1}. \tag{6.24}$$

The zero values for $\vec{E_0}$ and $\vec{B_0}$ reflect the assumption that there are no background electric or magnetic fields. The linearization requires expanding products and Taylor expanding the γ factors and keeping only terms at order ϵ^0 and ϵ^1. This can be performed automatically using a computer algebra system. The code I have written takes a set of partial differential equations and calculates its dispersion surface and is useful for rapidly experimenting with different wave equations. After linearization we have a system of linear equations for the perturbed field quantities, to which we can apply the methods of the previous section, altered only by extending the vector $[f, g]$ to a long vector containing all of the fields of the problem. For n relativistic fluids we have $4n + 6$ fields in the vector, four for the density and velocity of each fluid, and six for the components of the electromagnetic field. We then proceed as before to find the complex dispersion surface, which now consists of many branches corresponding to the larger number of degrees of freedom.

The fact that we have linearized the equations leads to the independent behavior of the modes $e^{i(-\Omega t + \vec{K}.\vec{x})}$; nonlinear terms in the F_1 would have introduced coupling between the pure modes proportional to $e^{i(-\Omega t + \vec{K}.\vec{x})}$, so no individual pure mode is a solution. In a treatment using the Fourier-Laplace transform this coupling shows up as convolutions arising from the products of the fields via the convolution theorem [97]. The nonlinear terms in the original equation still manifest themselves as the

interaction between zeroth order and first order terms; nonlinearity is one way in which the background plasma properties influence the properties of linear waves.

One spatial dimension

The above treatment can be applied to the one dimensional electrostatic case by using Gauss' law (6.17) in place of the dynamical pair of Maxwell's equations (6.18) and (6.19). For n relativistic fluids this gives a system of $2n + 1$ equations, two equations for each fluid (since there is only one velocity component in this case) together with Gauss' law. The resulting dispersion relation is only of order $2n$ in Ω since Gauss' law is not dynamical.

Figure 6.5 (a) shows the frequency and growth rate curves as a function of wavevector for a system of two electron beams in a background plasma. The electron beams have a relativistic kinetic energy of 1 MeV and a density of 1/100 times the background plasma density, corresponding to the beam parameters used in the 1D simulations in Chapter 7. The momentum equations for the fluids have been supplemented with a pressure term to account for the finite temperature of the beams, causing the unstable modes to lie in bands around $k = \pm 1.1$ rather than extending down to $k = 0$. Figure 6.5 (b) shows the dispersion curve in the space of frequency, wavevector and growth rate, making visible the association between given frequencies and growth rates.

The modes at different points on the dispersion curve have different polarizations. Calculating the polarization of the mode at the point marked in Figure 6.5 by the red sphere, the most unstable mode, gives the amplitude in the density fluctuation of the beam travelling in the positive x direction as 0.099 times the amplitude in the background plasma density fluctuation, while the beam travelling in the negative x direction has an amplitude of only 9.6×10^{-5}, so this mode is predominantly associated with one beam and the background plasma. For the stable mode marked by the green sphere, the amplitude of the density perturbation of the beam travelling in the positive x direction is 2.12 times the background density perturbation, while the beam travelling in the opposite direction's amplitude is at 1.04×10^{-4} times

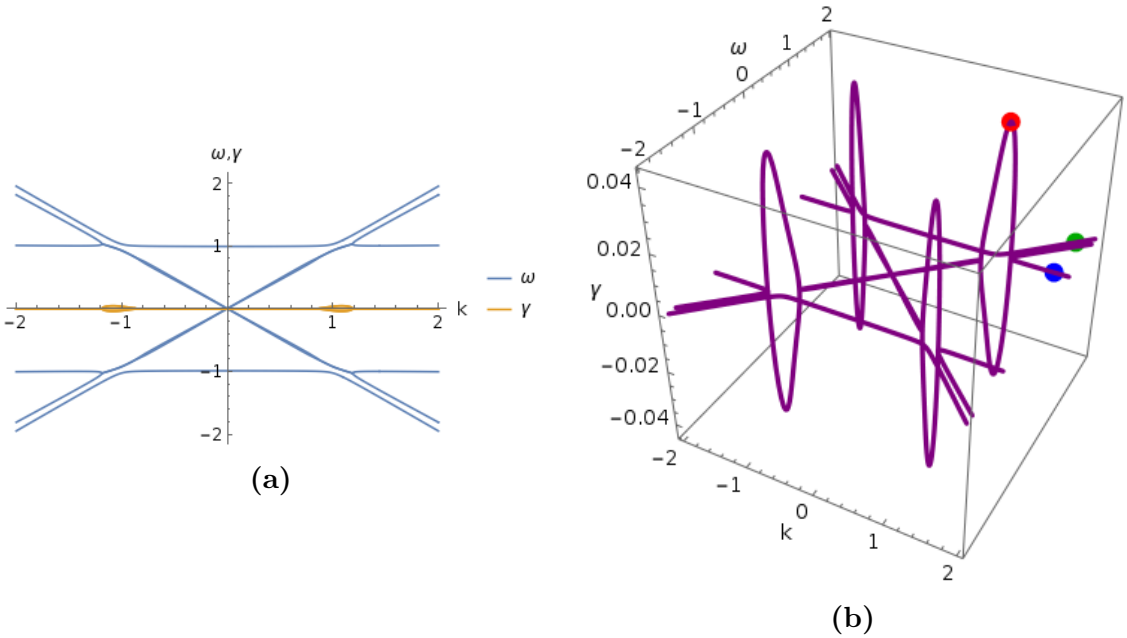

Figure 6.5: The frequencies and growth rates as a function of wavevector (a) and the dispersion curve (b) for a system of two electron beams in a background plasma.

the background, so this mode is primarily a mode along the beam travelling in the positive x direction. For the stable mode marked by the blue sphere both beam density fluctuation amplitudes are below 10^{-4}, this mode being essentially a Langmuir wave in the background plasma.

Two spatial dimensions

In two spatial dimensions the dynamical pair of Maxwell's equations (6.18) and (6.19) are required. The dispersion curves in this case, even setting the spatial growth rates to zero, naturally exist in the four dimensional space of two-component wavevectors $\vec{k}$, frequencies ω and growth rates γ, but projections of the dispersion curves can be usefully plotted.

Figure 6.6 shows the theoretical growth rate maps of the instability for 1 MeV electron beams with a density, n_b, of 0.01 times the background density, n_0, as in the 2D simulations in Chapter 7. Figure 6.6 (a) shows the growth rates in the case in which the two beams cross at 90°, travelling in the positive x and y directions, while (b) shows the case in which the beams cross at 180° travelling along the x axis. The system of two beams crossing at 90° has a symmetry about

the line $y = x$ which induces the symmetry of the growth rate maps in (a) under reflection in the line $k_y = k_x$. With the beams crossing at 180° the system has a symmetry under reflection in the x and y axes which is again inherited by the growth rate map. The case (a) in which the beams cross at 90° gives a higher maximum growth rate, corresponding to a mode with $k_x = k_y$ travelling diagonally between the two beams, as well as a spectrum of unstable modes which covers a wider range of angles. Since in the linear phase of the instability each mode grows independently, these growth rate maps show that beams crossing at 90° will initially couple their energy into Langmuir waves more rapidly.

Calculating the polarization of the fastest growing mode in the system of beams crossing at 90° in a background plasma, marked by a red dot in Figure 6.6 (a), both the beam travelling in the x direction and the beam travelling in the y direction have an amplitude of their density fluctuation of 0.13 times the background density fluctuation, so this fastest growing mode involves both beams interacting together with the background plasma. The velocity perturbation of the background plasma for this mode has equal x and y components, so in this mode the background plasma moves diagonally between the two beams. The electric field is also diagonal. The two beams velocity perturbations make an angle of 72.8° with their initial velocities, in the sense to bring their velocity vector closer to that of the other beam. For the mode marked with the blue point, which has a lower growth rate, the amplitude of the density perturbation of the beam propagating in the x direction is 0.15 times the background perturbation, while the beam travelling in the y direction's density perturbation is only 4.4×10^{-3}, so this slower growing mode is primarily associated with the background and the beam travelling in the x direction.

In the system of beams crossing at 180°, Figure 6.6 (b), for the modes labelled with the blue and red points the beam travelling in the negative x direction has a density fluctuation of less than 10^{-3} the background density perturbation, so both of these modes are predominantly associated with the beam travelling in the positive x direction and the background.

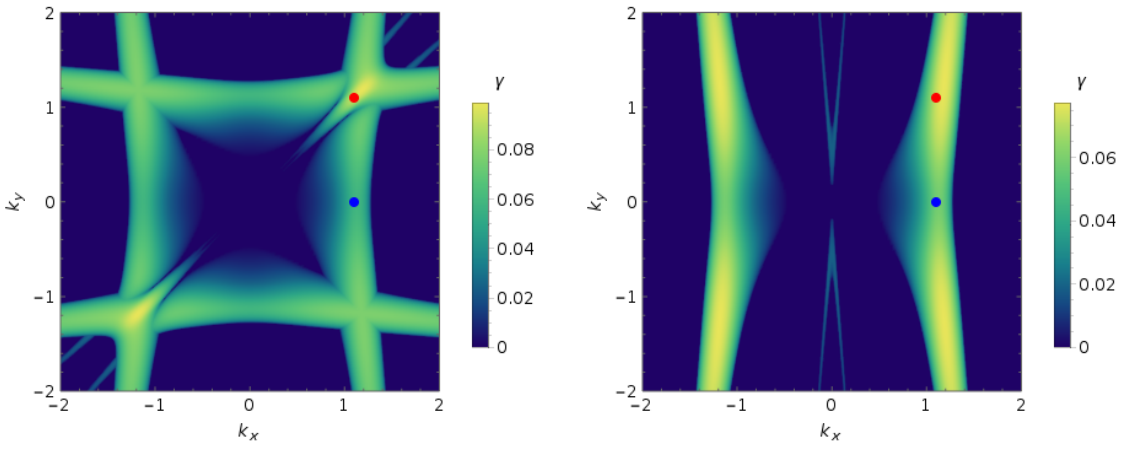

Figure 6.6: The growth rates of the modes of a system of beams crossing at (a) 90° and (b) 180° in a background plasma. The unstable modes of the system of beams crossing at 90° cover a broader range of angles in wavevector space and have a higher maximum growth rate.

Fig. 6.7 shows the real part of the frequencies which solve the 2D dispersion relation as a function of 2D wavevector $\vec{k}$. The different sheets of the dispersion surface correspond to different modes of the system. In particular the diagonal quasi-planar sheets correspond to beam modes propagating at the beam velocities. The unstable modes lie where the beam mode sheets turn away from the horizontal sheets associated with Langmuir waves. The curved sheets at the top and bottom are light modes. Only a small number of the modes shown here are unstable, that is, have a positive imaginary component of frequency.

6.4 Summary

In this chapter I have presented linear growth rate calculations for the system of electron beams crossing in a background plasma in preparation for the simulations presented in the next chapter. Examples of dispersion surfaces and complex dispersion surfaces were given, and the method for deriving growth rates illustrated with some model equations. Heuristics for understanding beam plasma instabilities in terms of transverse and longitudinal relativistic masses and by analogy with shear flow instabilities were presented. The dispersion curves for a system of two

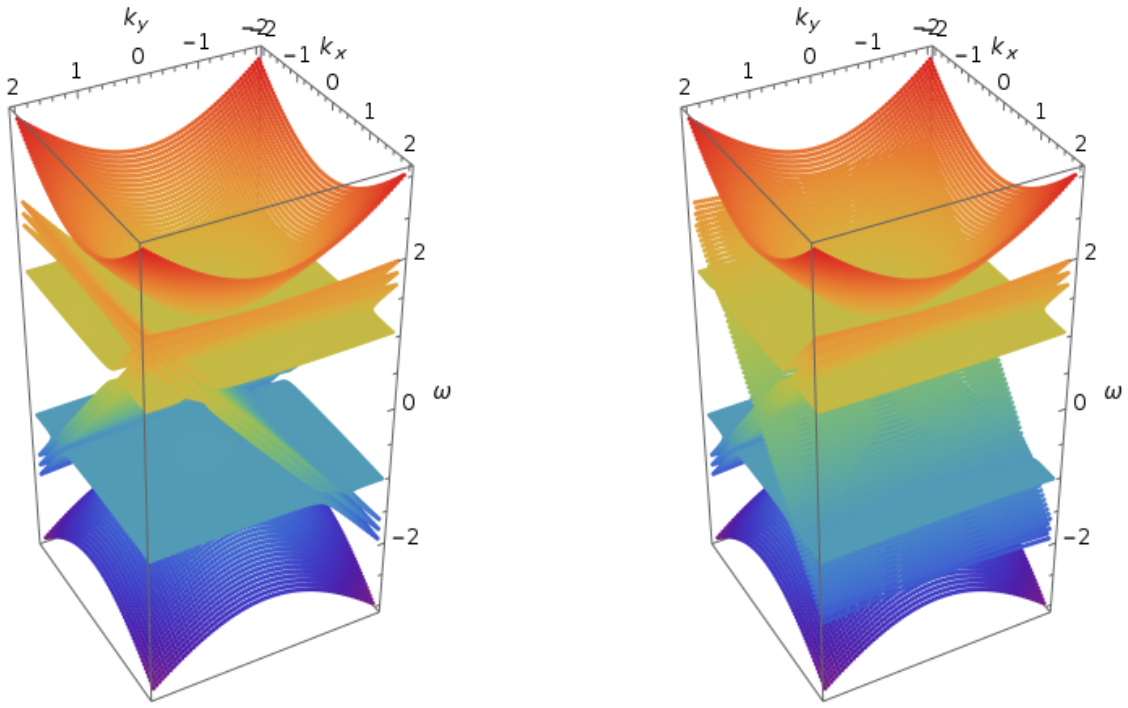

Figure 6.7: The frequencies of the modes of a system of electron beams crossing at (a) 90° and (b) 180° in a background plasma. The unstable modes lie where the diagonal sheets of the dispersion surface, which are associated with beam modes, turn away from the horizontal sheets associated with Langmuir waves. The paraboloidal surfaces are associated with light waves. Compare the 1D case shown in Figure 6.5 (a) where the growth rate (orange) is large where the different branches of the frequency (blue) turn away from each other.

beams crossing in a plasma were presented and the polarizations of some of the modes studied. The fastest growing unstable mode of the system of two beams crossing at 90° in a plasma was shown to be a mode with $k_x = k_y$ involving both beams interacting with the background. The next chapter presents Vlasov-Maxwell simulations of the systems of beams in a background plasma considered in this chapter.

7 Vlasov simulations with VALIS

7.1 VALIS

To follow the nonlinear evolution of the crossing beams and the coupling of Langmuir waves produced by the beam-plasma instability with ion-acoustic waves, I have performed simulations with the Vlasov-Maxwell code VALIS [200]. VALIS solves the relativistic Vlasov equation for the distribution functions $f_\alpha(\vec{x},\vec{p},t)$ of the various particle species α in the plasma,

$$\partial_t f_\alpha + \frac{\vec{p}}{\gamma}\cdot\nabla_x f_\alpha + q_\alpha\left(\vec{E}+\frac{\vec{p}}{\gamma}\times\vec{B}\right)\cdot\nabla_p f_\alpha = 0, \tag{7.1}$$

where $\vec{p}$ is the relativistic momentum defined in terms of the velocity $\vec{p} = m_\alpha\gamma\vec{v}$, where $\gamma = (1-|\vec{v}|^2/c^2)^{-1/2} = (1+|\vec{p}|^2/m_\alpha^2c^2)^{1/2}$ is the relativistic gamma factor. In fact the code works with $\vec{u}_\alpha = \vec{p}_\alpha/m_\alpha$. The Vlasov equations for the particle distribution functions are coupled to Maxwell's equations (as given in the previous chapter) for the electric and magnetic field, in which the charge density ρ and $\vec{J}$ are defined by

$$\rho(\vec{x}) = \sum_\alpha\left(q_\alpha\int f_\alpha(\vec{x},\vec{p})\,\mathrm{d}\vec{p}\right) \tag{7.2}$$

$$\vec{J}(\vec{x}) = \sum_\alpha\left(q_\alpha\int\frac{\vec{p}}{m_\alpha\gamma}f_\alpha(\vec{x},\vec{p})\,\mathrm{d}\vec{p}\right). \tag{7.3}$$

VALIS solves this system in up to two spatial and two momentum dimensions. VALIS advances the distribution functions from one time step to the next using an operator-split conservative scheme with separate 1D advections in each position and momentum coordinate [201], the advections being performed using the Piecewise Parabolic Method [202]. This numerical scheme has the advantages that it preserves the positivity of the distribution, it is monotonicity preserving and so avoids the introduction of spurious oscillations, and it handles in a physical manner the dissipation of fine structures in velocity which as we saw in Chapter 4 inevitably form as they fall beneath the grid scale [203].

VALIS uses dimensionless quantities defined in terms of the electron mass m_e, the elementary charge e, the speed of light c, and a reference density n_0. The coordinates are then defined in terms of the electron plasma frequency ω_p at the reference density n_0, defined by

$$\omega_p^2 = \frac{n_0 e^2}{\epsilon_0 m_e}. \tag{7.4}$$

Denoting the dimensionless quantities temporarily with tildes, they are defined in terms of the physical quantities of time t, position x, charge q, and temperature T by

$$t = \frac{1}{\omega_p}\tilde{t} \tag{7.5}$$

$$x = \frac{c}{\omega_p}\tilde{x} \tag{7.6}$$

$$q = e\tilde{q} \tag{7.7}$$

$$T = k_{\mathrm{B}} m_e c^2 \tilde{T}, \tag{7.8}$$

with other quantities such as velocity and the electric field deriving their dimensionless forms from these base quantities. These units have the useful property that light travels a dimensionless distance $\tilde{x} = 1$ in a dimensionless time $\tilde{t} = 1$.

Another popular numerical scheme for solving the Vlasov-Maxwell system is the particle-in-cell (PIC) scheme [204], which represents the distribution functions f_α as a sum of a finite number of localized pieces in phase space, picturesquely known as macroparticles, which move along the characteristics of the Vlasov equation. The scheme advances the positions and velocities of the macroparticles according to the

Lorentz force law given the electromagnetic field, interpolates to find the current and charge density on a grid, and uses these current and charge densities to update the electromagnetic field. For our work here a Vlasov code, which solves the Vlasov equation directly rather than in terms of macroparticles, is very suitable due to its ability to resolve well the regions of phase space at large velocity where the electron beams are situated, and to its intrinsically low noise, which is inherited by the computed phase space representations of the waves generated during the beam plasma instability rendering them easier to interpret.

7.2 Resolution tests

To establish the appropriate resolution for the simulations I carried out a series of resolution tests in which the number of grid points for the 1D simulation described below was increased. Figure 7.1 shows the results of these tests, with the left column showing the entropy and the electromagnetic energy (here smoothed to average out the oscillations on the scale of ω_{pe}) as the spatial resolution is doubled with a fixed number of momentum grid points $n_p = 2048$. The right column shows these same quantities for two numbers of spatial grid points $n_x = 4096$ and $n_x = 8192$ showing the effect of doubling the number of momentum grid points from $n_p = 2048$ to $n_p = 4096$. The electromagnetic energy is largely unchanged by the increasing resolutions past a spatial resolution of 2048 grid points, and while the behaviour of the entropy is more complicated due to the issues discussed above about the dissipation of fine scale structure in velocity, it also appears to converge.

7.3 1D simulation results

The 1D simulations describe electron beams crossing at 180° in a background plasma. The background electron and ion temperatures are 4 keV, corresponding to the range of temperatures of hot spots in inertial confinement fusion targets. The background plasma density in the simulation is a free parameter setting the scale of the units, though we have in mind an electron number density of $n = 10^{26}\,\mathrm{cm}^{-3}$. Both electron

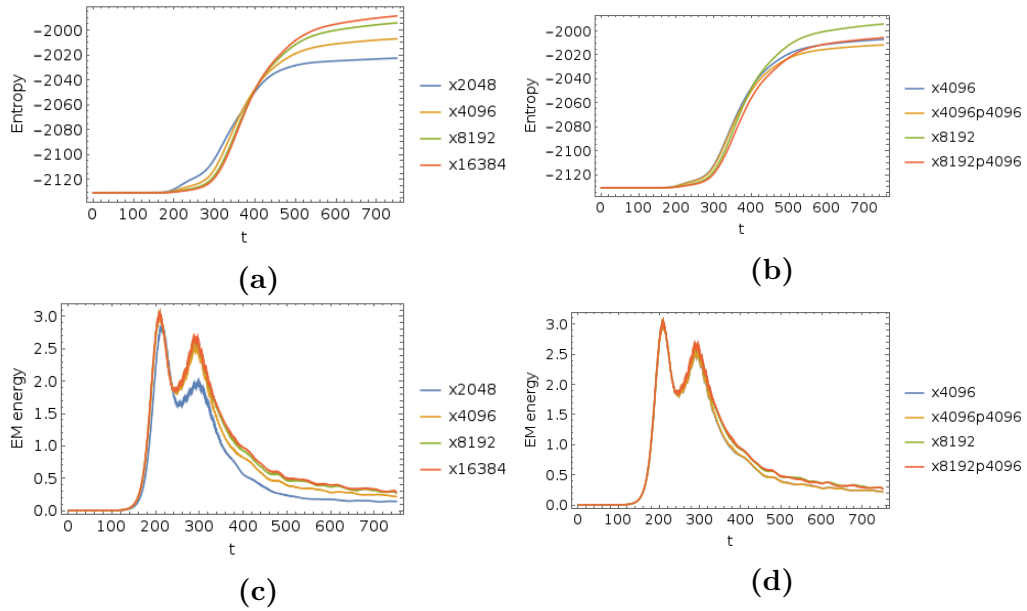

Figure 7.1: Plots showing the time evolution of the entropy (top row) and electromagnetic energy (bottom row) for simulations carried out to test the spatial (left column) and momentum (right column) resolution.

beams have a mean relativistic kinetic energy of 1 MeV and a density of one percent of the background density, in the practically relevant regime of high beam energy and low fractional beam density. The two beam distributions have a temperature of 40 keV. No collision operator is used since for a plasma of number density $n = 10^{26}\,\mathrm{cm}^{-3}$ and electron and ion temperatures $T_\mathrm{e} = T_\mathrm{i} = 4\,\mathrm{keV}$, the electron plasma frequency is $\omega_{pe} = 5.64 \times 10^{17}\,\mathrm{s}^{-1}$, over 200 times the electron collision frequency, while the simulations here ran for a time $2000/\omega_{pe}$ corresponding to 320 plasma periods, with much of the interesting dynamics occurring early in the simulation.

The initial electron distribution function is a sum of three drifting Maxwell-Jüttner distributions, the relativistic generalization of the Maxwellian distribution [205]. The distributions are initially homogeneous and periodic boundary conditions are employed. Due to the aforementioned low noise level in Vlasov codes, an initial low amplitude white noise perturbation is included in the electrons' spatial distribution to seed the initial beam-plasma instability. Since these simulations treat the system in one space and one momentum dimension, waves which would propagate obliquely to the beams cannot be captured. The ion mass in the simulations is

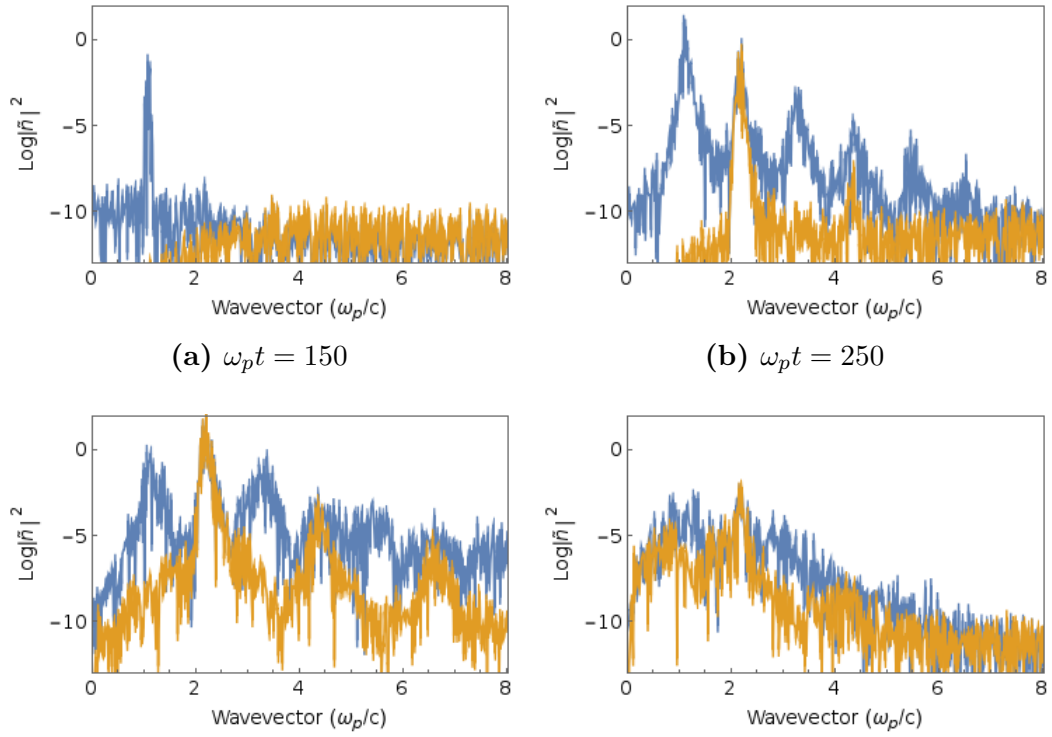

(a) $\omega_p t = 150$ **(b)** $\omega_p t = 250$

(c) $\omega_p t = 350$ **(d)** $\omega_p t = 750$

Figure 7.2: Time history of the power spectra of the electron (blue) and ion (orange) densities from a 1D Vlasov simulation of two electron beams crossing at 180°, showing the waves present during each stage of the heating process. Each timestep shows a different stage of the energy cascade: (a) the generation of Langmuir waves by the instability of the crossing beams, (b) the nonlinear coupling of the Langmuir waves into ion waves, (c) the instability of the ion-acoustic waves and (d) ion-acoustic turbulence.

$m_i = 1000 m_e$. While this ion mass is only 0.54 times the mass of a hydrogen ion (or 0.27 times the mass of a deuterium ion), this will not affect the results significantly since with $m_i = 1000 m_e$ the time scale of the natural oscillations of the ions is an order of magnitude greater than the electrons and so the ion population will evolve on a different timescale to the electrons. The spatial grid covers 400 c/ω_{p0} and the time $2000/\omega_{p0}$. The relativistic momentum space for the electrons spans $\pm 20 m_e c$, for the ions $\pm 0.25 m_i c$. The dimension of the (x, p) phase space grid was 4096×2048 for both electrons and ions.

Figure 7.2 shows a time history of the power spectra of the electron and ion densities (the modulus squared of their spatial Fourier transforms). Each frame shows a different stage of the process by which energy is transferred from the beams to the plasma particles. In (a) at $\omega_p t = 150$ there is a single peak in

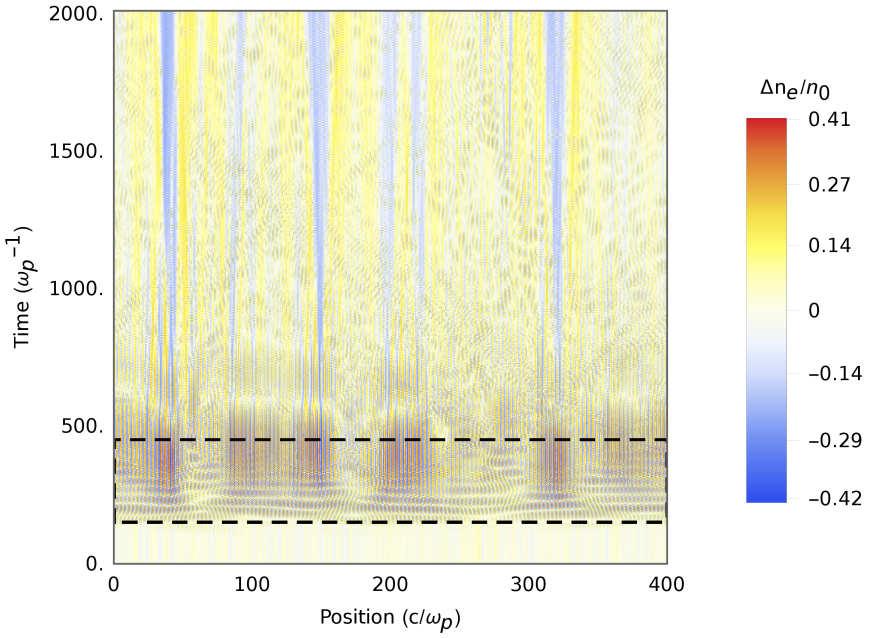

(a)

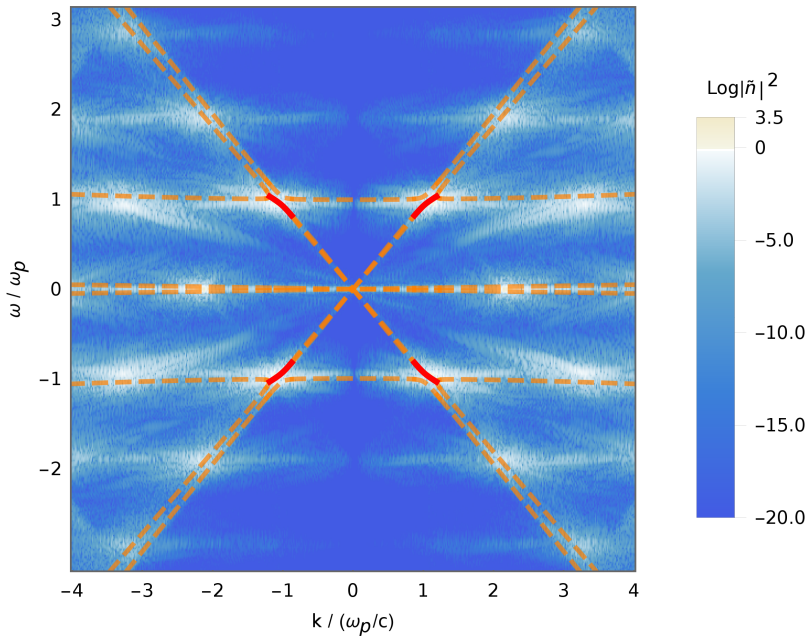

(b)

Figure 7.3: (a) Space-time plot of the electron density showing each stage of the energy cascade. (b) The numerically calculated frequency and wavevector, ω and k, of the waves produced by instability or nonlinear coupling in the dashed boxed portion of Fig. 7.3 (a). Overlaid are the theoretical dispersion curves. The red sections of the dispersion curves indicate frequencies with a positive imaginary part, showing instability.

the electron density spectrum representing a Langmuir wave driven by the two beams crossing in the plasma. It is at a wavevector $k_0 = 1.1\omega_p/c$, in agreement with the most unstable mode predicted by the multiple relativistic fluid theory of Chapter 6. In (b) at $\omega_p t = 250$ we see a peak at $2k_0$ in both the electron and ion spectra representing an ion-acoustic wave driven nonlinearly by the beam driven Langmuir wave [97]. The higher order peaks in the electron spectrum are Langmuir waves resulting from the nonlinear coupling. In (c) at $\omega_p t = 350$ the ion-acoustic feature in the electron and ion spectra from (b) has generated higher order peaks as the ion-acoustic wave becomes unstable. In (d) at $\omega_p t = 750$ sharp peaks are no longer visible in the electron and ion spectra, the continuous fall off with wavevector indicating a turbulent state.

Figure 7.3 (a) shows a space-time plot of the electron density from the simulation, giving a global picture of the interaction. Initially the beams drive Langmuir waves in the plasma via beam-plasma instability. These Langmuir waves become large and couple into ion-acoustic waves. The ion-acoustic waves are then damped, and the plasma ends in a state of ion-acoustic turbulence. The bunched structures in the dashed boxed region of Figure 7.3 (a) show that localized wavepackets are formed, information not visible in the Fourier spectra of Figure 7.2. Figure 7.3 (b) shows the Fourier transform of the portion of Figure 7.3 (a) indicated by the dashed box, highlighting the time in which the beams become unstable and ion-acoustic waves begin to form. Figure 7.3 (b) shows the distribution of waves in wavevector and frequency, i.e. in (k, ω) space. This provides a discrete approximation to the space-time Fourier transform $\tilde{n}(k, \omega)$ of the electron density $n(x, t)$. The orange curves in Figure 7.3 (b) show the roots of the dispersion relation from an electrostatic multiple relativistic fluid model for the two beams, background electrons and ions, with pressure terms included to take the temperature of the beams into account. The predominance of modes along the linear dispersion curves in Figure 7.3 (b) demonstrates the utility of the linear wave properties even in this nonlinear interaction. The red sections of the dispersion curves have a positive imaginary component of the frequency, leading to an exponential growth of the

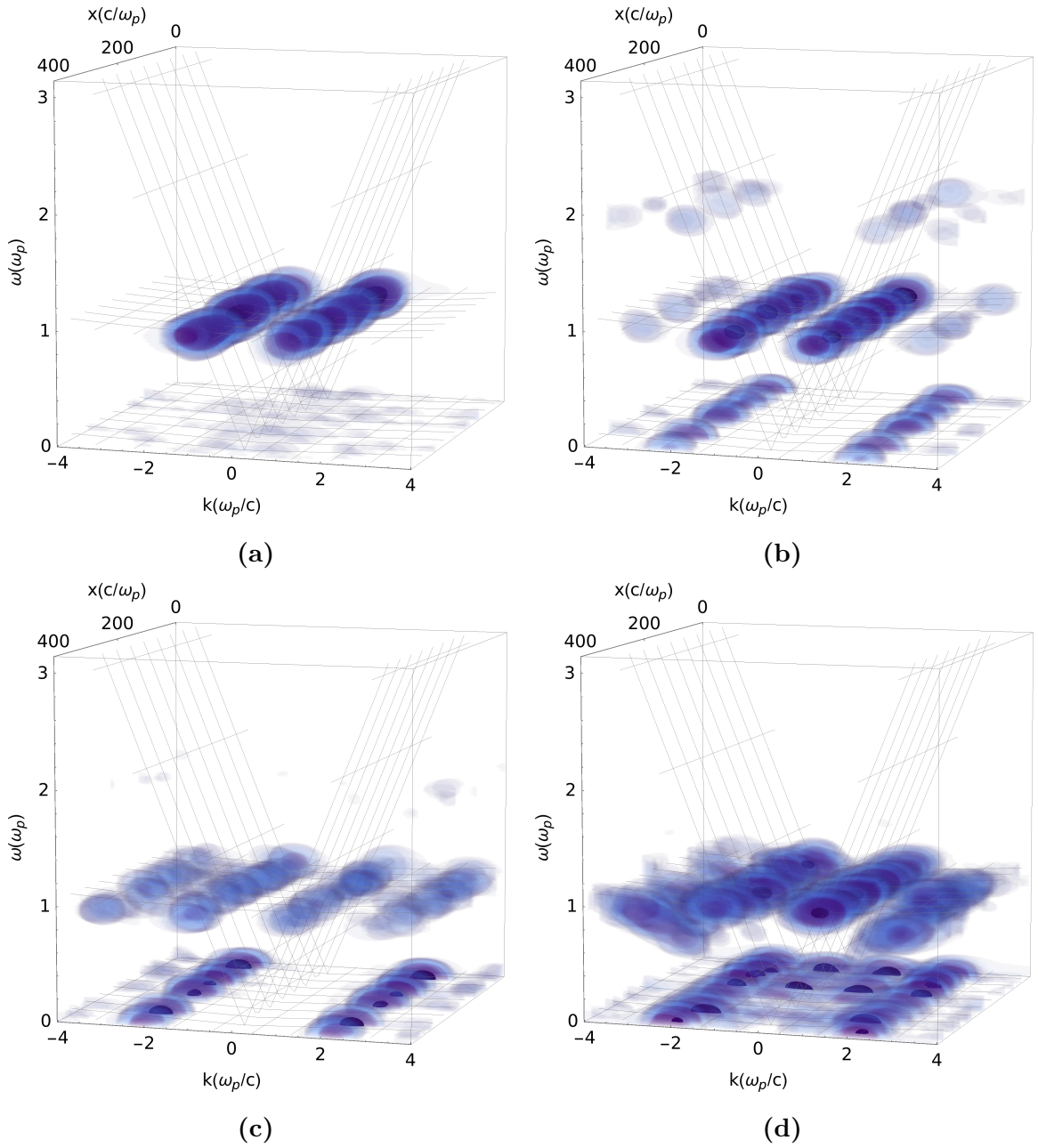

Figure 7.4: Time history of the wave phase space distribution of the electron density. This shows the distribution of the plasma waves in the space of position, wavevector and frequency (see text). The gridded surfaces are the theoretical dispersion surfaces.

mode amplitude and thus instability. Figure 7.3 shows the evolution of the waves responsible for the energy cascade from the electron beams to the plasma particles.

The Fourier spectra shown in Figure 7.2 and Figure 7.3 (b) make clear that the frequency and wavevector spectra of the electron and ion densities carry substantial physical information, while the space-time plot of the electron density in Figure 7.3 (a) shows the existence of localized bunches of waves, not visible in the Fourier spectra, but cannot directly reveal the information on the frequency and wavevector. The situation is thus ideal for the application of the phase space representation of the waves, revealing information on the localization of the waves and their frequency and wavevector spectra simultaneously. This distribution can be calculated numerically by scanning a window across the simulation data and using the fast Fourier transform to find the spectrum of each windowed slice of the data.

Figure 7.4 shows plots of the position-wavevector-time-frequency distribution $|W(x, k, t, \omega)|^2$, the modulus squared of the space-time windowed Fourier transform, for a range of times t, which can be interpreted as the distribution of waves in position, wavevector and frequency at the time t. The gridded surfaces show the dispersion surfaces from the multiple relativistic fluid theory used in Figure 7.3. Figure 7.4 (a) shows the early formation of bunched high frequency Langmuir waves, located along the Langmuir wave dispersion surface as predicted by the linear theory. (b) shows that the ion-acoustic waves generated are localized near the position of the large Langmuir wavepackets. This local information is important since the Langmuir waves are able to drive ion-acoustic waves more rapidly by bunching to increase the local Langmuir wave intensity, which in turn increases the coupling rate into ion-acoustic waves. (c) shows similarly localized daughter Langmuir waves together with bunched ion-acoustic waves, while in (d) the spread of the low frequency part of the distribution in k indicates ion-acoustic turbulence. Figure 7.4 unfolds the plasma dynamics into the interaction of localized wavepackets of a variety of frequencies and wavevectors, the phase space representation of the waves providing a detailed picture of the evolution of the waves responsible for the energy cascade process.

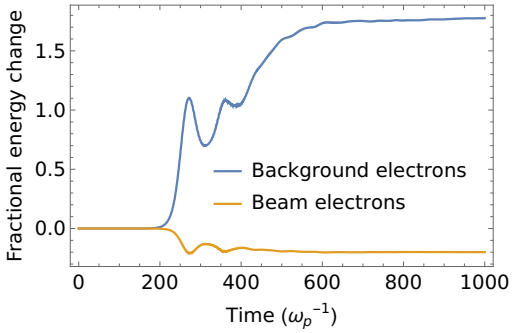

Figure 7.5: Time evolution of the fractional energy change of the background electrons (blue line) and beam electrons (orange line) during the collisionless heating process.

Figure 7.5 shows the time evolution of the fractional kinetic energy change of the beam electrons and the background electrons. These energies are calculated using a simulation in which the electron beams and the background electrons are separate species, allowing a clean calculation of the energy of each component. Figure 7.5 shows that 18% of the electron beam kinetic energy is coupled into the plasma electrons, giving a factor 2.8 increase in plasma electron kinetic energy.

7.3.1 Coherence

During the beam-plasma instability the plasma electron density evolves from an initial white noise perturbation into a series of localized Langmuir wave packets, ending in a turbulent state. Intuitively we would expect these states to have different degrees of coherence, and so for the level of coherence of the plasma to vary during the interaction. This expectation can be quantitatively verified by calculating the coherence length and field entropy discussed in Chapter 5 for the fields in the simulation as a function of time, as shown in Figure 7.6. At the beginning of the simulation the coherence length is very short, and the entropy large, as is to be expected for the initial white noise state. As the beam plasma instability develops the coherence length of the electrons increases rapidly, since initially it is Langmuir waves which are generated leaving the ions unaffected. As the Langmuir waves begin to couple into ion-acoustic waves the coherence of the ions increases as the waves form, and the coherence length of the electron density decreases, which is associated with incoherence in between the localized wavepackets

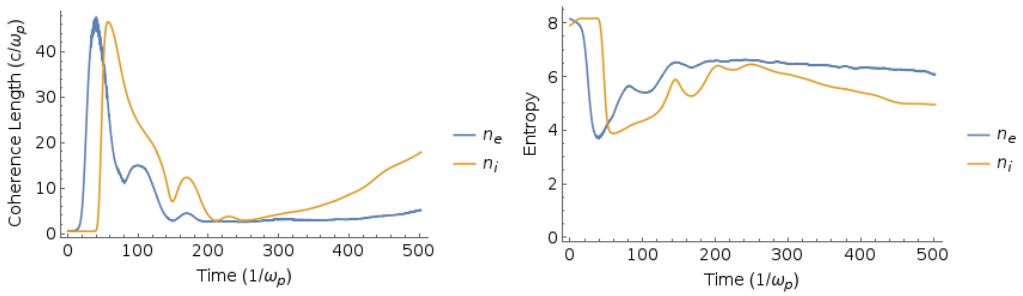

(a) **(b)**

Figure 7.6: The evolution of the coherence length (a) and field entropy (b) of the electron density n_e and ion density n_i as the beam plasma instability develops.

which form. After this coupling as shown in Figure 7.2 the waves begin to become turbulent, with an associated decrease in coherence. At large times structures begin to form in the ion density while the Langmuir waves remain noisy, reflected in an increase in the ion density coherence length.

In fact coherence initially builds up locally, as it must since early in the simulation distant parts of the plasma have not communicated. The local coherence length and entropy can be calculated by windowing the data as for the windowed Fourier transform and then calculating the coherence length and entropy while scanning the window across the data. Figure 7.7 shows snapshots of the local coherence length and entropy in the plasma as the instability develops, along with the electron density perturbation. The coherence length is lower, and the entropy higher, in between the wavepackets which have formed, consistent with the visual impression of the noisier field between the wavepackets in the plots of the electron density. The snapshot shown is taken at $t = 150$, which in these units mean that light has had a chance to propagate $x = 150$, a scale which is broadly consistent with the size of the wavepackets and the regions of coherence.

Following the work on coherence and phase dislocations presented in Chapter 5, the incoherence in the plasma should be associated with dislocations in the complex phase space distribution of the plasma waves. Figure 7.8 shows snapshots of the absolute value and phase of the position-wave vector distribution of the electron density at $t = 150$, the same time as in Figure 7.7. The dislocations visible are associated with a shorter local coherence length.

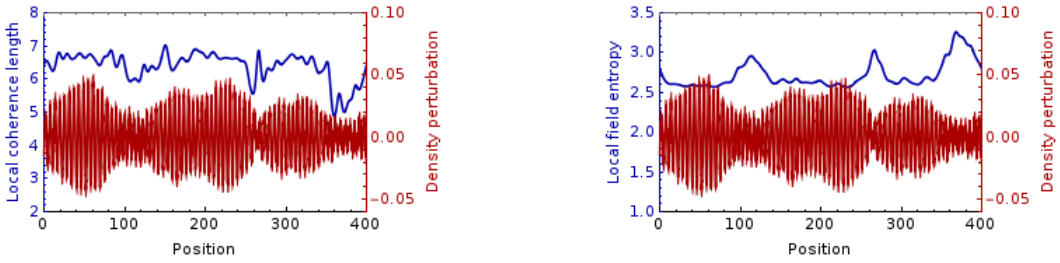

(a) **(b)**

Figure 7.7: Snapshots of the electron density and its local coherence length and field entropy as the beam-plasma instability develops.

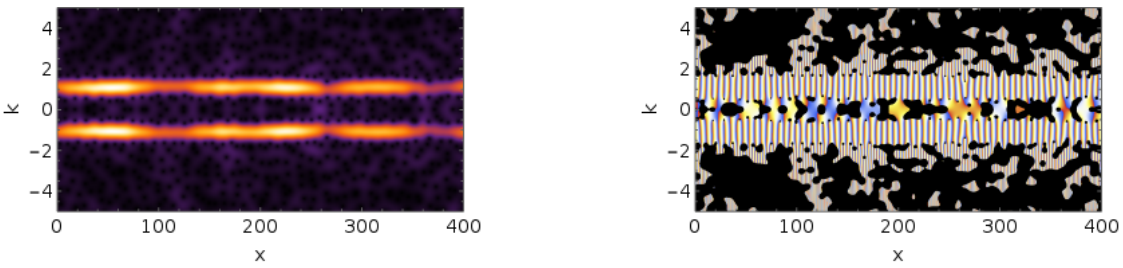

(a) **(b)**

Figure 7.8: Snapshots of the absolute value (a) and phase (b) of the position-wavevector distribution of the beam driven Langmuir waves, showing the phase dislocations associated with the regions of reduced coherence.

7.4 2D simulation results

Simulations in two spatial dimensions allow the study of waves propagating obliquely to the beams and also the geometry of two beams crossing at 90°. This section covers 2D simulations run with the same beam parameters as in the 1D simulations, for the cases in which the beams cross at 90° and 180°.

Figure 7.9 shows plots of the spatial Fourier transform of the electron density perturbation at two times for the two cases of beams crossing at 90° (a,b) and beams crossing at 180° (c,d). The spectra in the 90° case cover a broader range of angles in wavevector. There is a mode present with $k_x = 1.1$, $k_y = 1.1$ corresponding to the diagonal mode of the system of two beams crossing at 90° discussed in Chapter 6. As in the 1D simulations as the interaction progresses harmonics of the original

wavevectors are generated by the nonlinear interaction.

Figure 7.10 shows the electron density distribution in ω and k. The largest amplitude wave in (a) travels diagonally between the beams with positive projection of its phase velocity vector along each beam velocity vector, corresponding to the diagonal mode in the spatial Fourier transforms of Figure 7.9. It occurs at the wavevector and frequency predicted by the linear theory above, shown in (a) by the red spheres. The modes corresponding to the two red spheres have phase velocities in the same direction although their wavevectors point in opposite directions, since their frequencies differ by a factor of -1. The bases of the 3D plots show the wave distribution in $(\omega, \vec{k})$ integrated over ω, giving the distribution in $\vec{k}$ space which is here two-dimensional, matching the spectra in Figure 7.9.

7.5 Summary

In this chapter I have presented the results of Vlasov-Maxwell simulations of the system of beams crossing a background plasma using the VALIS code. Resolution tests were presented demonstrating the numerical convergence of the simulations. Simulations in one spatial dimension were explored using their spatial Fourier transforms, space-time Fourier transforms, and in real space, showing physical information both in wavevector through the harmonics associated with the nonlinear interaction and in the bunching of wavepackets in position. The phase space representation of the waves was used to understand the energy coupling process in terms of interacting wavepackets of varying position, frequency and wavevector. The energetics of the heating process were studied, with 18% of the electron beam energy coupled into the plasma electrons, giving a factor 2.8 increase in the plasma electron kinetic energy. The evolution of the global coherence properties during the interaction were studied in terms of the field entropy and the coherence length. The local coherence was then investigating using a windowing technique to find the local entropy and coherence length, showing regions of incoherence separating coherent bunches of Langmuir waves. The phase space distribution of the electron density was shown to contain phase dislocations associated with its local

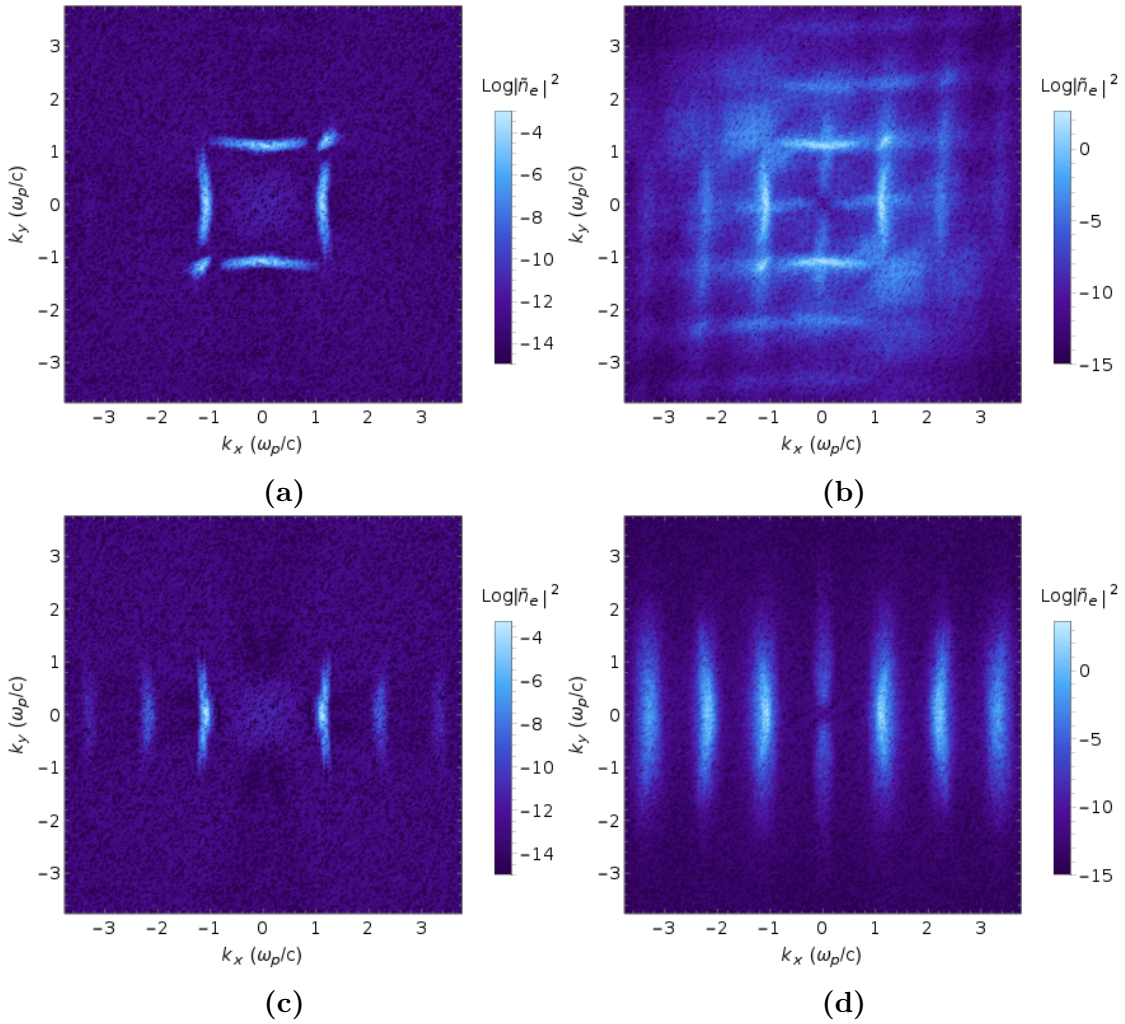

Figure 7.9: Snapshots of the spatial Fourier transform of the electron density perturbation from 2D Vlasov-Maxwell simulations of electron beams crossing at 90° (a,b) and 180° (c,d).

incoherence. Simulations in two spatial dimensions of systems of beams crossing at 90° and 180° were presented in which the 90° system showed the diagonal unstable mode calculated in Chapter 6.

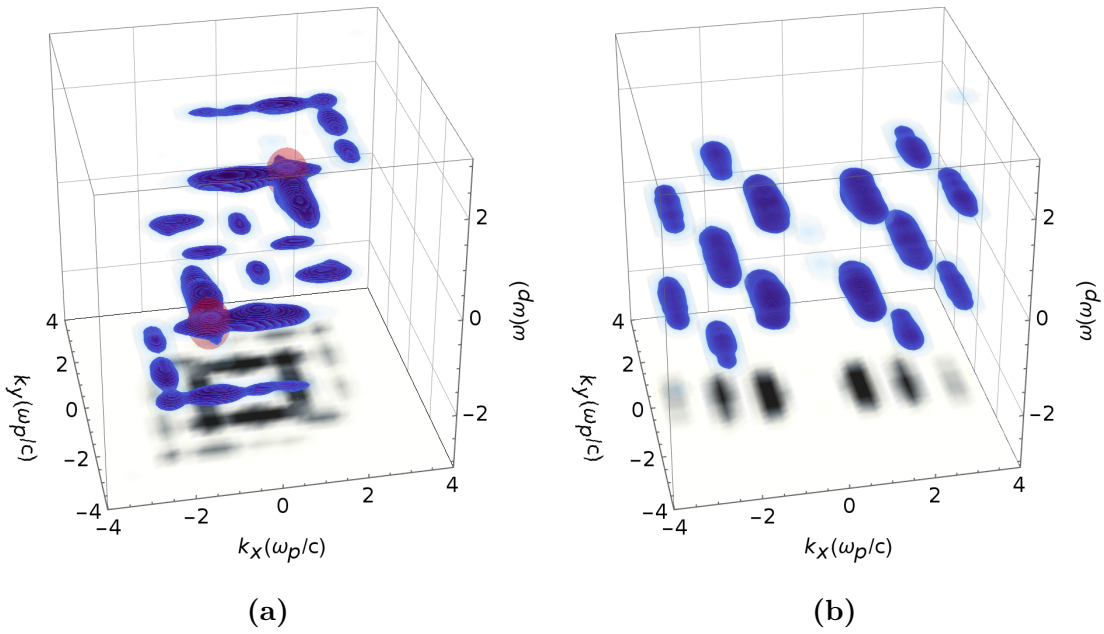

Figure 7.10: Numerically calculated ω-k distribution of the electron density from 2D Vlasov-Maxwell simulations of 1 MeV beams crossing at (a) 90° and (b) 180°. The bottom faces show the distribution in wavevector k integrated over frequency ω. The red spheres in (a) show the most unstable modes predicted by the multiple relativistic fluid theory of Chapter 6.

8

Summary and further work

8.1 Summary

This thesis presents results on the complex phase space representation of plasma waves. Chapters 2-5 presented a complex phase space representation of linear and nonlinear wave equations. The equations were derived using the Wick symbol calculus, a mathematical tool which uses Gaussian wavepackets to generalize many convenient properties of the Fourier transform to a local setting. The product formula of the Wick symbol calculus allowed the derivation of new exact equations for the phase space distribution and so the description of phenomena such as harmonic generation which are nonlocal in phase space. A general purpose asymptotic expansion of the product formula allowed treatment of dispersion, refraction, and photon acceleration, as well as nonlinear effects such as ponderomotive forces. Examples studied include an oscillator with varying frequency, wave propagation in a medium, the nonlinear Schrödinger equation, mode conversion, and the Vlasov equation. The coherence properties of wave fields were studied in terms of zeros resulting from dislocations in the phase of the distribution, which were related to the coherence length and the field entropy. Chapters 6 and 7 presented analytical and numerical work on plasma heating by crossing electron beams, including

the understanding of the wave coupling during this process using a phase space representation of the waves and their local coherence properties.

8.2 Further work

The work presented here suggests many extensions. A phase space description of waves has been used to develop numerical codes which efficiently simulate a variety of systems in plasma physics [75], [114] and it is possible that the Wick symbol equations derived above could be used to develop a phase space numerical code which tracks the phase of each wavepacket. This seems plausible since the equations obtained using the asymptotic expansion of the product formula can be solved along rays. Some method of treating the exact product formula numerically may allow a phase space numerical method in which the computational particles with different wavevectors could interact and generate a new particle at a new wavevector with the correct phase.

The Wick symbol method can also treat systems of equations straightforwardly; since the operator equation equivalent to each wave equation introduces only $\phi_0^\dagger$ and not additional copies of the fields, each equation can be treated as above, so for n fields we obtain n phase space equations. This is by contrast with the Wigner function for example, which due to its nonlinearity initially introduces n^2 phase space equations for a matrix of cross Wigner functions, before diagonalizing to reduce to n equations. An interesting possibility is to use spin coherent states [60], which introduce a complex coordinate like z above to describe the polarization of a set of fields, to give for n fields a single phase space equation depending on additional coordinates from the spin coherent states to describe the evolution of the polarization of the plasma waves.

The symbol as developed by Berezin [76] is not limited to the use of Gaussian wavepackets, and in particular can be applied using wavelets [82], [83], functions which are obtained from a given basic wavelet by translations and rescalings, to give equations in a phase space of position and scale. The efficacy of the formalism used here depended on the complex structure linking position and wavevector, and

in fact the analytic, or Paul, wavelets [54], [206] naturally come with a complex structure joining position and scale. Preliminary work suggests that the symbols defined using them satisfy equations similar to those above. A wavelet symbol calculus treatment may be well suited to the study of turbulence, where wavelets have found many applications [207], [208].

References

[1] G. J. Weisel, "Containing plasma physics: A disciplinary history, 1950–1980", 2001.

[2] J. Hendry and J. D. Lawson, "Fusion research in the UK 1945-1960", AEA Technology, Tech. Rep., 1993.

[3] W. P. Allis, S. J. Buchsbaum, and A. Bers, *Waves in anisotropic plasmas*. The MIT Press, 1963, p. 292.

[4] E. Whittaker, *A History of the Theories of Aether and Electricity: Vol. I: The Classical Theories; Vol. II: The Modern Theories, 1900-1926*. Courier Dover Publications, 1951, vol. 1.

[5] W. Crookes, "Experimental contributions to the theory of the radiometer.–Preliminary notice", *Proceedings of the Royal Society of London*, vol. 25, no. 171-178, pp. 303–314, 1876.

[6] H. A. Lorentz, *The Theory of Electrons and Its Applications to the Phenomena of Light and Radiant Heat: A Course of Lectures Delivered in Columbia University, New York, in March and April, 1906*. Columbia University Press, 1909, vol. 29.

[7] E. Hückel and P. Debye, "The theory of electrolytes: I. Lowering of freezing point and related phenomena", *Phys. Z*, vol. 24, pp. 185–206, 1923.

[8] I. Langmuir, "Oscillations in ionized gases", *Proceedings of the National Academy of Sciences*, vol. 14, no. 8, pp. 627–637, 1928.

[9] L. Tonks and I. Langmuir, "Oscillations in ionized gases", *Physical Review*, vol. 33, no. 2, p. 195, 1929.

[10] E. V. Appleton, "Wireless studies of the ionosphere", *Institution of Electrical Engineers-Proceedings of the Wireless Section of the Institution*, vol. 7, no. 21, pp. 257–265, 1932.

[11] W. H. Bennett, "Magnetically self-focussing streams", *Physical Review*, vol. 45, no. 12, p. 890, 1934.

[12] A. A. Vlasov, "The vibrational properties of an electron gas", *Physics-Uspekhi*, vol. 10, no. 6, pp. 721–733, 1968.

[13] H. Alfvén, "Existence of electromagnetic-hydrodynamic waves", *Nature*, vol. 150, no. 3805, pp. 405–406, 1942.

[14] L. D. Landau, "On the vibrations of the electronic plasma", *Zh. Eksp. Teor. Fiz.*, vol. 10, p. 25, 1946.

[15] I. Kurchatov, "On the possibility of producing thermonuclear reactions in a gas discharge", *Journal of Nuclear Energy (1954)*, vol. 4, no. 2, 193IN3199–198IN6202, 1957.

[16] L. Spitzer Jr, “A proposed stellarator”, Princeton Univ., NJ Forrestal Research Center, Tech. Rep., 1951.

[17] L. Spitzer Jr, *Physics of Fully Ionized Gases*, ser. Interscience Tracts on Physics and Astronomy. Interscience Publishers, 1955, vol. 3.

[18] O. Buneman, “Dissipation of currents in ionized media”, *Physical Review*, vol. 115, no. 3, p. 503, 1959.

[19] T. H. Maiman, “Stimulated optical radiation in ruby”, *Nature*, vol. 187, no. 4736, pp. 493–494, 1960.

[20] J. Nuckolls, L. Wood, A. Thiessen, and G. Zimmerman, “Laser compression of matter to super-high densities: Thermonuclear (CTR) applications”, *Nature*, vol. 239, no. 5368, pp. 139–142, 1972.

[21] Y. B. Zel’Dovich and Y. P. Raizer, “Physics of shock waves and high-temperature hydrodynamic phenomena”, *Vol. I*, pp. 93–101, 1966.

[22] R. Z. Sagdeev and A. A. Galeev, *Nonlinear Plasma Theory*. W. A. Benjamin, 1969.

[23] N. Ratan, N. Sircombe, L. Ceurvorst, J. Sadler, M. Kasim, J. Holloway, M. Levy, R. Trines, R. Bingham, and P. Norreys, “Dense plasma heating by crossing relativistic electron beams”, *Physical Review E*, vol. 95, no. 1, p. 013 211, 2017.

[24] A. P. Youschkevitch, “The concept of function up to the middle of the 19 th century”, *Archive for History of exact Sciences*, vol. 16, no. 1, pp. 37–85, 1976.

[25] N. Luzin, “Function: Part I”, *The American mathematical monthly*, vol. 105, no. 1, p. 59, 1998.

[26] L. Euler, “Introduction to analysis of the infinite, vol. 1”, *I (Translation by JD Blanton)(Springer, 1988)*, 1988.

[27] R. Beals, *Advanced mathematical analysis: periodic functions and distributions, complex analysis, Laplace transform and applications*. Springer-Verlag, 1973, vol. 12.

[28] R. D. Richtmyer, *Principles of advanced mathematical physics*. Springer, 1981, vol. 1.

[29] J. Lützen, *The prehistory of the theory of distributions*. Springer-Verlag, 1982, vol. 7.

[30] A. Robinson, *Non-standard analysis*. North-Holland Pub. Co., 1966.

[31] A. H. Lightstone and A. Robinson, *Nonarchimedean fields and asymptotic expansions*. North-Holland Pub. Co., 1975.

[32] R. Goldblatt, *Lectures on the hyperreals: an introduction to nonstandard analysis*. Springer, 1998, vol. 188.

[33] H. J. Keisler, *Elementary calculus: An infinitesimal approach*. Prindle, Weber and Schmidt, 1976.

[34] R. Penrose, “Republication of: Conformal treatment of infinity”, *General Relativity and Gravitation*, vol. 43, no. 3, pp. 901–922, 2011.

[35] ——, “Asymptotic properties of fields and space-times”, *Physical Review Letters*, vol. 10, no. 2, p. 66, 1963.

[36] J. Frauendiener, "Conformal infinity", *Living Reviews in Relativity*, vol. 7, no. 1, p. 1, 2004.

[37] D. V. Widder, *Laplace Transform (PMS-6)*. Princeton University Press, 1946.

[38] R. E. A. C. Paley and N. Wiener, *Fourier transforms in the complex domain*. American Mathematical Soc., 1934, vol. 19.

[39] C. Lanczos, *Applied analysis*. Isaac Pitman, 1957.

[40] G. Pólya and G. Latta, "Complex variables", 1974.

[41] G. B. Whitham, *Linear and nonlinear waves*, ser. Pure and applied mathematics. New York ; Chichester: Wiley, 1974.

[42] R. Courant and D. Hilbert, *Methods of mathematical physics, vol. 2: Partial differential equations, by R. Courant*, 1962.

[43] J. L. Synge, *Relativity: the special theory*. Prabhat Prakashan, 1965, vol. 1.

[44] M. Kac, "A stochastic model related to the telegrapher's equation", *Rocky Mountain Journal of Mathematics*, vol. 4, no. 3, 1974.

[45] M. Kac, "Some stochastic problems in physics and mechanics", Magnolia Petrolum Co. Colloq. Lect, 1956.

[46] S. Goldstein, "On diffusion by discontinuous movements, and on the telegraph equation", *The Quarterly Journal of Mechanics and Applied Mathematics*, vol. 4, no. 2, pp. 129–156, 1951.

[47] G. I. Taylor, "Diffusion by continuous movements", *Proceedings of the london mathematical society*, vol. 2, no. 1, pp. 196–212, 1922.

[48] R. Geroch, "Partial differential equations of physics", *General Relativity, Aberdeen, Scotland*, pp. 19–60, 1996.

[49] D. Gabor, "Theory of communication. part 1: The analysis of information", *Journal of the Institution of Electrical Engineers-Part III: Radio and Communication Engineering*, vol. 93, no. 26, pp. 429–441, 1946.

[50] J. d. Ville, "Théorie et applications de la notion de signal analytique", *Cables et transmission*, vol. 2, no. 1, pp. 61–74, 1948.

[51] ——, *Theory and applications of the notion of the analytic signal*, https://archive.org/details/VilleSigAnalytiqueCablesEtTrans1948En, Trans. by M D Godfrey, 1948.

[52] N. De Bruijn, "Uncertainty principles in Fourier analysis", *Inequalities*, vol. 2, pp. 57–71, 1967.

[53] G. B. Folland, *Harmonic Analysis in Phase Space.(AM-122)*. Princeton University Press, 1989, vol. 122.

[54] I. Daubechies and T. Paul, "Time-frequency localisation operators-a geometric phase space approach: Ii. the use of dilations", *Inverse Problems*, vol. 4, no. 3, p. 661, 1988.

[55] E. Wigner, "On the quantum correction for thermodynamic equilibrium", *Physical review*, vol. 40, no. 5, p. 749, 1932.

[56] G. Kaiser, *A friendly guide to wavelets*. Birkhäuser, 1994.

[57] M. V. Berry, "Semi-classical mechanics in phase space: A study of Wigner's function", *Philosophical Transactions of the Royal Society of London A: Mathematical, Physical and Engineering Sciences*, vol. 287, no. 1343, pp. 237–271, 1977.

[58] E. J. Heller, "Wigner phase space method: Analysis for semiclassical applications", *The Journal of Chemical Physics*, vol. 65, no. 4, pp. 1289–1298, 1976.

[59] R. J. Glauber, "Coherent and incoherent states of the radiation field", *Physical Review*, vol. 131, no. 6, p. 2766, 1963.

[60] J. Klauder and B. Skagerstam, *Coherent states: applications in physics and mathematical physics*. World scientific, 1985.

[61] S. T. Ali, J. Antoine, J. Gazeau, and U. Mueller, "Coherent states and their generalizations: A mathematical overview", *Rev. Math. Phys*, vol. 7, no. 7, pp. 1013–1104, 1995.

[62] W. Noll, *Finite-dimensional spaces: algebra, geometry and analysis*. Springer Science & Business Media, 2012, vol. 1.

[63] M. J. Ablowitz and A. S. Fokas, *Complex variables: introduction and applications*. Cambridge University Press, 2003.

[64] R. Remmert, *Theory of complex functions*, ser. Graduate texts in mathematics. Springer-Verlag, 1991, vol. 122.

[65] I. N. Vekua, *Generalized analytic functions*, ser. International series of monographs in pure and applied sciences. Pergamon Press, 1962, vol. 25.

[66] J. L. Synge, *Geometrical optics: an introduction to Hamilton's method*, 37. CUP Archive, 1937.

[67] V. I. Arnold, *Mathematical methods of classical mechanics*, ser. Graduate Texts in Mathematics. 1991, vol. 60.

[68] W. L. Burke, *Applied differential geometry*. Cambridge University Press, 1985.

[69] O. Heaviside, "On operators in physical mathematics. Part I", *Proceedings of the Royal Society of London*, vol. 52, no. 315-320, pp. 504–529, 1892.

[70] ——, "On operators in physical mathematics. Part II", *Proceedings of the Royal Society of London*, vol. 54, no. 326-330, pp. 105–143, 1893.

[71] K. Oldham and J. Spanier, *The fractional calculus theory and applications of differentiation and integration to arbitrary order*. Elsevier, 1974, vol. 111.

[72] I. B. Bernstein and L. Friedland, "Geometric optics in space and time varying plasmas", in *Basic Plasma Physics I*, A. A. Galeev and R. N. Sudan, Eds., North-Holland, 1983, ch. 2.5, pp. 367–418.

[73] S. W. McDonald, "Phase-space representations of wave equations with applications to the eikonal approximation for short-wavelength waves", *Physics Reports*, vol. 158, no. 6, pp. 337–416, 1988.

[74] S. W. McDonald and A. N. Kaufman, "Weyl representation for electromagnetic waves: The wave kinetic equation", *Physical Review A*, vol. 32, no. 3, p. 1708, 1985.

[75] E. R. Tracy, A. J. Brizard, A. Richardson, and A. Kaufman, *Ray tracing and beyond: phase space methods in plasma wave theory*. Cambridge University Press, 2014.

[76] F. A. Berezin, "Covariant and contravariant symbols of operators", *Izvestiya: Mathematics*, vol. 6, no. 5, pp. 1117–1151, 1972.

[77] F. A. Berezin and M. A. Shubin, *The Schrödinger Equation*. Kluwer Academic, Dordrecht, 1991.

[78] V. Bargmann, "On a Hilbert space of analytic functions and an associated integral transform part I", *Communications on pure and applied mathematics*, vol. 14, no. 3, pp. 187–214, 1961.

[79] R. E. Peierls, *Quantum theory of solids*, 23. Oxford University Press, 1955.

[80] A. A. Galeev and R. Z. Sagdeev, "Wave-wave interaction", in *Basic Plasma Physics I*, A. A. Galeev and R. N. Sudan, Eds., North-Holland, 1983, ch. 4.2, pp. 367–418.

[81] V. N. Tsytovich, *Theory of turbulent plasma*. Consultants Bureau, New York, 1977.

[82] I. Daubechies, "The wavelet transform, time-frequency localization and signal analysis", *IEEE transactions on information theory*, vol. 36, no. 5, pp. 961–1005, 1990.

[83] Y. Meyer, *Wavelets and operators*. Cambridge university press, 1995, vol. 1.

[84] H. Weyl, *The theory of groups and quantum mechanics*. Methuen, 1931.

[85] J. E. Moyal, "Quantum mechanics as a statistical theory", in *Mathematical Proceedings of the Cambridge Philosophical Society*, Cambridge Univ Press, vol. 45, 1949, pp. 99–124.

[86] R. G. Littlejohn, "The semiclassical evolution of wave packets", *Physics reports*, vol. 138, no. 4-5, pp. 193–291, 1986.

[87] E. J. Heller, "Phase space interpretation of semiclassical theory", *The Journal of Chemical Physics*, vol. 67, no. 7, pp. 3339–3351, 1977.

[88] Y. Weissman, "Semiclassical approximation in the coherent states representation", *The Journal of Chemical Physics*, vol. 76, no. 8, pp. 4067–4079, 1982.

[89] E. J. Heller, "Frozen gaussians: A very simple semiclassical approximation", *The Journal of Chemical Physics*, vol. 75, no. 6, pp. 2923–2931, 1981.

[90] J. Lu and X. Yang, "Frozen gaussian approximation for high frequency wave propagation", *Communications in Mathematical Sciences*, vol. 9, no. 3, pp. 663–683, 2011.

[91] J. R. Klauder, "Global, uniform, semiclassical approximation to wave equations", *Physical Review Letters*, vol. 56, no. 9, p. 897, 1986.

[92] ——, "Global, uniform, asymptotic wave-equation solutions for large wavenumbers", *Annals of Physics*, vol. 180, no. 1, pp. 108–151, 1987.

[93] A. Voros, "Wentzel-Kramers-Brillouin method in the Bargmann representation", *Physical Review A*, vol. 40, no. 12, p. 6814, 1989.

[94] ——, "The return of the quartic oscillator. The complex WKB method", in *Annales de l'Institut Henri Poincare. Section A, Physique Theorique*, vol. 39, 1983, pp. 211–338.

[95] A. A. Galeev and V. I. Karpman, "Turbulence theory of a weakly nonequilibrium low-density plasma and structure of shock waves", *Soviet Physics JETP*, vol. 17, no. 2, pp. 403–409, 1963.

[96] A. Vedenov, A. Gordeev, and L. Rudakov, "Oscillations and instability of a weakly turbulent plasma", *Plasma Physics*, vol. 9, no. 6, p. 719, 1967.

[97] V. N. Tsytovich, *Nonlinear Effects in Plasma*. Plenum, 1970.

[98] I. M. Besieris and F. D. Tappert, "Propagation of frequency-modulated pulses in a randomly stratified plasma", *Journal of Mathematical Physics*, vol. 14, no. 6, pp. 704–707, 1973.

[99] ——, "Stochastic wave-kinetic theory in the Liouville approximation", *Journal of Mathematical Physics*, vol. 17, no. 5, pp. 734–743, 1976.

[100] J. T. Mendonça, *Theory of photon acceleration*. CRC Press, 2000.

[101] T. Biro and K. Rönnmark, "Phase-space description of plasma waves. Part 1. Linear theory", *Journal of plasma physics*, vol. 47, no. 03, pp. 465–477, 1992.

[102] K. Rönnmark and T. Biro, "Phase-space description of plasma waves. Part 2. Nonlinear theory", *Journal of plasma physics*, vol. 47, no. 03, pp. 479–489, 1992.

[103] K. Rönnmark, "Quantitative methods for waves in space plasmas", *Space Science Reviews*, vol. 54, no. 1-2, pp. 1–73, 1990.

[104] N. Marcuvitz, "Quasiparticle view of wave propagation", *Proceedings of the IEEE*, vol. 68, no. 11, pp. 1380–1395, 1980.

[105] S.-Y. Lee and N. Marcuvitz, "Quasiparticle description of pulse propagation in a lossy dispersive medium", *IEEE transactions on antennas and propagation*, vol. 32, no. 4, pp. 395–398, 1984.

[106] ——, "Quasiparticle description of wave propagation and reflection in inhomogeneous media", *IEEE transactions on antennas and propagation*, vol. 34, no. 5, pp. 613–625, 1986.

[107] H. Pécseli and J. Trulsen, "Wavenumber-in-cell simulation of weak Langmuir turbulence", *Physical review letters*, vol. 64, no. 3, p. 285, 1990.

[108] ——, "A wavenumber-in-cell simulation of weak Langmuir turbulence", *Physica Scripta*, vol. 46, no. 2, p. 159, 1992.

[109] E. Kontar and H. Pécseli, "Nonlinear development of electron-beam-driven weak turbulence in an inhomogeneous plasma", *Physical Review E*, vol. 65, no. 6, p. 066 408, 2002.

[110] L. Silva, W. Mori, R. Bingham, J. Dawson, T. M. Antonsen, and P. Mora, "Photon kinetics for laser-plasma interactions", *IEEE transactions on plasma science*, vol. 28, no. 4, pp. 1128–1134, 2000.

[111] R. Trines, R. Bingham, L. Silva, J. Mendonça, P. Shukla, and W. Mori, "Quasiparticle approach to the modulational instability of drift waves coupling to zonal flows", *Physical review letters*, vol. 94, no. 16, p. 165 002, 2005.

[112] A. Reitsma, R. Trines, R. Bingham, R. Cairns, J. Mendonça, and D. Jaroszynski, "Photon kinetic modeling of laser pulse propagation in underdense plasma", *Physics of Plasmas (1994-present)*, vol. 13, no. 11, p. 113 104, 2006.

[113] R. Trines, R. Bingham, M. Dunlop, A. Vaivads, J. Davies, J. Mendonça, L. Silva, and P. Shukla, "Spontaneous generation of self-organized solitary wave structures at earth's magnetopause", *Physical review letters*, vol. 99, no. 20, p. 205 006, 2007.

[114] R. Trines, R. Bingham, L. Silva, J. Mendonça, P. Shukla, C. Murphy, M. Dunlop, J. Davies, R. Bamford, A. Vaivads, *et al.*, "Applications of the wave kinetic approach: From laser wakefields to drift wave turbulence", *Physics of Plasmas (1994-present)*, vol. 16, no. 5, p. 055 904, 2009.

[115] K. Hasselmann, "On the non-linear energy transfer in a gravity-wave spectrum Part 1. General theory", *Journal of Fluid Mechanics*, vol. 12, no. 4, pp. 481–500, 1962.

[116] K. Hasselmann, "On the non-linear energy transfer in a gravity wave spectrum Part 2. Conservation theorems; wave-particle analogy; irrevesibility", *Journal of Fluid Mechanics*, vol. 15, no. 2, pp. 273–281, 1963.

[117] K. Hasselmann, "On the non-linear energy transfer in a gravity-wave spectrum. Part 3. Evaluation of the energy flux and swell-sea interaction for a Neumann spectrum", *Journal of Fluid Mechanics*, vol. 15, no. 3, pp. 385–398, 1963.

[118] J. L. Synge, "Geometrical optics in moving dispersive media", *Commun. Dublin Inst. Adv. Stud., A*, 1956.

[119] J. L. Synge, "The Hamiltonian method and its application to water waves", in *Proceedings of the Royal Irish Academy. Section A: Mathematical and Physical Sciences*, JSTOR, 1963, pp. 1–34.

[120] ——, *Geometrical mechanics and de Broglie waves*. Cambridge University Press, 1954.

[121] J. L. Synge, "Water waves and hydrons", *Science*, vol. 138, no. 3536, pp. 13–15, 1962.

[122] W. L. Burke, *Spacetime, geometry, cosmology*, English, ser. A Series of books in astronomy. Mill Valley, Calif.: University Science Books, 1980.

[123] A. Schekochihin, J. Parker, E. Highcock, P. Dellar, W. Dorland, and G. Hammett, "Phase mixing versus nonlinear advection in drift-kinetic plasma turbulence", *Journal of Plasma Physics*, vol. 82, no. 02, p. 905 820 212, 2016.

[124] J. T. Parker and P. J. Dellar, "Fourier–Hermite spectral representation for the Vlasov–Poisson system in the weakly collisional limit", *Journal of Plasma Physics*, vol. 81, no. 02, p. 305 810 203, 2015.

[125] W. H. Louisell, *Coupled mode and parametric electronics*. Wiley, 1960.

[126] G. N. Watson, *A treatise on the theory of Bessel functions*. Cambridge University Press, 1944.

[127] M. Baranger, M. A. de Aguiar, F. Keck, H.-J. Korsch, and B. Schellhaaß, "Semiclassical approximations in phase space with coherent states", *Journal of Physics A: Mathematical and General*, vol. 34, no. 36, p. 7227, 2001.

[128] A. Schuster, "The propagation of waves through dispersive media", in *Festschrift Ludwig Boltzmann*, S. Meyer, Ed., Leipzig: J.A. Barth, 1904, ch. 72, pp. 569–575.

[129] A. Sommerfeld and L. Brillouin, *Wave Propagation and Group Velocity*. Academic Press, New York, 1960.

[130] A. H. Nayfeh, *Perturbation methods*. John Wiley & Sons, 1973.

[131] S. Wilks, J. Dawson, W. Mori, T. Katsouleas, and M. Jones, "Photon accelerator", *Physical review letters*, vol. 62, no. 22, p. 2600, 1989.

[132] W. L. Kruer, "The physics of laser plasma interactions", 1988.

[133] G. G. Howes and K. D. Nielson, "Alfvén wave collisions, the fundamental building block of plasma turbulence. I. Asymptotic solution", *Physics of Plasmas*, vol. 20, no. 7, p. 072 302, 2013.

[134] K. E. Oughstun, *Electromagnetic and optical pulse propagation 1*, ser. Springer series in optical sciences. Springer, 2006, vol. 125.

[135] A. Shabat and V. Zakharov, "Exact theory of two-dimensional self-focusing and one-dimensional self-modulation of waves in nonlinear media", *Soviet physics JETP*, vol. 34, no. 1, p. 62, 1972.

[136] M. J. Ablowitz and H. Segur, *Solitons and the inverse scattering transform*. SIAM, 1981.

[137] R. Y. Chiao, E. Garmire, and C. Townes, "Self-trapping of optical beams", *Physical Review Letters*, vol. 13, no. 15, p. 479, 1964.

[138] V. E. Zakharov, "Collapse of Langmuir waves", *Sov. Phys. JETP*, vol. 35, no. 5, pp. 908–914, 1972.

[139] D. R. Nicholson, *Introduction to Plasma Theory*. Wiley, 1983.

[140] F. Tappert, W. Cole, R. Hardin, and N. Zabusky, "Wave kinetic equation emulation by numerical particle-in-cell simulation methods", in *Proceedings of the Fourth Conference on Numerical Simulation of Plasmas*, J. P. Boris and R. A. Shanny, Eds., Naval Research Laboratory, 1970, pp. 196–208.

[141] T. H. Stix, *Waves in plasmas*. American Institute of Physics, 1992.

[142] D. G. Swanson, *Theory of mode conversion and tunneling in inhomogeneous plasmas*. John Wiley & Sons, 1998.

[143] R. Cairns and C. Lashmore-Davies, "A unified theory of a class of mode conversion problems", *The Physics of Fluids*, vol. 26, no. 5, pp. 1268–1274, 1983.

[144] A. N. Kaufman and L. Friedland, "Phase-space solution of the linear mode-conversion problem", *Physics Letters A*, vol. 123, no. 8, pp. 387–389, 1987.

[145] E. Tracy and A. N. Kaufman, "Wave-kinetic formulation of incoherent linear mode conversion", *Physical review letters*, vol. 64, no. 14, p. 1621, 1990.

[146] ——, "Metaplectic formulation of linear mode conversion", *Physical Review E*, vol. 48, no. 3, p. 2196, 1993.

[147] E. Schrödinger, "Der stetige übergang von der mikro-zur makromechanik", *Naturwissenschaften*, vol. 14, no. 28, pp. 664–666, 1926.

[148] ——, "The continuous transition from micro- to macro-mechanics", in *Collected papers on wave mechanics*, AMS Chelsea, 1982, pp. 41–44.

[149] F. Hioe, "An approach to the study of quantum systems", *Journal of Mathematical Physics*, vol. 15, no. 4, pp. 445–452, 1974.

[150] S. Schweber, "On the application of Bargmann Hilbert spaces to dynamical problems", *Annals of Physics*, vol. 41, no. 2, pp. 205–229, 1967.

[151] V. P. Maslov and M. V. Fedoriuk, *Semi-classical approximation in quantum mechanics*. Springer Science & Business Media, 2001, vol. 7.

[152] V. P. Maslov, *Operational methods*. Mir, 1976.

[153] V. Fuchs, A. Bers, and L. Harten, "On the theory of pairwise coupling embedded in more general local dispersion relations", *The Physics of fluids*, vol. 28, no. 1, pp. 177–189, 1985.

[154] D. C. Montgomery and D. A. Tidman, *Plasma kinetic theory*, ser. McGraw-Hill Advanced Physics Monograph Series. McGraw-Hill, 1964.

[155] K. M. Case, "Plasma oscillations", *Annals of Physics*, vol. 7, no. 3, pp. 349–364, 1959.

[156] N. G. Van Kampen, "On the theory of stationary waves in plasmas", *Physica*, vol. 21, no. 6-10, pp. 949–963, 1955.

[157] C. Mouhot and C. Villani, "On Landau damping", *Acta mathematica*, vol. 207, no. 1, pp. 29–201, 2011.

[158] J. Dawson, "On Landau damping", *The Physics of Fluids*, vol. 4, no. 7, pp. 869–874, 1961.

[159] H. Grad, "On the kinetic theory of rarefied gases", *Communications on pure and applied mathematics*, vol. 2, no. 4, pp. 331–407, 1949.

[160] ——, "Principles of the kinetic theory of gases", in *Thermodynamik der Gase/Thermodynamics of Gases*, Springer, 1958, pp. 205–294.

[161] C. Truesdell and R. G. Muncaster, *Fundamentals of Maxwell's Kinetic Theory of a Simple Monatomic Gas: Treated as a Branch of Rational Mechanics*. Academic Press, 1980, vol. 83.

[162] F. C. Grant and M. R. Feix, "Fourier-Hermite solutions of the Vlasov equations in the linearized limit", *The Physics of Fluids*, vol. 10, no. 4, pp. 696–702, 1967.

[163] A. Zocco and A. A. Schekochihin, "Reduced fluid-kinetic equations for low-frequency dynamics, magnetic reconnection, and electron heating in low-beta plasmas", *Physics of Plasmas*, vol. 18, no. 10, p. 102 309, 2011.

[164] N. Wiener, "Hermitian polynomials and fourier analysis", *Studies in Applied Mathematics*, vol. 8, no. 1-4, pp. 70–73, 1929.

[165] G. Szeg, *Orthogonal polynomials*. American Mathematical Soc., 1939, vol. 23.

[166] L. Mandel and E. Wolf, *Optical coherence and quantum optics*. Cambridge university press, 1995.

[167] I. Białynicki-Birula and J. Mycielski, "Uncertainty relations for information entropy in wave mechanics", *Communications in Mathematical Physics*, vol. 44, no. 2, pp. 129–132, 1975.

[168] J. Nye and M. Berry, "Dislocations in wave trains", in *Proceedings of the Royal Society of London A: Mathematical, Physical and Engineering Sciences*, The Royal Society, vol. 336, 1974, pp. 165–190.

[169] J. Hannay, "The chaotic analytic function", *Journal of Physics A: Mathematical and General*, vol. 31, no. 49, p. L755, 1998.

[170] P. Leboeuf and A. Voros, "Chaos-revealing multiplicative representation of quantum eigenstates", *Journal of Physics A: Mathematical and General*, vol. 23, no. 10, p. 1765, 1990.

[171] D. J. Hoarty, S. F. James, H. Davies, C. R. D. Brown, J. W. O. Harris, C. C. Smith, S. J. Davidson, E. Kerswill, B. J. B. Crowley, and S. J. Rose, "Heating of buried layer targets by 1ω and 2ω pulses using the HELEN CPA laser", *High Energy Density Physics*, vol. 3, no. 1, pp. 115–119, 2007.

[172] G. Sarri, K. Poder, J. M. Cole, W. Schumaker, A. Di Piazza, B. Reville, T. Dzelzainis, D. Doria, L. A. Gizzi, G. Grittani, *et al.*, "Generation of neutral and high-density electron-positron pair plasmas in the laboratory", *Nature communications*, vol. 6, 2015.

[173] M. Tabak, J. Hammer, M. E. Glinsky, W. L. Kruer, S. C. Wilks, J. Woodworth, E. M. Campbell, M. D. Perry, and R. J. Mason, "Ignition and high gain with ultrapowerful lasers", *Physics of Plasmas (1994-present)*, vol. 1, no. 5, pp. 1626–1634, 1994.

[174] H. Shiraga, H. Nagatomo, W. Theobald, A. A. Solodov, and M. Tabak, "Fast ignition integrated experiments and high-gain point design", *Nuclear Fusion*, vol. 54, no. 5, p. 054 005, 2014.

[175] M. C. Levy, S. C. Wilks, M. Tabak, S. B. Libby, and M. G. Baring, "Petawatt laser absorption bounded", *Nature communications*, vol. 5, 2014.

[176] International Commission on Radiation Units and Measurements, *ICRU Report 37, Stopping Powers for Electrons and Positrons*. Bethesda, MD, 1984.

[177] S. Atzeni, A. Schiavi, and J. Davies, "Stopping and scattering of relativistic electron beams in dense plasmas and requirements for fast ignition", *Plasma Physics and Controlled Fusion*, vol. 51, no. 1, p. 015 016, 2008.

[178] A. Solodov and R. Betti, "Stopping power and range of energetic electrons in dense plasmas of fast-ignition fusion targets", *Physics of Plasmas (1994-present)*, vol. 15, no. 4, p. 042 707, 2008.

[179] A. P. L. Robinson, D. J. Strozzi, J. R. Davies, L. Gremillet, J. J. Honrubia, T. Johzaki, R. J. Kingham, M. Sherlock, and A. A. Solodov, "Theory of fast electron transport for fast ignition", *Nuclear Fusion*, vol. 54, no. 5, p. 054 003, 2014.

[180] O. A. Hurricane, D. A. Callahan, D. T. Casey, P. M. Celliers, C. Cerjan, E. L. Dewald, T. R. Dittrich, T. Döppner, D. E. Hinkel, L. F. B. Hopkins, *et al.*, "Fuel gain exceeding unity in an inertially confined fusion implosion", *Nature*, 2014.

[181] J. Milovich, H. Robey, D. Clark, K. Baker, D. Casey, C. Cerjan, J. Field, A. MacPhee, A. Pak, P. Patel, *et al.*, "Design of indirectly driven, high-compression inertial confinement fusion implosions with improved hydrodynamic stability using a 4-shock adiabat-shaped drive", *Physics of Plasmas (1994-present)*, vol. 22, no. 12, p. 122 702, 2015.

[182] O. Hurricane, D. Callahan, D. Casey, E. Dewald, T. Dittrich, T. Döppner, S. Haan, D. Hinkel, L. B. Hopkins, O. Jones, *et al.*, "Inertially confined fusion plasmas dominated by alpha-particle self-heating", *Nature Physics*, 2016.

[183] V. M. Malkin and N. J. Fisch, "Collective deceleration of relativistic electrons precisely in the core of an inertial-fusion target", *Physical Review Letters*, vol. 89, no. 12, p. 125 004, 2002.

[184] S. A. Bludman, K. M. Watson, and M. N. Rosenbluth, "Statistical mechanics of relativistic streams. II", *Physics of Fluids (1958-1988)*, vol. 3, no. 5, pp. 747–757, 1960.

[185] A. Bret, L. Gremillet, and M. E. Dieckmann, "Multidimensional electron beam-plasma instabilities in the relativistic regime", *Physics of Plasmas (1994-present)*, vol. 17, no. 12, p. 120 501, 2010.

[186] T. Tajima, "Plasma heating by a relativistic electron beam with secondary instabilities", *Journal of Plasma Physics*, vol. 19, no. 01, pp. 63–75, 1978.

[187] J. Mendonça, P. Norreys, R. Bingham, and J. Davies, "Beam instabilities in laser-plasma interaction: Relevance to preferential ion heating", *Physical review letters*, vol. 94, no. 24, p. 245 002, 2005.

[188] N. J. Sircombe, R. Bingham, M. Sherlock, J. T. Mendonca, and P. Norreys, "Plasma heating by intense electron beams in fast ignition", *Plasma Physics and Controlled Fusion*, vol. 50, no. 6, p. 065 005, 2008.

[189] T. Chapman, S. Brunner, J. W. Banks, R. L. Berger, B. I. Cohen, and E. A. Williams, "New insights into the decay of ion waves to turbulence, ion heating, and soliton generation", *Physics of Plasmas (1994-present)*, vol. 21, no. 4, p. 042 107, 2014.

[190] M. J. Everett, A. Lal, C. E. Clayton, W. B. Mori, T. W. Johnston, and C. Joshi, "Coupling between high-frequency plasma waves in laser-plasma interactions", *Physical Review Letters*, vol. 74, no. 12, p. 2236, 1995.

[191] Y. Kitagawa, Y. Mori, O. Komeda, K. Ishii, R. Hanayama, K. Fujita, S. Okihara, T. Sekine, N. Satoh, T. Kurita, *et al.*, "Fusion using fast heating of a compactly imploded cd core", *Physical Review Letters*, vol. 108, no. 15, p. 155 001, 2012.

[192] P. Koester, N. Booth, C. A. Cecchetti, H. Chen, R. G. Evans, G. Gregori, L. Labate, T. Levato, B. Li, M. Makita, *et al.*, "Evidence of locally enhanced target heating due to instabilities of counter-streaming fast electron beams", *Physics of Plasmas (1994-present)*, vol. 22, no. 2, p. 020 701, 2015.

[193] A. J. Kemp, F. Fiuza, A. Debayle, T. Johzaki, W. B. Mori, P. K. Patel, Y. Sentoku, and L. O. Silva, "Laser–plasma interactions for fast ignition", *Nuclear Fusion*, vol. 54, no. 5, p. 054 002, 2014.

[194] P. Clemmow, *The plane wave spectrum representation of electromagnetic fields*. Oxford: Pergamon Press, 1966.

[195] R. J. Briggs, *Electron-stream interaction with plasmas*. MIT, 1964.

[196] A. Bers, "Space-time evolution of plasma instabilities-absolute and convective", in *Basic plasma physics. 1*, 1983.

[197] P. C. Clemmow and J. P. Dougherty, *Electrodynamics of particles and plasmas*. Addison-Wesley, 1969.

[198] J. M. Dawson, "Plasma oscillations of a large number of electron beams", *Physical Review*, vol. 118, no. 2, p. 381, 1960.

[199] D. S. Jones, *Introduction to asymptotics: a treatment using nonstandard analysis*. World Scientific, 1997.

[200] N. J. Sircombe and T. D. Arber, "VALIS: A split-conservative scheme for the relativistic 2D Vlasov–Maxwell system", *Journal of Computational Physics*, vol. 228, no. 13, pp. 4773–4788, 2009.

[201] C.-Z. Cheng and G. Knorr, "The integration of the Vlasov equation in configuration space", *Journal of Computational Physics*, vol. 22, no. 3, pp. 330–351, 1976.

[202] P. Colella and P. R. Woodward, "The piecewise parabolic method (PPM) for gas-dynamical simulations", *Journal of Computational Physics*, vol. 54, no. 1, pp. 174–201, 1984.

[203] T. Arber and R. Vann, "A critical comparison of Eulerian-grid-based Vlasov solvers", *Journal of computational physics*, vol. 180, no. 1, pp. 339–357, 2002.

[204] J. M. Dawson, "Particle simulation of plasmas", *Reviews of modern physics*, vol. 55, no. 2, p. 403, 1983.

[205] J. L. Synge, *The relativistic gas*. North-Holland Amsterdam, 1957, vol. 32.

[206] T. Paul, "Functions analytic on the half-plane as quantum mechanical states", *Journal of mathematical physics*, vol. 25, no. 11, pp. 3252–3263, 1984.

[207] M. Farge, "Wavelet transforms and their applications to turbulence", *Annual review of fluid mechanics*, vol. 24, no. 1, pp. 395–458, 1992.

[208] G. Kowal and A. Lazarian, "Velocity field of compressible magnetohydrodynamic turbulence: Wavelet decomposition and mode scalings", *The Astrophysical Journal*, vol. 720, no. 1, p. 742, 2010.